AD-A044 818 HUGHES AIRCRAFT CO CULVER CITY CALIF ANTENNA DEPT F/G 9/5
DYNAMIC IMPEDANCE MATCHING IN CONFORMAL ARRAYS.(U)
JAN 74 P C BARGELIOTES, W H KUMMER N00019-73-C-0127
UNCLASSIFIED 2265.30/184 NL

1 OF 1
ADA
044818

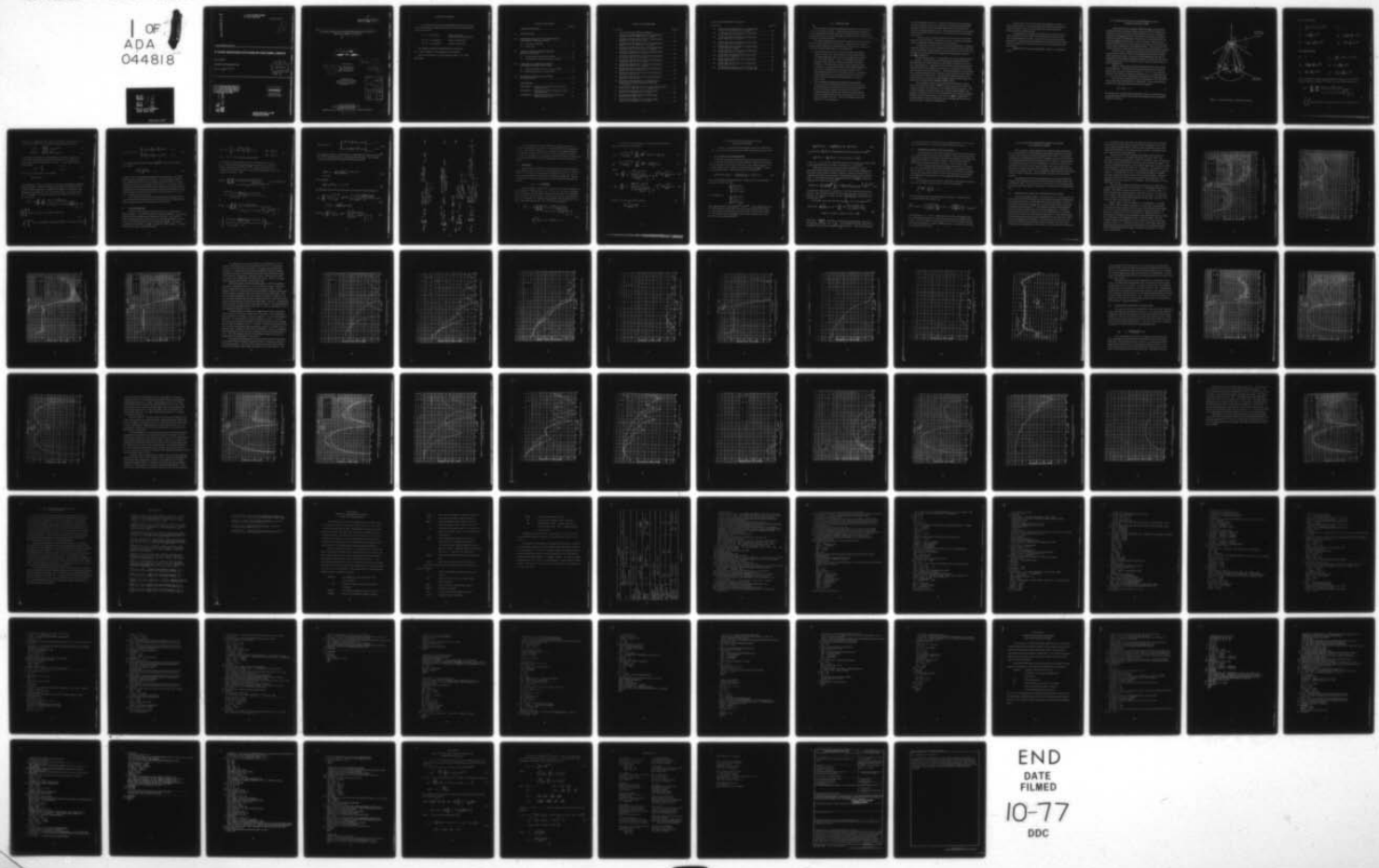

END
DATE
FILMED
10-77
DDC

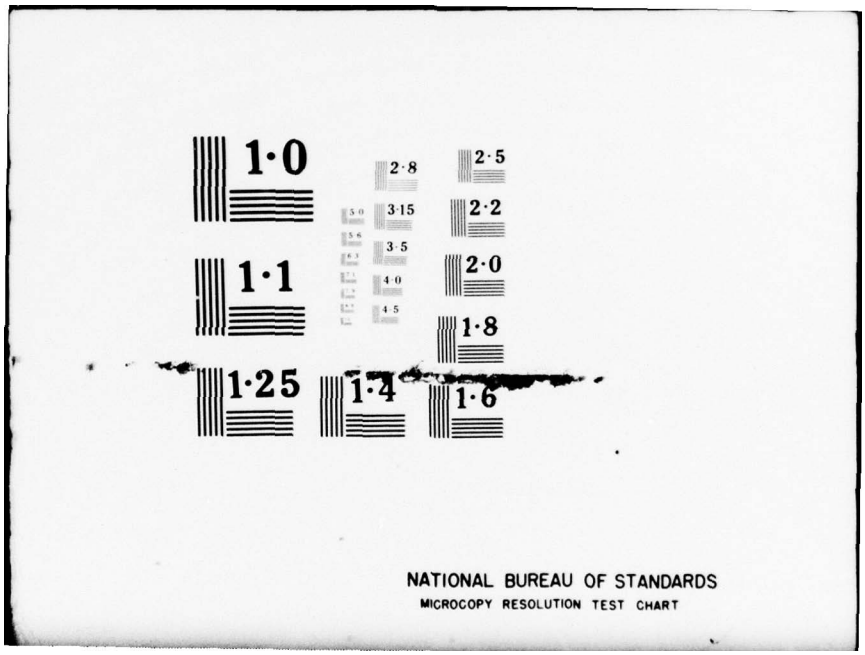
1·0
1·1
1·25
1·4
1·6
1·8
2·0
2·2
2·5
2·8
3·15
3·5
4·0
4·5
5·0
5·6
6·3
NATIONAL BUREAU OF STANDARDS
MICROCOPY RESOLUTION TEST CHART

REPORT NO. 2265.30/184
HAC REF. NO. C 7488

B. S.

Contract N000 19-73-C-0127

DYNAMIC IMPEDANCE MATCHING IN CONFORMAL ARRAYS

FINAL REPORT

JANUARY 1973 TO JANUARY 1974

Prepared for the AIR SYSTEMS COMMAND
Department of the NAVY

Creating a new world with electronics
HUGHES
ANTENNA DEPARTMENT
AEROSPACE GROUP
HUGHES AIRCRAFT COMPANY
CULVER CITY, CA 90230

(14)

Report No. 2265.30/184
HAC Ref. C-7488

(6)

DYNAMIC IMPEDANCE MATCHING IN CONFORMAL ARRAYS.

CONTRACT N00019-73-C-0127

(15)

(9)

FINAL REPORT.

Jan 1973 to Jan 1974.

(11) Jan 74

Prepared by

(10) Peter C./Bargeliotes,
Wolfgang H./Kummer
alfred T./Villeneuve

(12) 90 p.

Prepared for
Air Systems Command
Department of the Navy
Washington, D. C.

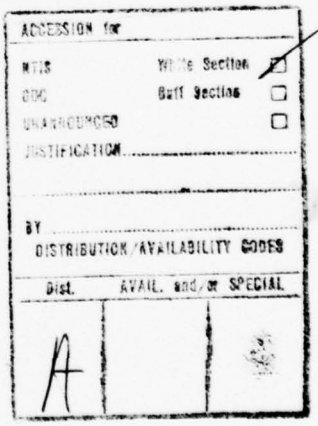

Antenna Department
Engineering Equipment Division
AEROSPACE GROUP
Hughes Aircraft Company - Culver City, California 90230

402 429

ACKNOWLEDGMENTS

The following personnel of the Hughes Radar Division contributed to the Dynamic Impedance Matching in Conformal Arrays Study during this program.

Dr. W. H. Kummer	Program Manager Radar Microwave Laboratory
Dr. P. C. Bargeliotes	Antenna Department
Dr. A. T. Villeneuve	Antenna Department

The authors gratefully acknowledge the assistance of Mrs. Yvonna Hartke in the preparation of this report.

The Technical Officer for this program is Mr. J. W. Willis (AIR-310B).

TABLE OF CONTENTS

LIST OF ILLUSTRATIONS

LIST OF ILLUSTRATIONS - Continued

1.0 INTRODUCTION

Several topics relating to conformal arrays have received detailed attention in the last few years. These topics include pattern synthesis, types of appropriate radiating elements, and their impedance and mutual coupling characteristics, and wide angle scanning of linear arrays located on planar and conical surfaces.

Synthesis techniques for the far field patterns from current distributions on planar surfaces are well known. Since there are no proven techniques for synthesizing antenna patterns from arrays on conical surfaces, two different approaches have been pursued:

1. An equivalence principle was used to determine the distribution of sources on a cone to produce a prescribed pattern. Using this approach, planar arrays are replaced by sources on a conformal surface. Thus, it is possible to generate patterns using well known synthesis techniques for planar surfaces. The equivalent sources are continuous functions on the cone. The practical validity of the method depends on the accuracy with which the continuous functions can be approximated by physically realizable radiators. Equivalent source distributions were computed at discrete points on a conical surface to approximate the patterns of a specific planar array.
2. The computation of approximate patterns from discrete radiators judiciously positioned on the cone was carried out. An optimization was performed to obtain element weightings that yield the highest signal-to-noise ratio in the beam pointing direction neglecting the effects of mutual coupling. Uniform weighting schemes were also used for beams in the region about the cone axis. This second approach has been termed a heuristic approach.

In the Final Report on Contract N00019-72-C-0212,[1] the results from the above two approaches were reported. In the equivalence principle approach, excitations and radiation patterns were computed for two particular beam pointing directions. These patterns were then compared to the far-field pattern that would have been produced by the generating planar array.

In the use of the heuristic approach several layouts of radiating elements were considered. Parameters such as variations of sidelobe levels, grating lobes and beamwidths were investigated.

In conjunction with the use of the above two approaches, computer programs were written for the approximate computation of the fields and patterns of different configurations of elements on the surface on the cone. The program used in the heuristic approach was appended in the first Quarterly Report [2].

In the present report, the computation of an exact element pattern is described. The report begins with the general expressions for two potential functions representing the modal fields of arbitrary apertures on a conducting cone. Expressions for the electric field components are then derived from the potential functions for circumferential and radial slots with particular slot excitations. The field expressions are the basis for a computer program which computes radiation patterns from both circumferential and radial slots. The appropriate approximations for the Legendre functions and the spherical Bessel functions used for their computations are summarized in Section 3 of this report.

The computer program is a modification and extension of one described by Pridmore-Brown [3] and has been executed on the IBM 370 computer system, now operational at the Hughes Aircraft Company. The program computes the special functions in DOUBLE PRECISION, thus giving the required accuracy of the computations. The complete program together with a brief description of its use is included in Appendix A. A second program, useful in studying the exact element modal patterns at minimum cost, is included in Appendix B.

Several test cases were excuted on the program in order to check its correctness. In each test case, the results compared favorably with identical cases of a circumferential slot considered by Pridmore-Brown and Stewart [4].

A comprehensive analysis of the modal series patterns is presented in Section 4 of this report for a slot 39 radians from the tip. The computed patterns are then compared with previously measured patterns [5]. Also presented are patterns of circumferential and radial slots at 30 radians from the cone tip for comparison with the previous slot location.

Suggestions for further investigations, Section 5, conclude the report.

2.0 RADIATION FIELDS OF CIRCUMFERENTIAL AND RADIAL SLOTS ON A CONE

Expressions for the radiation fields from slot-excited conical antennas were first obtained by Bailin and Silver.[6] The fields were expressed in terms of normal-mode expansions using the orthogonal properties of the eigenfunctions. Although some corrections appeared in the literature[7] modifying the first results, the expressions for the fields need additional examination. More recently Pridmore-Brown and Stewart[4] presented a more rigorous calculation of the θ-polarized electric field component of circumferential slots. Their numerical calculation is based on expressions derived from integral transform methods.

In this section, complete expressions of two potential functions representing the modal fields will be presented for both the circumferential and the radial slot. The electric field components will then be obtained from the potential functions and will be available for calculation of radiation patterns of the individual slots or arrays of slots of any desired configuration.

Figure 1 shows typical circumferential and radial slots and the conical geometry. The usual spherical coordinate system centered at the cone tip is associated with the structure. The cone axis coincides with the Z-axis of the rectangular coordinates (x, y, z) associated with (r, θ, ϕ). Primes denote coordinates of the apertures on the structure.

The two scalar potential functions in question are Π^{TE} and Π^{TM}, TE and TM to the radial direction, respectively. For an assumed time dependence of exp $\left\{ j\omega t \right\}$ both satisfy the wave equation:

$$(\nabla^2 + k^2)\,\Pi = 0. \tag{1}$$

The electric and magnetic field components are then conveniently given by superposition of TE and TM partial fields obtained from the potential functions as follows:

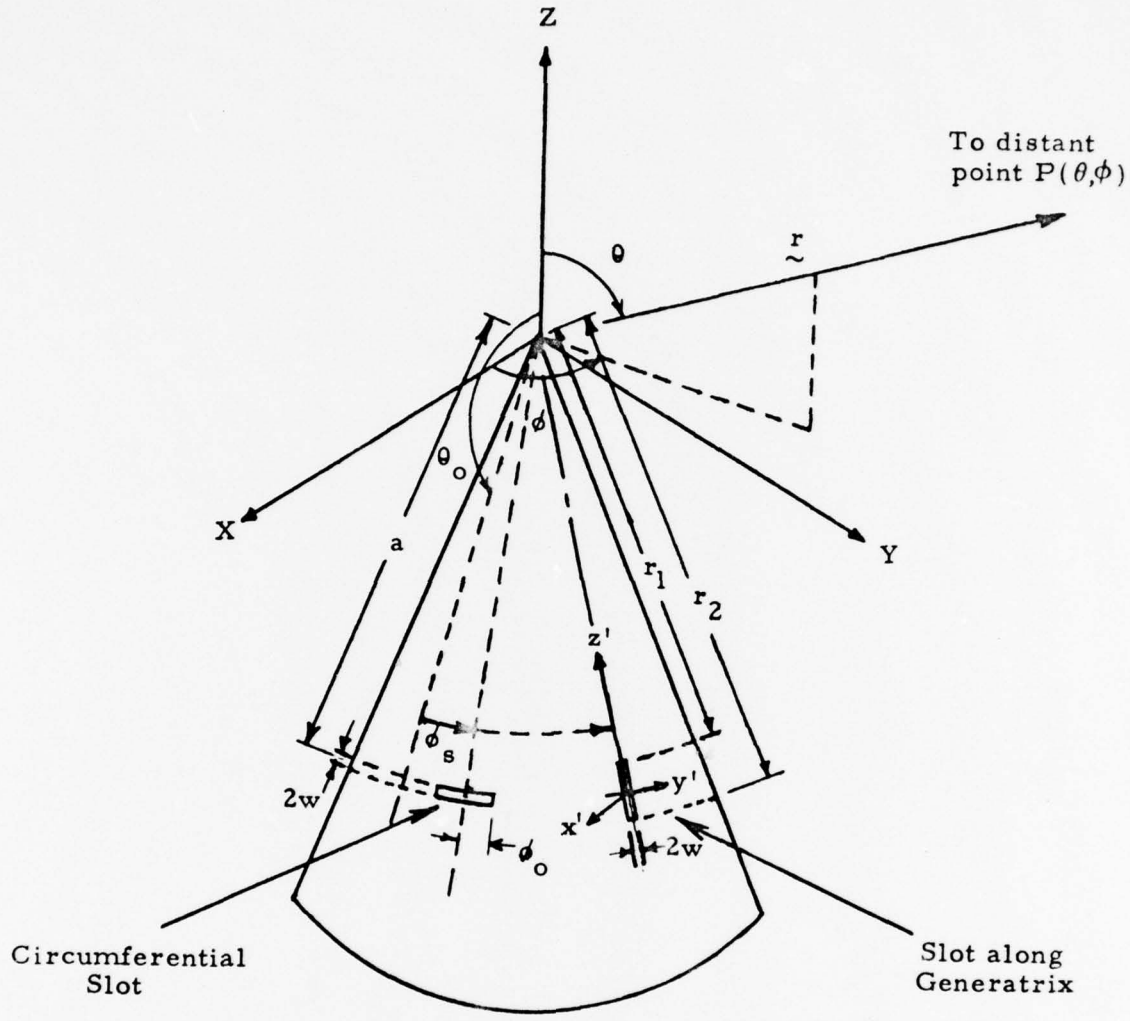

Figure 1. Conical Geometry and Slot Coordinates

TM - Partial Fields:

$$E_r = \frac{\partial^2}{\partial r^2}(r\Pi^{TM}) + k^2(r\Pi^{TM}) \qquad H_r = 0$$

$$E_\theta = \frac{1}{r}\frac{\partial^2}{\partial r \partial \theta}(r\Pi^{TM}) \qquad H_\theta = \frac{j\omega\epsilon}{r\sin\theta}\frac{\partial}{\partial \phi}(r\Pi^{TM}) \tag{2}$$

$$E_\phi = \frac{1}{r\sin\theta}\frac{\partial^2}{\partial r \partial \phi}(r\Pi^{TM}) \qquad H_\phi = \frac{-j\omega\epsilon}{r}\frac{\partial}{\partial \theta}(r\Pi^{TM})$$

TE - Partial Fields:

$$E_r = 0 \qquad H_r = \frac{\partial^2}{\partial r^2}(r\Pi^{TE}) + k^2(r\Pi^{TE})$$

$$E_\theta = -\frac{j\omega\mu}{r\sin\theta}\frac{\partial}{\partial \phi}(r\Pi^{TE}) \qquad H_\theta = \frac{1}{r}\frac{\partial^2}{\partial r \partial \theta}(r\Pi^{TE}) \tag{3}$$

$$E_\phi = \frac{j\omega\mu}{r}\frac{\partial}{\partial \theta}(r\Pi^{TE}) \qquad H_\phi = \frac{1}{r\sin\theta}\frac{\partial^2}{\partial r \partial \phi}(r\Pi^{TE})$$

For an arbitrarily shaped source excitation the expression for the Π^{TM} is given by Bailin and Silver.[7] (There is (-) sign in their expression.)

$$\Pi^{TM} = \sum_{m=0}^{\infty}\sum_{i=1}^{\infty} \frac{(jk)(2\nu_i + 1)P_{\nu_i}^m(\cos\theta)}{\nu_i(\nu_i+1)(1+\delta_{om})\pi\sin\theta_o \left.\frac{\partial P_\nu^m}{\partial \nu}\right|_{\substack{\theta=\theta_o \\ \nu=\nu_i}}} \cdot \int_{r_1}^{r_2}\int_{\phi_1}^{\phi_2} f_1(r',\phi')\cos m(\phi'-\phi)\, j_{\nu_i}(k r_<)\, h_{\nu_i}(k r_>)\, r' \sin\theta_o \, dr'\, d\phi' \tag{4}$$

where $r_>$, $r_<$ symbolizes the larger and smaller of the coordinates r, r', respectively. $P_\nu^m(\cos\theta)$ is the associated Legendre function and

$$j_\nu(kr) = \sqrt{\frac{\pi}{2kr}}\ J_{\nu+1/2}(kr) \tag{5}$$

$$h_\nu^{(2)}(kr) = \sqrt{\frac{\pi}{2kr}}\ H_{\nu+1/2}^{(2)}(kr) \tag{6}$$

are the spherical Bessel and spherical Hankel functions, respectively. J_ν is the Bessel function of the first kind and order ν and $H_\nu^{(2)}$ is the Hankel function of the second kind and order ν. δ_{om} is the Kronecker delta function

$$\delta_{om} = \begin{cases} 1 & m = 0 \\ 0 & m \neq 0 \end{cases} \tag{7}$$

while the ν_i are the roots of the equation

$$P_\nu^m(\cos\theta_o) = 0 \tag{8}$$

The function $f_1(r', \phi')$ in equation (4) is the electric field source excitation in the r direction. Following the general procedure described by Ballin and Silver where the boundary conditions are applied in conjunction with the Lorentz reciprocity theorem to the modal fields, an expression for Π^{TE} is obtained. The TE scalar function with arbitrary source excitation is given by,

$$\Pi^{TE} = \frac{1}{\eta}\sum_{m=o}^{\infty}\sum_{i=1}^{\infty} \frac{(2\nu_i' + 1)\ P_{\nu_i'}^m(\cos\theta)}{\pi(1+\delta_{om})\,\nu_i'(\nu_i'+1)\sin\theta_o \left.\frac{\partial^2 P_\nu^m}{\partial\nu\,\partial\theta}\right|_{\substack{\theta=\theta_o \\ \nu=\nu_i'}}}$$

$$\cdot \left\{ \int_{r_1}^{r_2}\int_{\phi_1}^{\phi_2} m f_1(r', \phi')\ \Gamma_1(r, r')\sin m(\phi' - \phi)\, dr'\, d\phi' \right. \tag{9}$$

$$\left. + \int_{r_1}^{r_2}\int_{\phi_1}^{\phi_2} \nu_i'(\nu_i'+1)\sin\theta_o\, f_2(r', \phi')\, j_{\nu_i'}(kr_<)\, h_{\nu_i'}^{(2)}(kr_>)\cos m(\phi' - \phi)\, dr'\, d\phi' \right\}$$

$$\text{where } \Gamma_1(r, r') = \begin{cases} j_{\nu'_i}(kr) \frac{d}{dr'} [r' h^{(2)}_{\nu'_i}(kr')] & r < r' \\ h^{(2)}_{\nu'_i}(kr) \frac{d}{dr'} [r' j_{\nu'_i}(kr')] & r > r' \end{cases} \tag{10}$$

and η is the free space wave impedance $\sqrt{\frac{\mu}{\epsilon}}$. The ν'_i are the roots of the equation

$$\frac{\partial P_\nu^m(\cos\theta_o)}{\partial \theta} = 0 \tag{11}$$

and $f_2(r', \phi')$ is the E_ϕ component of the source excitation. All other quantities are as defined for the TM case. It is interesting to observe that, unlike the TM mode, the TE mode is excited by both the r- and ϕ-components of the source excitation in the aperture. Conversely, the r-component of the source excitation *excites* both the TM and the TE modes. It should also be noted that the expression in Equation (9) differs from the expression given by Bailin and Silver [7] in the expression for $\Gamma_1(r, r')$ and a common factor of $1/\sin\theta_o$.

The modal functions and the corresponding field components from particular aperture configurations on the cone structure with appropriate field excitations are given in Sections 2.1 and 2.2 below.

2.1 Circumferential Slot

A narrow circumferential slot of width $2w << \lambda$ is considered as shown in Figure 1. The narrow slot has an azimuthal length $d = 2\phi_o a \sin\theta_o$ where $2\phi_o$ is the azimuthal angle subtended by the slot, θ_o is the cone exterior angle measured from the axis, a is the distance from the cone tip to the center of the slot and λ is the operating wavelength. The slot is assumed to be excited by a voltage V_o across its center and has a resulting field across it in the r direction given by

$$E_r(r', \phi') = \begin{cases} V_o \cos\left[\dfrac{\pi(\phi' - \phi_s)}{2\phi_o}\right] \delta(r' - a) & \left|\phi' - \phi_s\right| < \phi_o \\ 0 & \left|\phi' - \phi_s\right| > \phi_o \end{cases} \tag{12}$$

where $\delta(r' - a)$ is the Dirac delta function.

Substituting the expression of $E_r(r', \phi')$ in Equations (4) and (9) for $f_1(r', \phi')$ and integrating over the primed coordinates, we obtain the explicit expression for Π^{TM} and Π^{TE}. The function $f_2(r', \phi')$ is set equal to zero in the TE case, as only the E_r component of the source excitation is assumed. Thus,

$$\underset{\sim}{\Pi}^{TM}(\underset{\sim}{r}) = \sum_{m=0}^{\infty}\sum_{i=1}^{\infty} \frac{(jka V_o)(2\nu_i+1) P_{\nu_i}^m(\cos\theta)}{\nu_i(\nu_i+1)(1+\delta_{om})\pi \dfrac{\partial P_\nu^m(\cos\theta)}{\partial \nu}\Bigg|_{\substack{\theta=\theta_o \\ \nu=\nu_i}}} j_{\nu_i}(kr<)\, h_{\nu_i}^{(2)}(kr>)$$

$$\cdot \frac{2ka \sin\theta_o \cos\left(\dfrac{m\pi}{2ka\sin\theta_o}\right) \cos m(\phi - \phi_s)}{(ka\sin\theta_o)^2 - m^2} \tag{13}$$

and

$$\underset{\sim}{\Pi}^{TE}(\underset{\sim}{r}) = \frac{1}{\eta}\sum_{m=0}^{\infty}\sum_{i=1}^{\infty} \frac{(2\nu_i' + 1) P_{\nu_i'}^m(\cos\theta)}{\pi(1+\delta_{om})\nu_i'(\nu_i'+1)\sin\theta_o \dfrac{\partial^2 P_\nu^m(\cos\theta)}{\partial\nu\,\partial\theta}\Bigg|_{\substack{\theta=\theta_o \\ \nu=\nu_i'}}}$$

$$\cdot \left\{ \frac{-2ka\sin\theta_o \cos\left(\dfrac{m\pi}{2ka\sin\theta_o}\right) m \sin m(\phi - \phi_s)}{(ka\sin\theta_o)^2 - m^2} \right\} \cdot \Gamma_1(r, a) \tag{14}$$

$$\text{where } \Gamma_1(r, a) = \begin{cases} h^{(2)}_{\nu'_i}(kr)\,\frac{d}{dr}\left(r' j_{\nu'_i}(kr')\right)\Big|_{r'=a} & r > a \\ j_{\nu'_i}(kr)\,\frac{d}{dr}\left(r' h^{(2)}_{\nu'_i}(kr')\right)\Big|_{r'=a} & r < a \end{cases} \tag{15}$$

The radiation fields are readily found by substituting the expression of Π^{TM} and Π^{TE} corresponding to $r > a$ into Equations (2) and (3). On using the asymptotic expansion for the spherical Hankel functions,

$$h^{(2)}_{\nu}(kr) \underset{kr\to\infty}{=} \sqrt{\frac{\pi}{2kr}}\sqrt{\frac{2j}{\pi kr}}\, j^{\nu+1/2}\, e^{-jkr} \tag{16}$$

and noting that

$$\frac{\partial}{\partial r}\left(r\, h^{(2)}_{\nu}(kr)\right) = j^{\nu}\, e^{-jkr} \tag{17}$$

the following expressions are obtained for the electric field components:

$$E_\theta = \sum_{m=0}^{\infty} \frac{V_o\, e^{-j(kr - \pi/4)}}{r\pi(1+\delta_{om})} \sqrt{2\pi ka}\, \frac{2ka\sin\theta_o \cos\left(\frac{m\pi}{2ka\sin\theta_o}\right)}{(ka\sin\theta_o)^2 - m^2} \cos m\phi \cdot \left\{ P_{1\theta} + \frac{j m^2}{\sin\theta_o \sin\theta} P_{2\theta} \right\} \tag{18}$$

$$\text{where } P_{1\theta} = \sum_{i=1}^{\infty} j^{\nu_i} \frac{\nu_i}{\nu_i^2 - 1/4} J_{\nu_i}(ka)\, \frac{\frac{\partial}{\partial\theta} P^{-m}_{\nu_i - 1/2}(\cos\theta)}{\frac{\partial}{\partial\nu} P^{-m}_{\nu-1/2}(\cos\theta)}\Bigg|_{\substack{\theta=\theta_o \\ \nu=\nu_i}} \tag{19}$$

$$\text{and } P_{2\theta} = \sum_{i=1}^{\infty} j^{\nu_i'} \frac{\nu_i'}{\nu_i'^2 - 1/4} \left. \frac{P^{-m}_{\nu_i' - 1/2}(\cos\theta)}{\frac{\partial^2 P^{-m}_{\nu - 1/2}(\cos\theta)}{\partial\nu\,\partial\theta}} \right|_{\substack{\theta = \theta_o \\ \nu = \nu_i'}} \left[\frac{\left(\nu_i' + \frac{1}{2}\right) J_{\nu_i'}(ka)}{ka} - J_{\nu_i'+1}(ka) \right] \tag{20}$$

$$E_\phi = \sum_{m=0}^{\infty} m \frac{V_o e^{-j(kr - \pi/4)}}{r\pi} \sqrt{2\pi ka} \cdot \frac{2ka \sin\theta_o \cos\left(\frac{m\pi}{2ka \sin\theta_o}\right)}{(ka \sin\theta_o)^2 - m^2} \sin m\phi \tag{21}$$

$$\cdot \left\{ \frac{-j}{\sin\theta} P_{1\phi} + \frac{1}{\sin\theta_o} P_{2\phi} \right\} \tag{22}$$

where

$$P_{1\phi} = \sum_{i=1}^{\infty} \frac{\nu_i}{\nu_i^2 - 1/4} j^{\nu_i} J_{\nu_i}(ka) \left. \frac{P^{-m}_{\nu_i - 1/2}(\cos\theta)}{\frac{\partial P^{-m}_{\nu - 1/2}(\cos\theta)}{\partial\nu}} \right|_{\substack{\theta = \theta_o \\ \nu = \nu_i}}$$

$$\text{and } P_{2\phi} = \sum_{i=1}^{\infty} \frac{\nu_i'}{\nu_i'^2 - 1/4} j^{\nu_i'} \left. \frac{\frac{\partial}{\partial\theta} P^{-m}_{\nu_i' - 1/2}(\cos\theta)}{\frac{\partial^2 P^{-m}_{\nu - 1/2}(\cos\theta)}{\partial\nu\,\partial\theta}} \right|_{\substack{\theta = \theta_o \\ \nu = \nu_i'}} \cdot \left[\frac{(\nu_i' + 1/2) J_{\nu_i'}(ka)}{ka} - J_{\nu_i'+1}(ka) \right] \tag{23}$$

It is pointed out that the θ-dependence is represented by the Legendre function $P_{\nu - 1/2}^{-m}(\cos\theta)$ instead of $P_\nu^m(\cos\theta)$ as originally derived. This choice simplifies the evaluation of the Legendre function in the digital computer and is preferred. Also, except for a constant factor of $1/\pi$, the expression for E_θ agrees with that reported by Pridmore-Brown and Stewart[4] derived by the Kontrorovitch-Lebedev transform method.

2.2 Radial Slot

A narrow slot of width 2 w≪circumference is assumed to be positioned along a generatrix of the cone and extends from r_1 to r_2 as shown in Figure 1. It is further assumed that the length of the slot, $(r_2 - r_1)$, is such as to allow definition of the ends of the slot by constant ϕ'. The slot is excited by a voltage V_o' resulting in an electric field in the ϕ-direction given by

$$E_\phi = V_o' \frac{g(r')\,\delta(\phi')}{r' \sin\theta_o}$$

The function g(r') describes the variation of the source excitation in the r' direction. Clearly, since $f_1(r', \phi') = 0$, i.e., no source excitation in the r'-direction, the TM mode of the potential function is not supported. The TE mode, on the other hand, is obtained only from the contribution of $f_2(r', \phi')$ in Equation (9). Substitution of Equation (24) into Equation (9) results in the following expression for Π^{TE} for the radial slot:

$$\underset{\sim}{\Pi}^{TE}(r) = \frac{V_o'}{\eta} \sum_{m=0}^{\infty} \sum_{i=1}^{\infty} \frac{(2\nu_i' + 1)\, P_{\nu_i'}^m(\cos\theta)\cos m\phi}{\sin\theta_o\, \pi(1+\delta_{om}) \dfrac{\partial^2 P_\nu^m(\cos\theta)}{\partial\nu\,\partial\theta}\Bigg|_{\substack{\theta=\theta_o \\ \nu=\nu_i'}}} \cdot \int_{r_1}^{r_2} \frac{g(r')}{r'} j_{\nu_i'}(kr'_<)\, h_{\nu_i'}^{(2)}(k r_>)\, d r' \tag{25}$$

The electric field components are obtained from Equation (2) operating on Equation (25) giving:

$$E_\theta = \frac{V_o' e^{-j(k r - \pi/4)}}{r \sin \theta_o} \sum_{m=1}^{\infty} j \sqrt{\frac{2}{\pi}} \; m \sin m\phi \; \frac{1}{\sin \theta} P_\theta \tag{26}$$

$$E_\phi = \frac{V_o' e^{-j(k r - \pi/4)}}{r \sin \theta_o} \sum_{m=0}^{\infty} j \sqrt{\frac{2}{\pi}} \; \frac{\cos m\phi}{(1 + \delta_{om})} P_\phi \tag{27}$$

where

$$P_\theta = \sum_{i=1}^{\infty} \nu_i' j^{\nu_i'} \frac{P_{\nu_i'}^{-m} - 1/2 (\cos \theta)}{\dfrac{\partial^2 P_{\nu - 1/2}^{-m}(\cos \theta)}{\partial \nu \, \partial \theta}} \Bigg|_{\substack{\theta = \theta_o \\ \nu = \nu_i'}} \cdot \int_{r_1}^{r_2} \frac{g(r')}{r'} \frac{J_{\nu_i'}(k r')}{\sqrt{k r'}} \, dr' \tag{28}$$

$$P_\phi = \sum_{i=1}^{\infty} \nu_i' j^{\nu_i'} \frac{\dfrac{\partial}{\partial \theta} P_{\nu_i'}^{-m} - 1/2 (\cos \theta)}{\dfrac{\partial^2 P_{\nu - 1/2}^{-m}(\cos \theta)}{\partial \nu \, \partial \theta}} \Bigg|_{\substack{\theta = \theta_o \\ \nu = \nu_i'}} \cdot \int_{r_1}^{r_2} \frac{g(r')}{r'} \frac{J_{\nu_i'}(k r')}{\sqrt{k r'}} \, dr' \tag{29}$$

and the ν_i' are the roots of the equation (30)

$$\frac{\partial P_{\nu - 1/2}^{-m}(\cos \theta_o)}{\partial \theta} = 0$$

3.0 COMPUTATIONAL PROCEDURES FOR SPECIAL FUNCTIONS

A brief description of the procedures used in the computation of some functions appearing in the far field expressions is given below.

3.1 Computation of Legendre Functions

From the expressions of the field components given in Section 2, it is seen that the calculation of radiation patterns requires the evaluation of the function $P_\nu^m(\cos\theta)$ and its derivatives with respect to ν and θ. As stated previously, we have chosen to work with the function $P_\nu^{-m}(\cos\theta)$ rather than $P_\nu^m(\cos\theta)$. The two functions are related by[8]

$$P_\nu^m(\cos\theta)\cos(m\pi) = \frac{\Gamma(\nu+m+1)}{\Gamma(\nu-m+1)} P_\nu^{-m}(\cos\theta) \tag{31}$$

where $\Gamma(k)$ is Euler's gamma function. Using the above relationship, it is easy to show that the ratio

$$\frac{\frac{\partial}{\partial\theta} P_\nu^m(\cos\theta)}{\frac{\partial}{\partial\nu} P_\nu^m(\cos\theta_o)}$$

can be replaced by

$$\frac{\frac{\partial}{\partial\theta} P_\nu^{-m}(\cos\theta)}{\frac{\partial}{\partial\nu} P_\nu^{-m}(\cos\theta_o)}$$

in the expression of the functions Π^{TM} and Π^{TE}. From equation (31) it is also evident that the roots of $P_\nu^m(\cos\theta_o)$ are also roots of $P_\nu^{-m}(\cos\theta_o)$. The same holds true for the derivatives of the two functions with respect to θ. Derivatives of the Legendre Functions with respect to θ are computed by the recurrence formula[9]

$$\frac{d}{d\theta} P_\nu^m(\cos\theta) = m \frac{\cos\theta}{\sin\theta} P_\nu^m(\cos\theta) + P_\nu^{m+1}(\cos\theta) \qquad (32)$$

The derivatives $\frac{d}{d\nu} P_\nu^m$ are computed numerically using the formula[10]

$$\frac{d}{d\nu} f(\nu_i) = \frac{1}{12h} \left\{ f(\nu_o) - 8 f(\nu_1) + 8 f(\nu_2) - f(\nu_3) \right\}$$

where $\nu_i = \nu_o + i\,h$, h is a selected increment in ν, and $f(\nu_i)$ are the values of the Legendre functions of order m and degree ν_i, $P_{\nu_i}^m(\cos\theta)$.

Thus far we have given expressions for computing the various derivatives of the Legendre functions in terms of the functions themselves. The computations of these functions, however, require extreme care, as valid approximations must be used for the different ranges of the variables θ and ν. For relatively small values of θ such that $\theta < \frac{9}{72+2m}$ where θ is expressed in radians, the formula[11]

$$P_\nu^{-m}(\cos\theta) = \left(\frac{1 - \cos\theta}{1 + \cos\theta}\right)^{\frac{m}{2}} \sum_{n=o}^{\infty} (-1)^n \frac{\Gamma(\nu + n + 1)}{\Gamma(\nu - n + 1)\,\Gamma(m+n+1)} \frac{(\frac{1}{2} - \frac{1}{2}\cos\theta)^n}{n!} \qquad (33)$$

is suitable for computations. As before, $\Gamma(k)$ is the usual Euler's gamma function. The computation of $P_\nu^m(\cos\theta)$ is then obtained from Equation (31). However, for ν large, ($\nu > 100$), the ratio $\frac{\Gamma(\nu + m + 1)}{\Gamma(\nu - m + 1)}$ is replaced by its limiting value ν^{2m}.

For large values of θ such that $\theta \geq \frac{9}{72+2m}$ we use the expansion[12]

$$P_\nu^{-m}(\cos\theta) = \sqrt{\frac{2}{\pi \sin\theta}}\, \Gamma(\nu - m + 1) \sum_{k=o}^{\infty} (-1)^k \frac{(1/2 + m)_k\, (1/2 - m)_k}{k!\, (2\sin\theta)^k\, (\nu + 3/2)_k}$$

$$\sin\left[(\nu + k + 1/2)\,\theta + \pi\,(1/2\,k + 1/2\,m + 1/4)\right] \qquad (34)$$

where $(b)_k = \frac{\Gamma(b+k)}{\Gamma(b)}$. The above expansion gives satisfactory results for all values of ν and $\frac{\pi}{6} < \theta < 5\frac{\pi}{6}$. For θ outside this range, the series is asymptotic and its accuracy depends on the value of ν. This last expression

is used for numerical computations in the neighborhood of $\nu = 70 + 2m$ and the desired functions are obtained through backward recursion.

3.2 Computation of Spherical Bessel Functions

The computation of the fields involves the spherical Bessel function $j_\nu(x)$ and the spherical Hankel function $h_\nu^{(2)}(x)$. Since these functions are related to corresponding cylindrical functions by Equations (5) and (6), the cylindrical functions are computed instead. For the Hankel function, $H_\nu^{(2)}(x)$, the asymptotic expansion, Equation (16), has been used.

In the accompanying computer program, Appendix A, the Bessel functions are computed in DOUBLE PRECISION using computer system library routines. If such library routines are not available or accessible, high speed computational subroutines for these functions may be written from appropriate approximations. These approximations are given in Appendix C.

The computation of the radiation field from a slot along a generator of the conical surface requires the evaluation of the integral

$$\int_{r_1}^{r_2} \frac{g(r)}{r} \frac{J_\nu(k r)}{\sqrt{k r}} \, d r \quad .$$

A series solution of the indicated integral when $g(r')$ is a polynomial in r' is obtained from the formula [13]

$$\int_0^z t^\mu J_\nu(t)\, dt = \frac{z^\mu \, \Gamma\left(\frac{\nu+\mu+1}{2}\right)}{\Gamma\left(\frac{\nu-\mu+1}{2}\right)} \sum_{k=0}^{\infty} (\nu + 2k + 1) \frac{\Gamma\left(\frac{\nu-\mu+1}{2} + k\right)}{\Gamma\left(\frac{\nu+\mu+3}{2} + k\right)} J_{\nu+2k+1}(z)$$

with Real part $(\mu + \nu + 1) > 0$. Alternatively, the indicated integral may be evaluated with sufficient accuracy by known numerical integration techniques. The latter method, using Simpson's "3/8 Rule", has been chosen for the present program. Either method, however, requires the evaluation of the Bessel function $J_\nu(x)$.

4.0 ANALYSIS OF COMPUTED ELEMENT PATTERNS FOR SLOTS ON A CONE

The convergence of the modal series representing the far fields of the circumferential and radial slots was examined by looking at the pattern change in the sequential summation of higher order modes. In each case, patterns were calculated for every 10° in azimuth and every 5° in elevation for both the θ-polarization and the ϕ-polarization. However, elevation cuts were plotted only at $\phi = 0^{\circ}$ and $\phi = 180$ degrees. These two cuts have been plotted on an extended θ scale to give a single view of the elevation cut. Since the cone under study has a 10° half angle, the position of $\theta = 80^{\circ}$ was selected for azimuthal cuts. This corresponds to the broadside of the conical surface. Figure 1 shows the relative position of slots in the coordinate system.

The patterns to be shown subsequently have been normalized to the largest value computed for both polarizations for the particular modal sum or individual mode. For convenience, we shall refer to the individual mode patterns by the small letter "m" and to the sum patterns by the capital letter "M".

4.1 RADIATION PATTERNS OF CIRCUMFERENTIAL SLOTS

A slot of azimuthal length $d = \lambda/2$ located at $ka = 39$ radians$(k = 2\pi/\lambda)$ from the tip of the 10° half angle cone was selected for pattern computations. This particular location was selected because it corresponds to a case of a circumferential slot at 8.15 GHz and 9 inches from the cone tip previously investigated experimentally.[17] The computed results will be compared with the available experimental results where appropriate. The slot is assumed to be excited by a voltage across its center and has a resulting field across it in the r direction given by Equation (12). Near the tip of the cone this excitation function may be represented by a few terms of a cosine series with appropriate coefficients. A greater number of terms are required for adequate representation of the same function when the slot is located many wavelengths away from the tip. It will be seen later that there

is a correlation between the number of expansion terms in the excitation function and the number of terms required for convergence of the modal series representing the fields. However, this correlation is not easily determined beforehand. The dominant TE_{10} mode of a rectangular waveguide may be used to excite the slot.

Figures 2 and 3 show the θ-polarized pattern of the lowest two modes, m = 0 and m = 1, respectively, for $\phi = 0^{\circ}$ and $\phi = 180^{\circ}$. As expected, the modal patterns for $\phi = 180^{\circ}$ are identical to the $\phi = 0^{\circ}$ patterns, since the variation of the fields in the ϕ-direction is purely sinusoidal. The pattern corresponding to the m = 0 mode shows significant variation at broadside with extrema at $\theta = 0^{\circ}$ and $\theta = \theta_o = 170$ degrees. The peaks at $\theta = 12^{\circ}$ and $\theta = 30^{\circ}$ of this particular mode are particularly noteworthy. In contrast to the m = 0 mode pattern, the m = 1 mode pattern of Figure 3 exhibits a relatively small and smooth variation at the broadside region. The maximum now occurs at $\theta = 0^{\circ}$ with a pronounced first minimum at $\theta = 15^{\circ}$ followed by a local maximum at $\theta = 25$ degrees. Also, the pattern is about 1 dB down at $\theta = \theta_o$.

The total or sum θ-polarized pattern of the first two modes, M = 1, is also shown in Figure 2 for $\phi = 0^{\circ}$ and for $\phi = 180^{\circ}$ together with the M = 2 pattern. The addition of the second mode, m = 1, to the first mode, in effect dominates the resulting pattern. The effect of the m = 0 mode, however, is still evident in the region near the cone axis with a -3.5 dB value at $\theta = 1$ degree. The forward-back difference varies from 1 dB at $\theta = 1^{\circ}$ to 9 dB at $\theta = 80^{\circ}$ and to 14 dB at $\theta = \theta_o$.

Higher order mode sum patterns, M = 3 through M = 5, for both $\phi = 0^{\circ}$ and $\phi = 180^{\circ}$ are shown in Figure 4. In each case, the sequential summation of a higher order mode in the sum series effectively decreases the variation at the broadside region with the average level of the $\phi = 0^{\circ}$ patterns at -9 dB for M = 2 and -4 dB for M = 4. Addition of the m = 5 mode raises the pattern level only slightly at broadside while in the vicinity of $\theta = 40^{\circ}$ and $\theta = 150^{\circ}$ changes of about -1.5 dB are noted. The next significant changes in the pattern are seen in the M = 7 modal sum shown in Figure 5 for $\phi = 0^{\circ}$. At the same time, the $\phi = 180^{\circ}$ pattern shows that the pattern level decreases with increased modes at the broadside region while maintaining the level of about -5.5 dB and -15.5 dB at $\theta = 1^{\circ}$ and $\theta = \theta_o$, respectively.

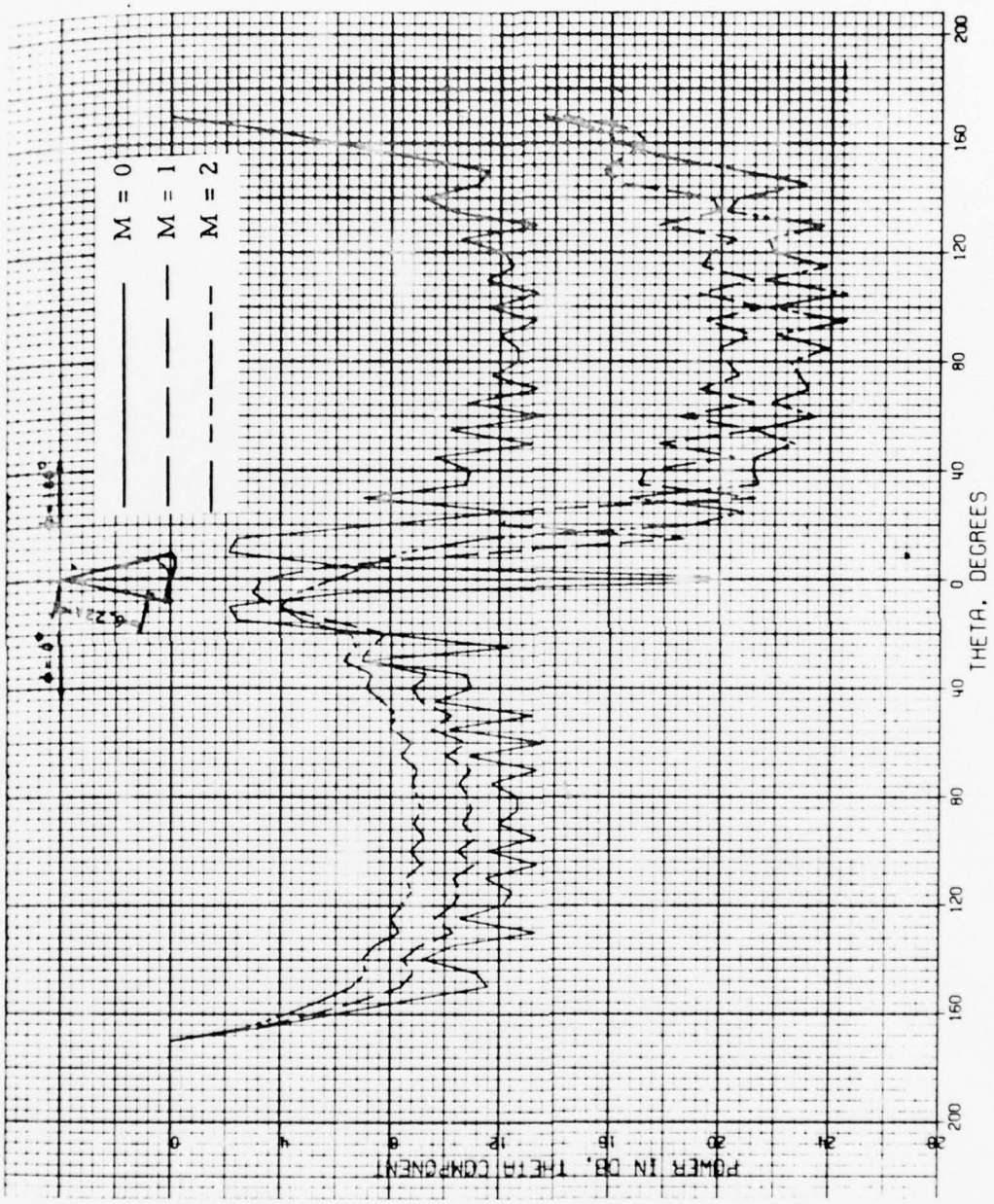

Figure 2. θ-Polarized Total Patterns of λ/2 Circumferential Slot for $\phi = 0^{o}$, $\phi = 180^{o}$, M = 0, 1, and 2

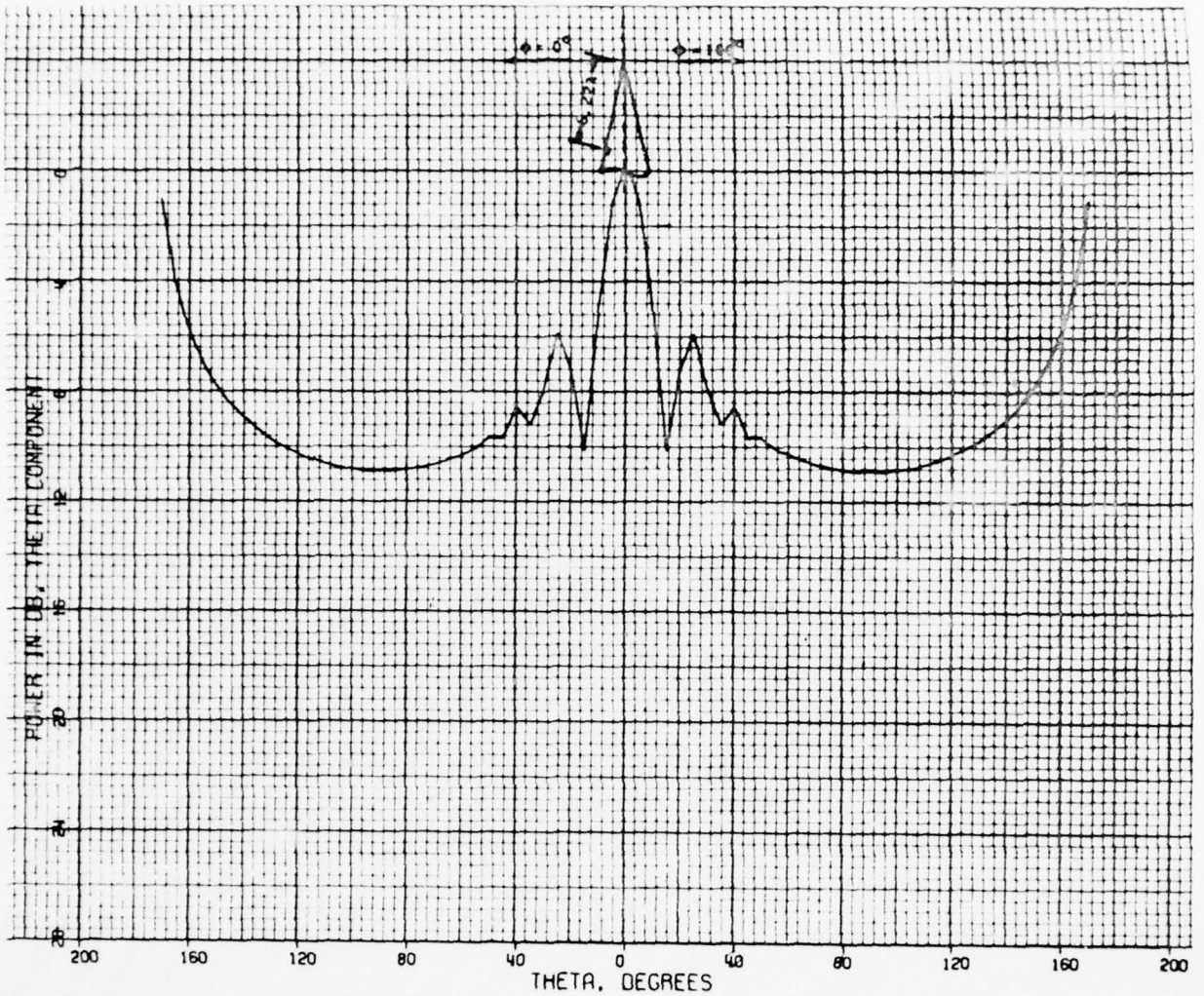

Figure 3. θ-Polarized Modal Pattern of $\lambda/2$ Circumferential Slot for m = 1, $\phi = 0^{o}$, $\phi = 180^{o}$

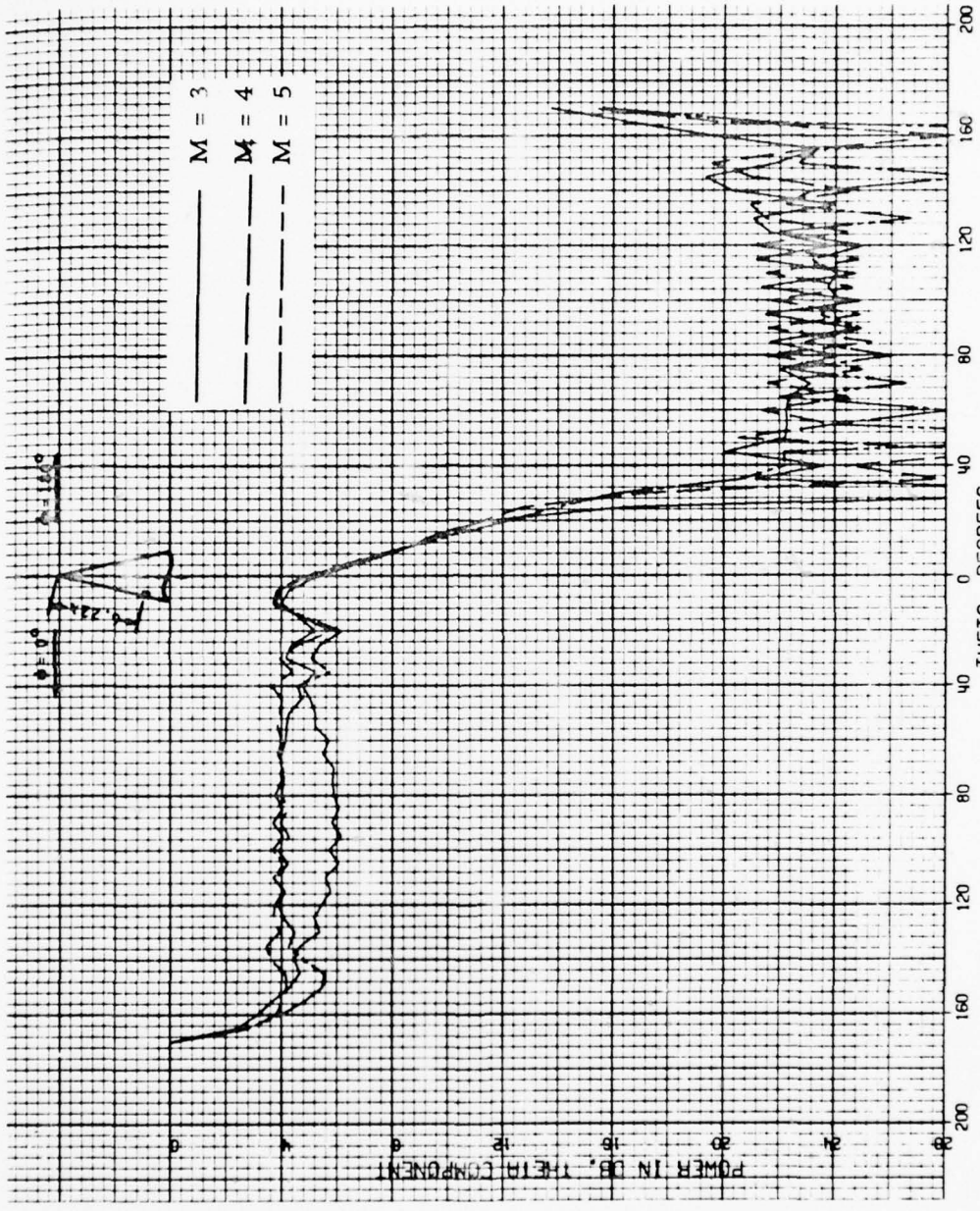

Figure 4. θ-Polarized Total Patterns of /2 Circumferential Slot for $\phi = 0^{o}$, $\phi = 180^{o}$, M = 3, 4 and 5

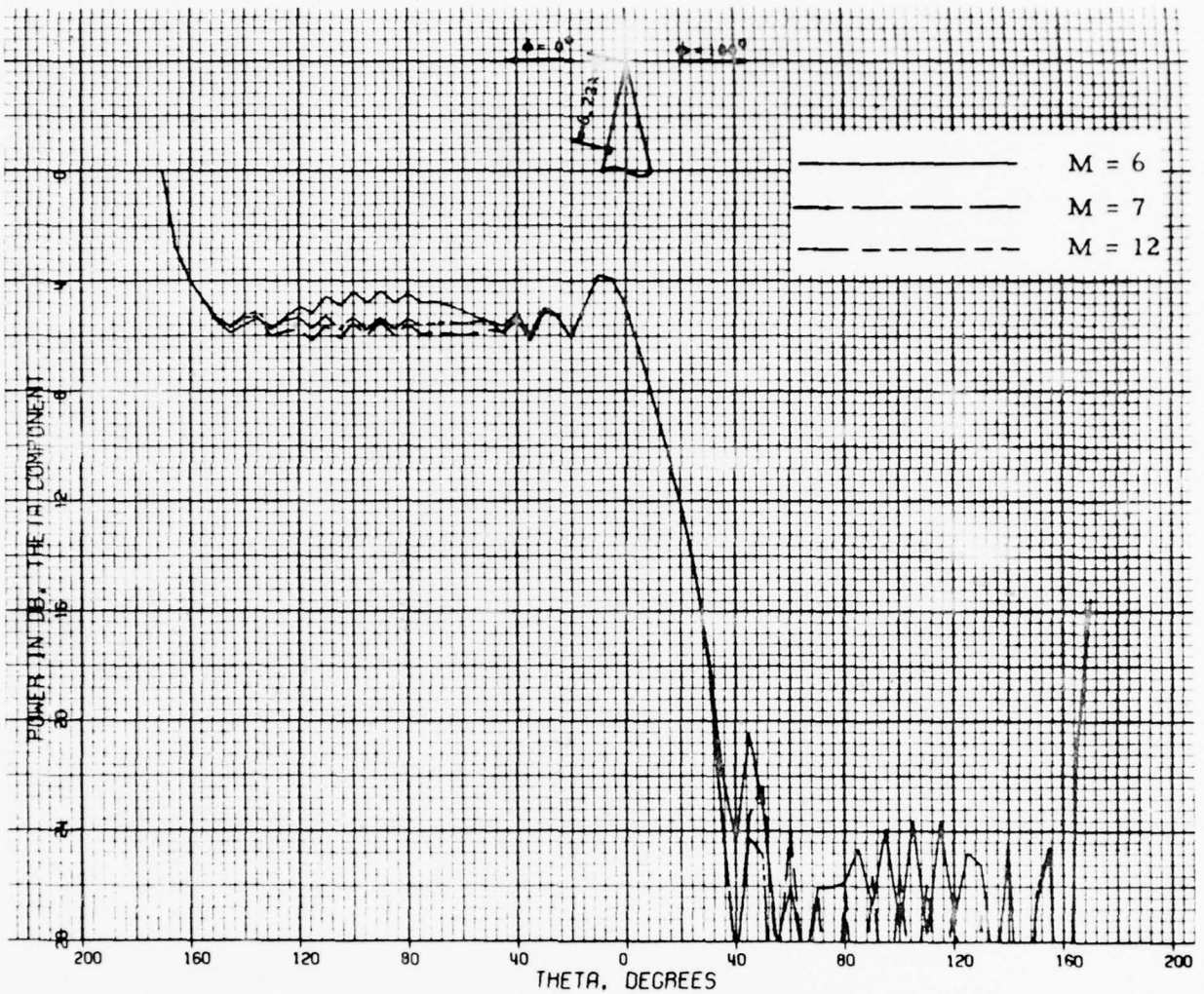

Figure 5. θ-Polarized Total Pattern of λ/2 Circumferential Slot for $\phi = 0^{o}$, $\phi = 180^{o}$, M = 6, 7, and 12

The addition of the next five modes, m = 8 through m = 12, to the M = 7 total pattern gives the total pattern of M = 12. The patterns for this case are also shown in Figure 5. Comparison of this pattern with the M = 7 total pattern shows that the addition of these five modes results in a decrease of the pattern level of less than .4 dB in the range of $\theta = 40^{\circ}$ to $\theta = 140$ degrees. Similarly, the $\phi = 180^{\circ}$ pattern for this case shows only a slight decrease in the same range. There is no significant change to either pattern outside this range.

Azimuthal patterns for the broadside angle $\theta = 80^{\circ}$ were plotted for both θ- and ϕ-polarizations. These are shown in Figures 6 through 8 for the θ-polarization and in Figure 9 for the ϕ-polarization. From Figures 6 and 7 it is seen that the θ-polarized pattern changes considerably with the addition of higher order mode almost at all azimuth angles. The M = 7, θ-polarized pattern, however, Figure 8, is down -5.8 dB at $\phi = 0^{\circ}$ and decreases almost monotonically to about -26 dB at $\phi = 100^{\circ}$ and remains below that level for the remaining azimuthal region. The M = 7, ϕ-polarized pattern is below -23 dB for all azimuth angles, Figure 9. Smoother patterns are observed in both polarizations of the M = 12 case as compared to corresponding pattern of the M = 7 case.

To study further the effects of the higher order modes to the total pattern, the m = 13 mode was added to M = 12 pattern. The resulting M = 13 sum pattern in elevation is shown in Figure 10. The azimuthal patterns for the M = 13 case have been included in Figures 11 and 12. It is seen that there are no noticeable changes in either the elevation or the azimuthal patterns with the addition of the m = 13 mode. It should be pointed out, however, that the normalized θ-polarized pattern of the m = 13 mode, has its maximum at $\theta = 90$ degrees rather than at broadside. This is a consequence of the θ-dependence of the associated Legendre functions and their derivatives. This also explains why only the broadside range of the pattern is changed with increased higher order modes.

The measured E-plane pattern of the circumferential slot fed from a half-height X-band waveguide is shown in Figure 13 together with the M = 12 computed pattern. The two patterns agree very well near the cone tip and for the broadside region where both patterns are quite uniform. The

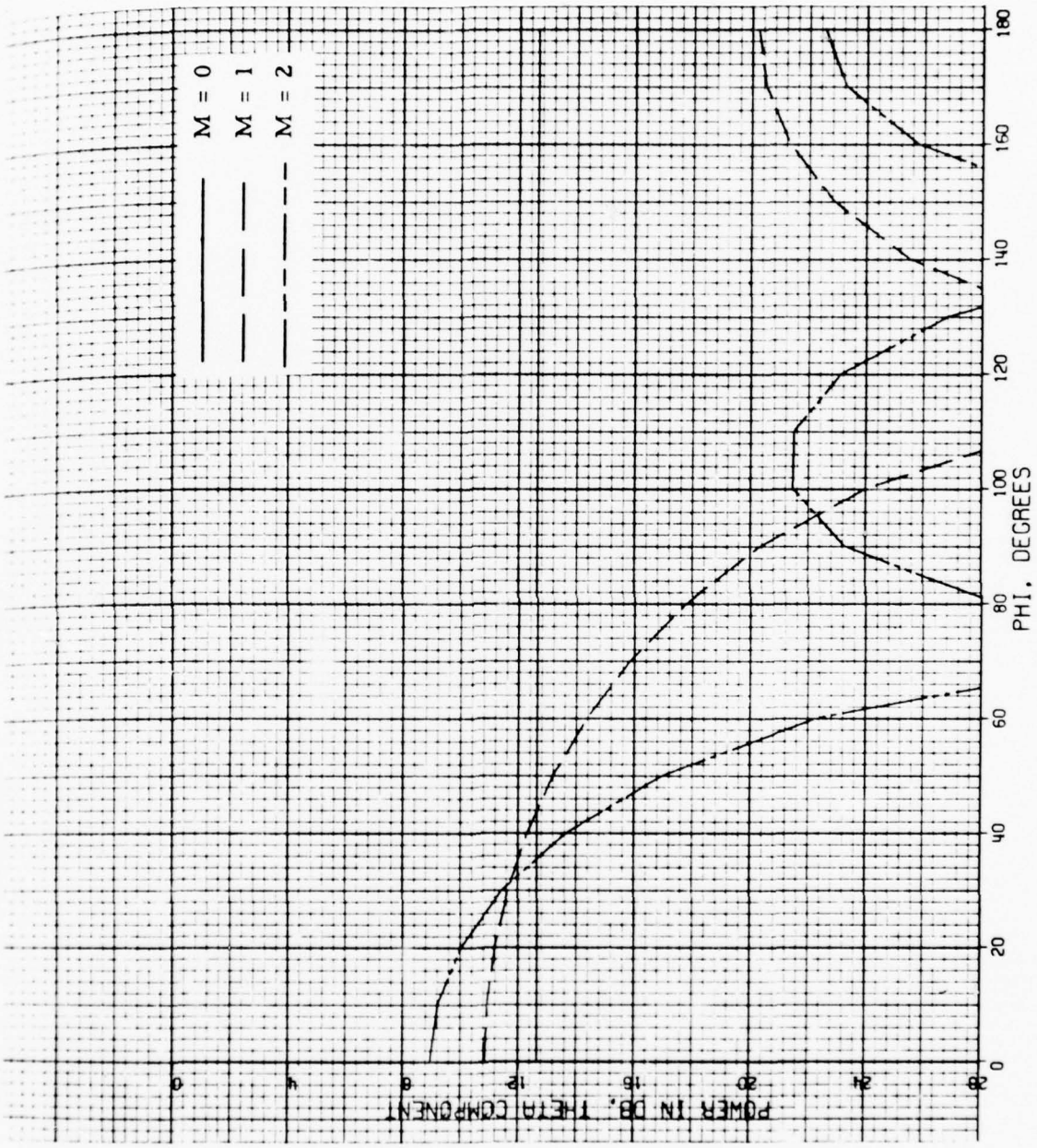

Figure 6. θ-Polarized Total Patterns of $\lambda/2$ Circumferential Slot for $\theta = 80^{\circ}$, M = 0, 1, and 2

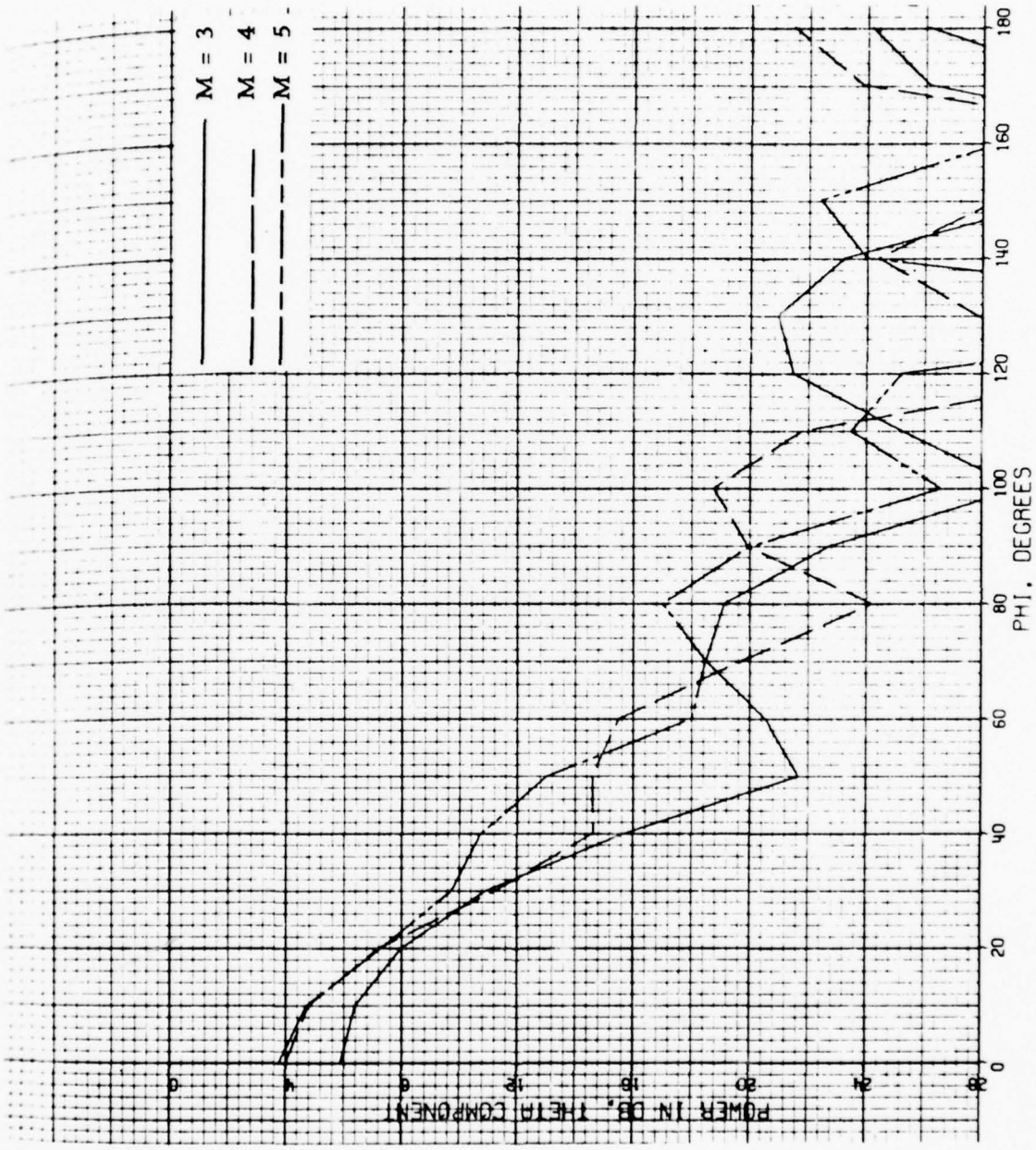

Figure 7. θ-Polarized Total Patterns of λ/2 Circumferential Slot for $\theta = 80°$, M = 3, 4, and 5

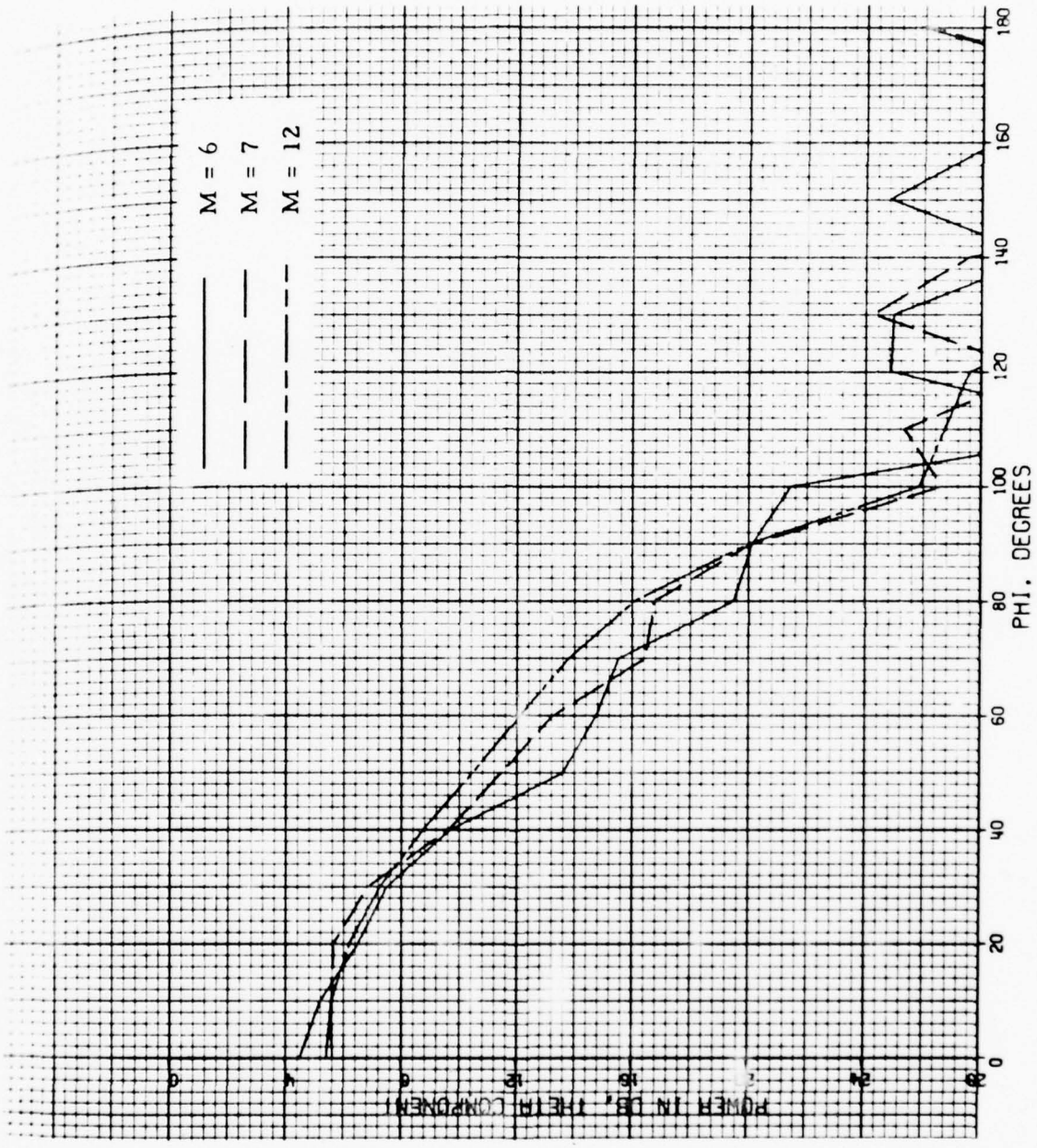

Figure 8. θ-Polarized Total Patterns of λ/2 Circumferential Slot for $\theta = 80^{\circ}$, M = 6, 7, and 12

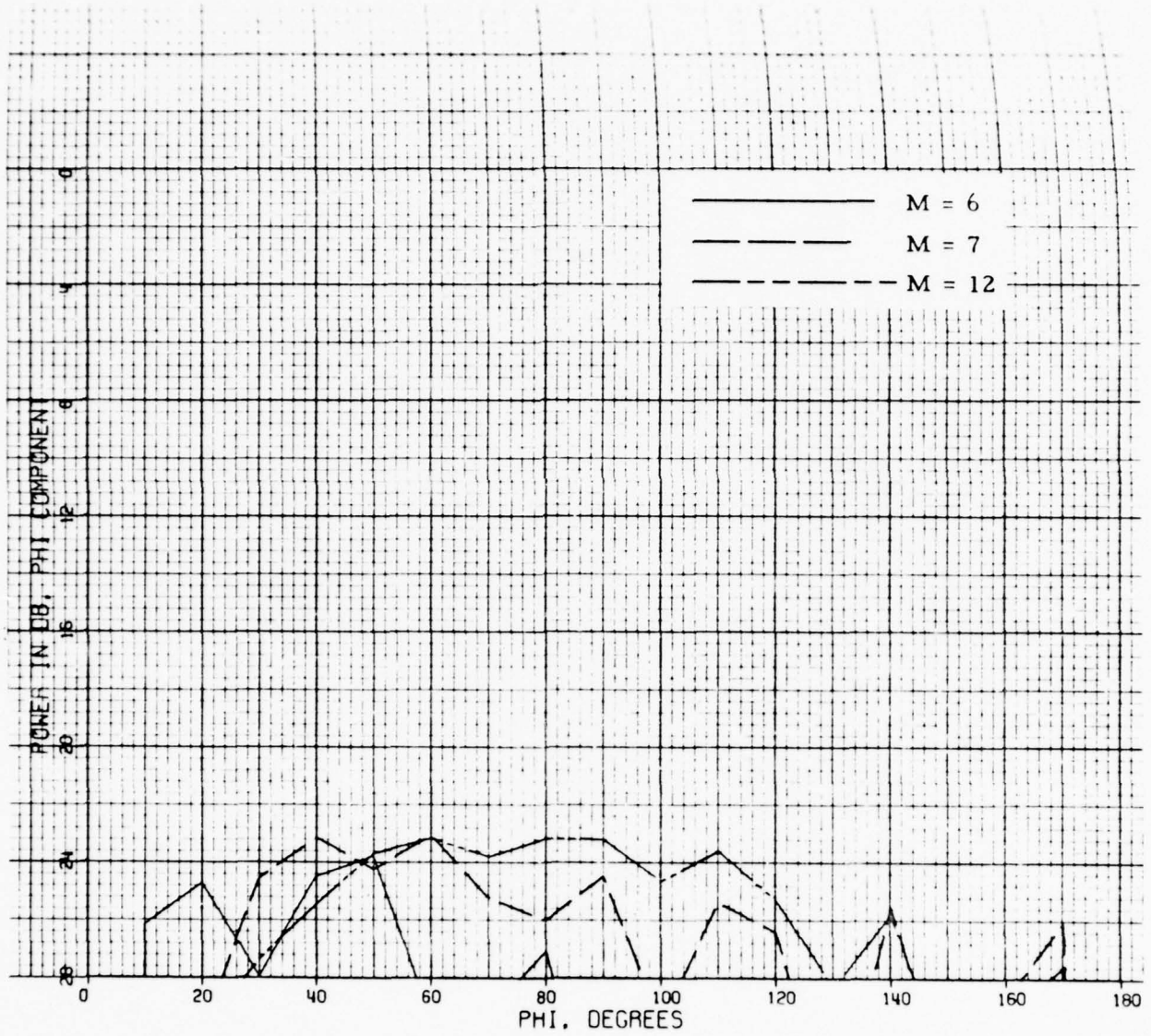

Figure 9. ϕ-Polarized Total Patterns of $\lambda/2$ Circumferential Slot for $\theta = 80^{\circ}$, M = 6, 7, and 12

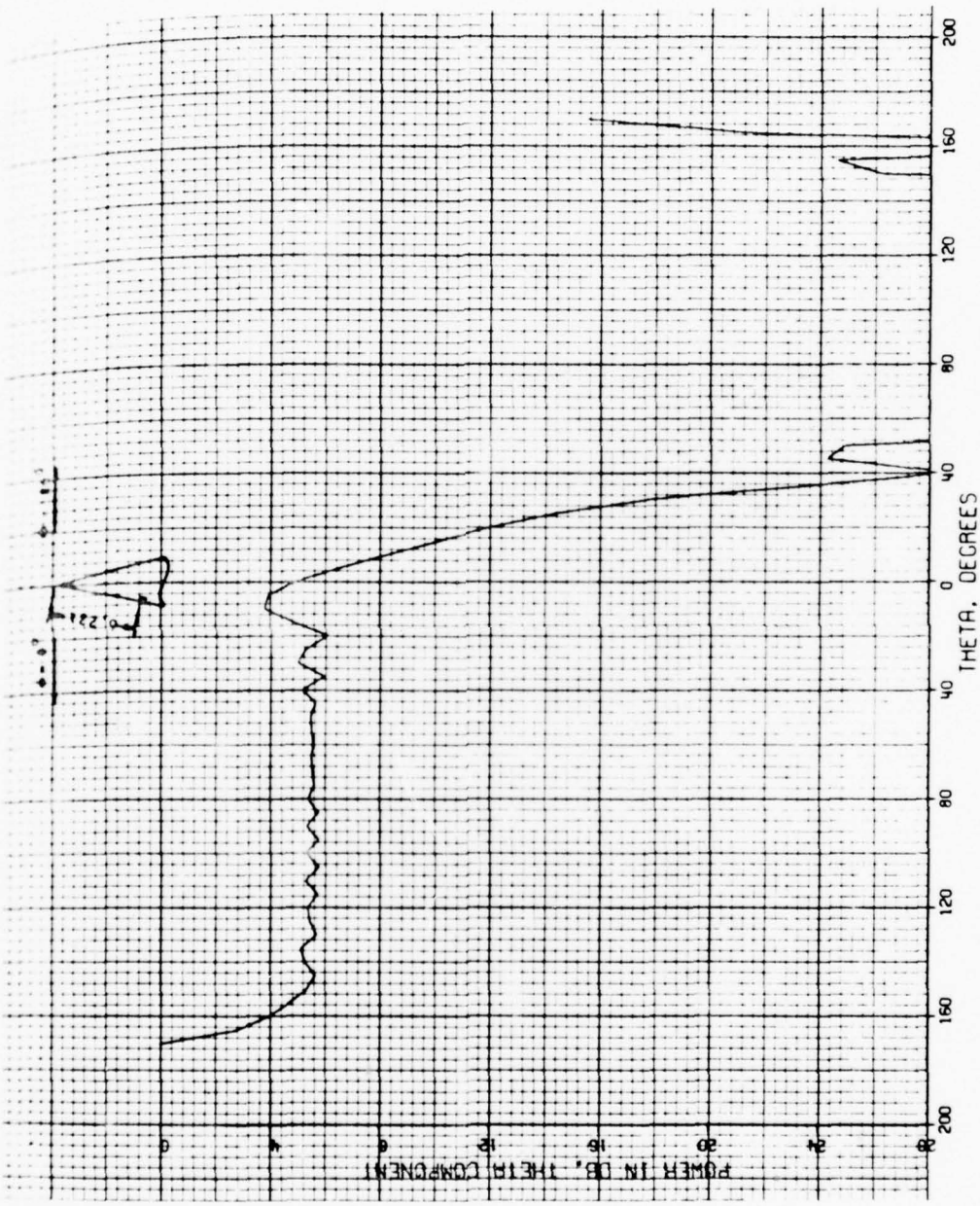

Figure 10. θ-Polarized Total Patterns of λ/2 Circumferential Slot for $\phi = 0^{o}$, $\phi = 180^{o}$, M = 13

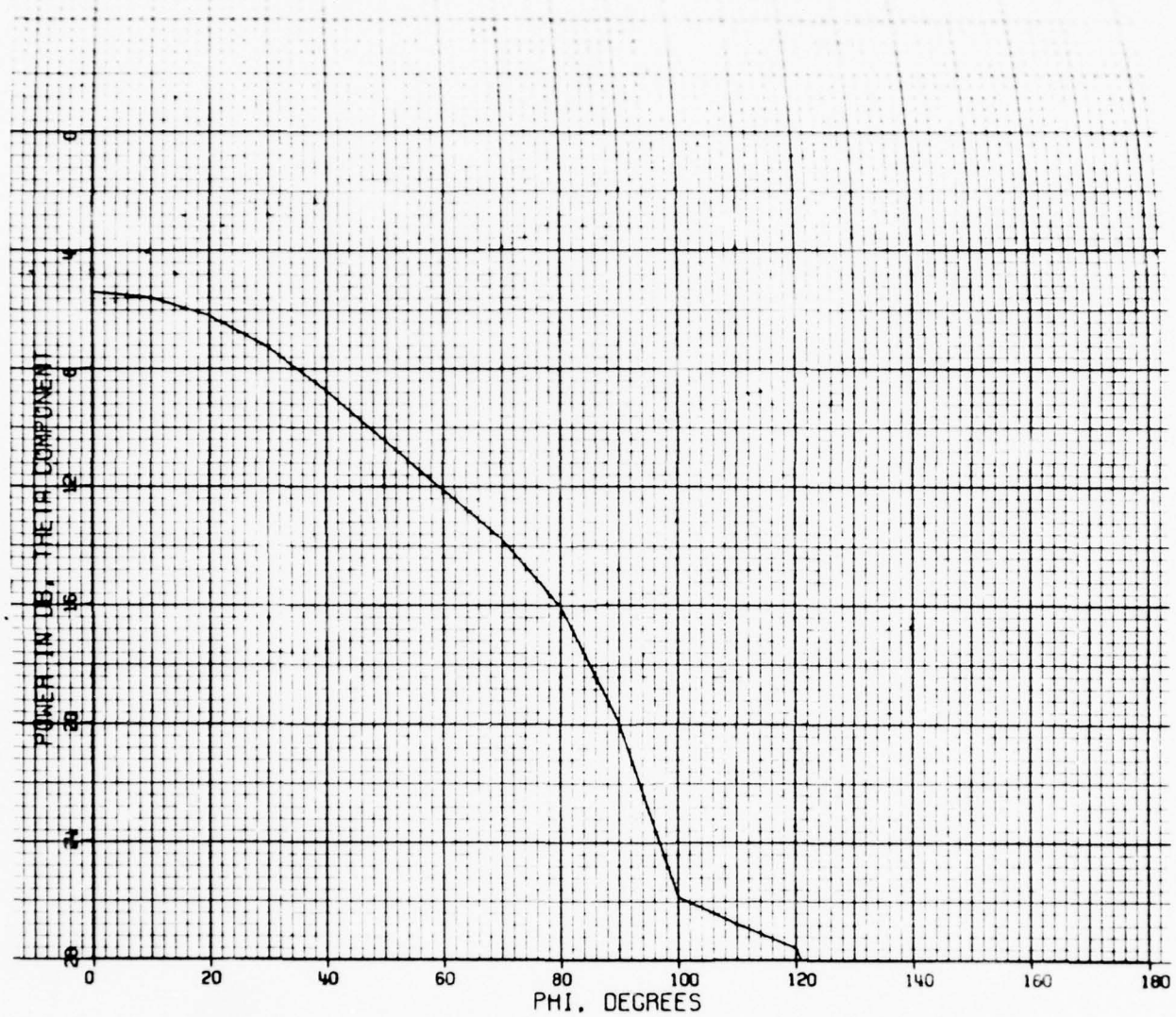

Figure 11. θ-Polarized Total Pattern of $\lambda/2$ Circumferential Slot for $\theta = 80^{\circ}$, M = 13

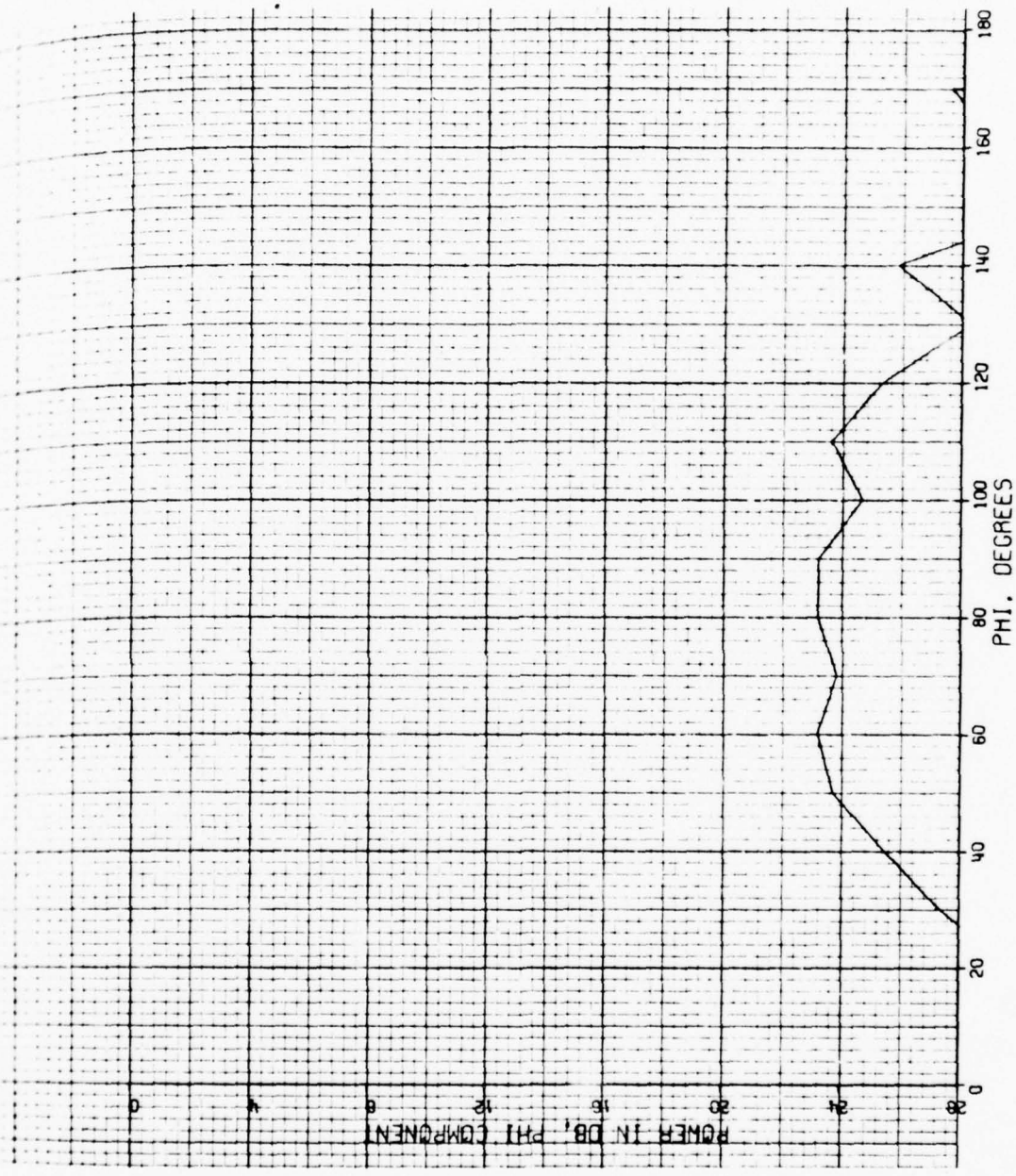

Figure 12. ϕ-Polarized Total Pattern of $\lambda/2$ Circumferential Slot for $\theta = 80^{o}$, M = 13

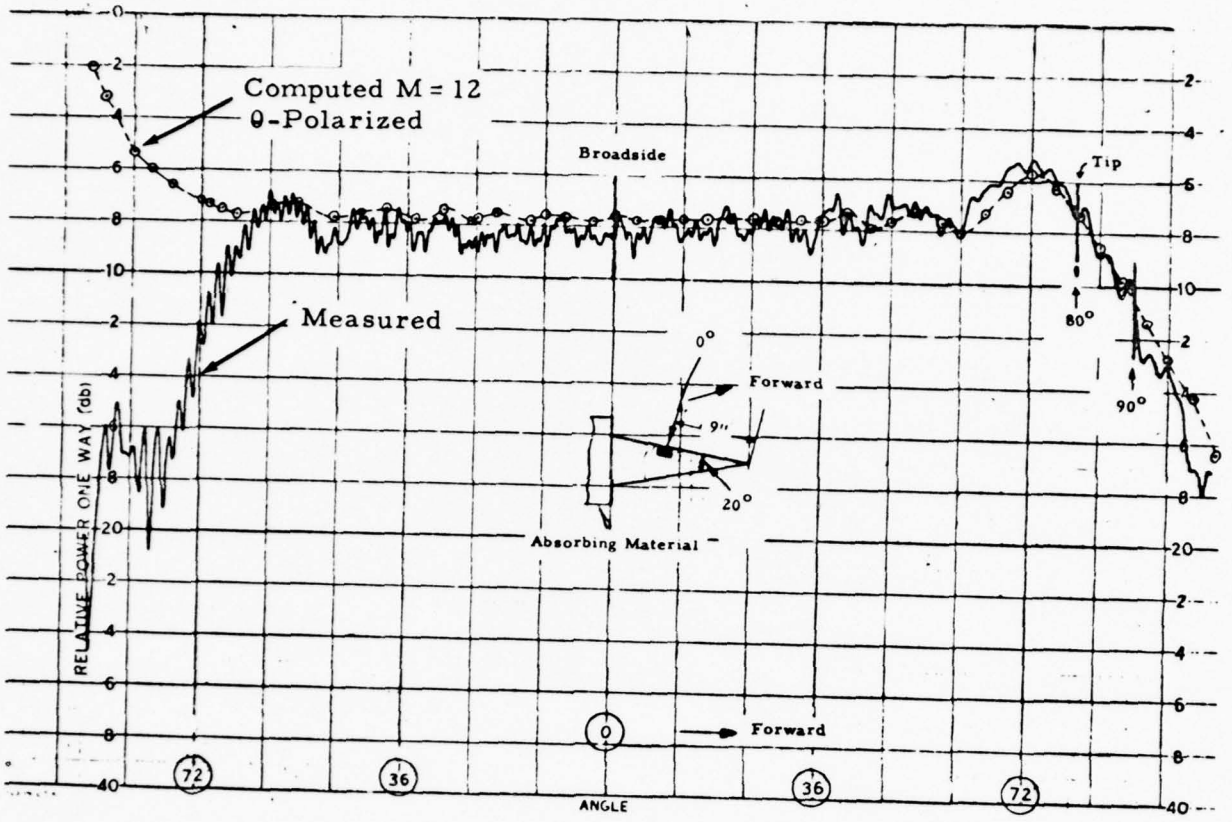

Figure 13. Measured and Computed (M = 12) θ-Polarized Pattern of Circumferential Slot on 20° Cone, f = 8.15 GHz

measured pattern drop off to the rear is a consequence of shadowing at the base of the cone by the absorbant material in which the cone was set. Thus, it is concluded that about 13 terms of the modal series are required to correctly represent the radiation from this slot configuration. Furthermore, the tip diffraction effects are generally accounted by the lower order modes of the series.

Elevation patterns were also computed for a similar slot located at ka = 30 radians from the tip of the cone. These three patterns corresponding to M = 4, M = 5 and M = 6 are shown in Figure 14. It is pointed out that the two cuts shown here are for $\phi = 0^{\circ}$ and $\phi = 90^{\circ}$. Although additional modes are required to describe the radiation characteristics of this case adequately, the figures do shown the effect of tip diffraction as the slot is moved along a generatrix of the cone. The first minimum of the $\phi = 0^{\circ}$ patterns now occurs at $\theta = 25^{\circ}$ from the tip of the cone as compared to $\theta = 20^{\circ}$ for the ka = 39 position (Figure 5).

4.2 RADIATION PATTERNS OF A RADIAL SLOT

In the present section we consider the narrow slot along a generatrix of the cone which was described in Section 2.2. For the present study the length of the slot has been chosen as one-half wavelength at the operating frequency. The cone characteristics and the operating frequency, as well as the location of the center of the slot remain the same as for the circumferential slot described in Section 4.1. The slot is excited by a voltage V_o' resulting in an electric field in the ϕ-direction given by

$$E_{\phi} = V_o' \frac{\cos (kr' - ka)}{r' \sin \theta_o} \delta (\phi')$$

It is interesting to follow the convergence of the modal series of the radial slot in the same manner that was done for the circumferential slot. We first look at the m = 0 and m = 1 mode patterns of the ϕ-polarized components at $\phi = 0^{\circ}$ depicted in Figures 15 and 16. The effect of the cone's tip on the modal patterns is clearly seen by the behavior of the patterns near the axis of the cone. This effect continues

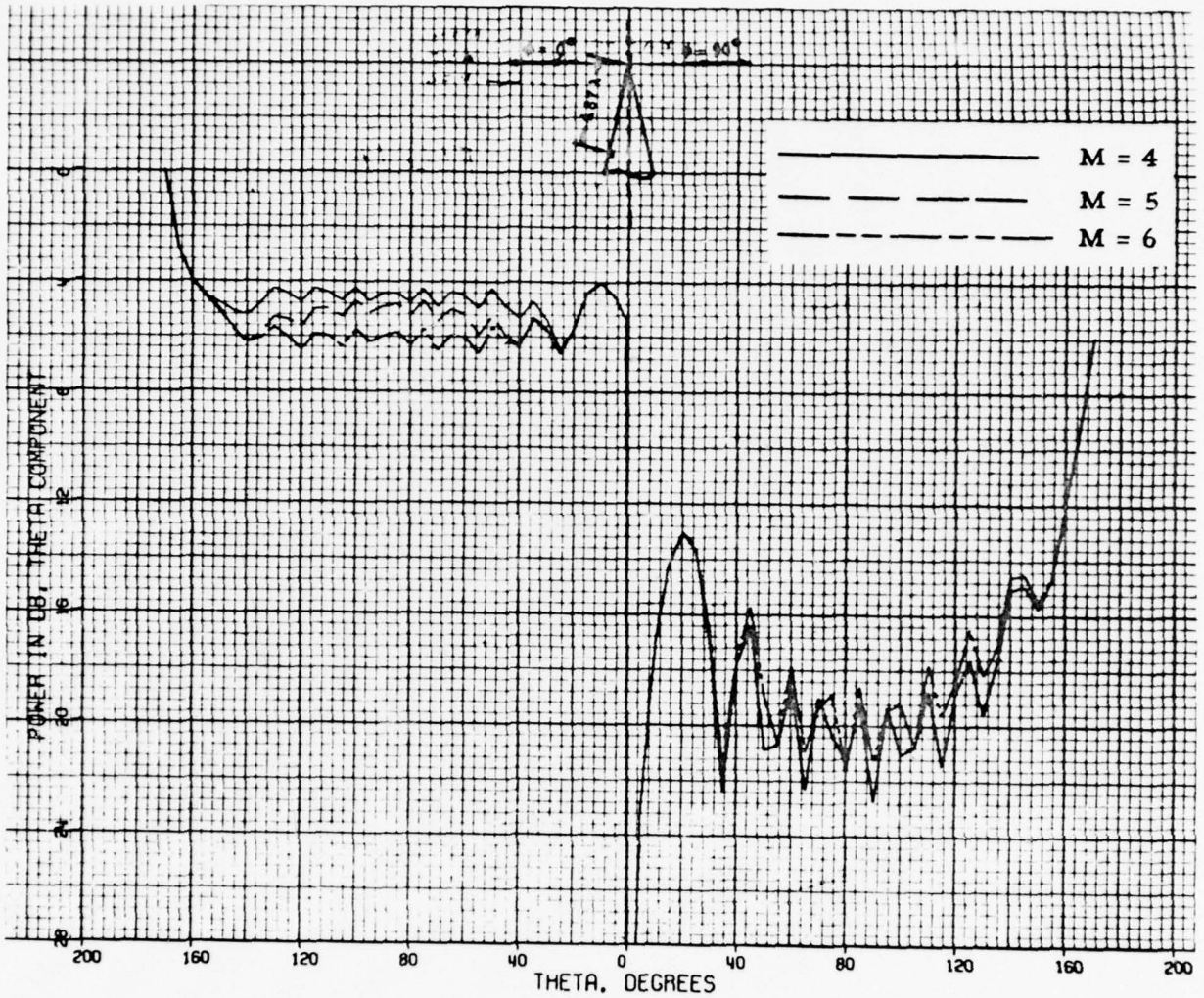

Figure 14. θ-Polarized Total Patterns of λ/2 Circumferential Slot for $\phi = 0^{\circ}$, $\phi = 90^{\circ}$, M = 4, 5, 6, and ka = 30

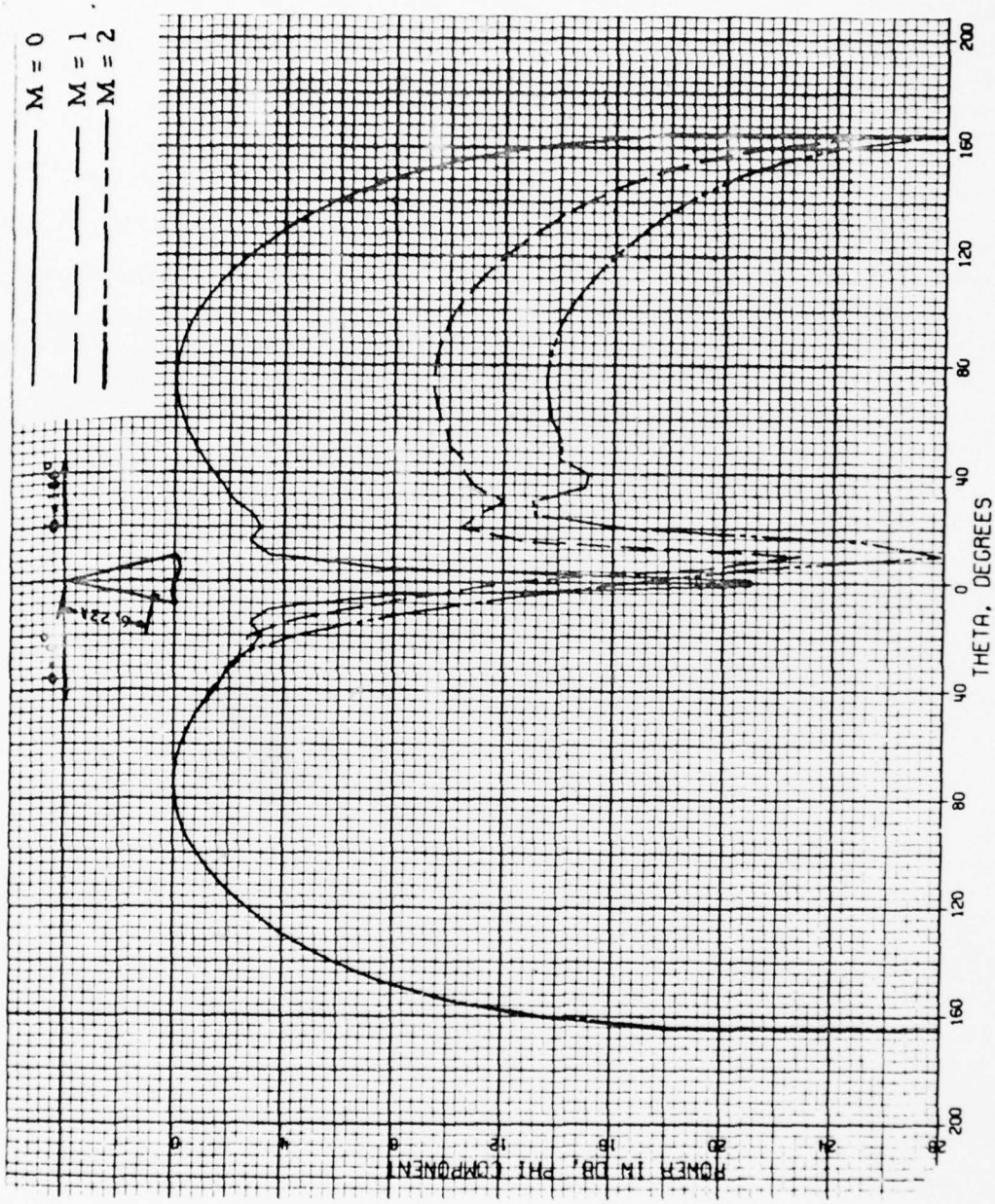

Figure 15. ϕ-Polarized Total Patterns of $\lambda/2$ Radial Slot for $\phi = 0^{o}$, $\phi = 180^{o}$, M = 0, 1, and 2

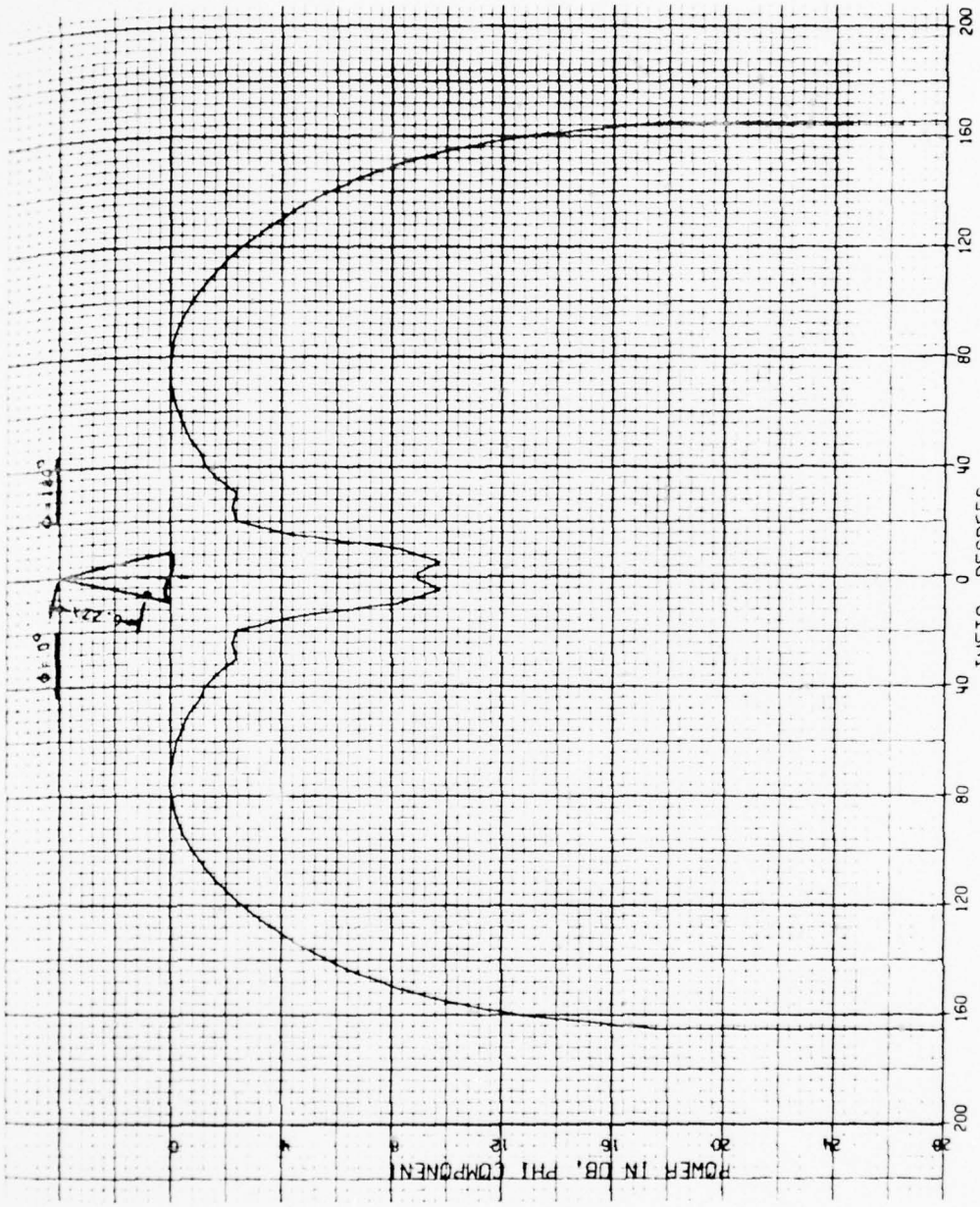

Figure 16. ϕ-Polarized Modal Pattern of $\lambda/2$ Radial Slot for $\phi = 0^{o}$, $\phi = 180^{o}$, m = 1

to persist also in the total patterns of M = 1 through M = 5, shown in Figures 15 and 17. It is evident from the Figures that the total patterns are dominated by the m = 1 mode. Both the patterns for $\phi = 0^{\circ}$ and $\phi = 180^{\circ}$ exhibit a local maximum at about 20 degrees from the axis. This maximum moves toward the broadside region with increased number of terms of the modal series. Also, the higher order total patterns are increasingly narrower. The higher order patterns of M = 6, 7, and 12 are shown in Figure 18.

The M = 12 for $\phi = 0^{\circ}$ pattern shows a minimum of -18 dB at $\theta = 1^{\circ}$ and has its maximum at exactly broadside. The pattern for $\phi = 180^{\circ}$ of the same case dips to a minimum near $\theta = 15^{\circ}$ and then increases to about -14 dB at θ = 100 degrees. Both patterns decrease rapidly near $\theta = \theta_{o}$. The irregularities noticed in all the previous total patterns are not present at all in the M = 12 patterns.

Azimuth patterns for the ϕ-polarized component and the θ-polarized component for the radial slot are shown by Figures 19 through 23. As it is seen from the Figures, all of the low order sum patterns for both polarizations exhibit considerable variation in azimuth. This can be viewed as an indication of the slow convergence of the modal series and the requirement for additional terms in the series representation. On the other hand, the M = 12, ϕ-polarized total pattern shows a smooth transition from 0 dB at $\phi = 0^{\circ}$ to -13 dB at $\phi = 140^{\circ}$ while maximum of the θ-polarized pattern occurs near broadside at about -17 dB.

From the above considerations, it appears that more than eight but less than fourteen terms of the modal series are required to represent the fields of this slot configuration correctly. The upper limit was further checked by looking at the M = 13 patterns and comparing them with the M = 12 patterns. These patterns are shown in Figures 24 through 26. There were no noticeable changes in either the elevation or the azimuthal patterns.

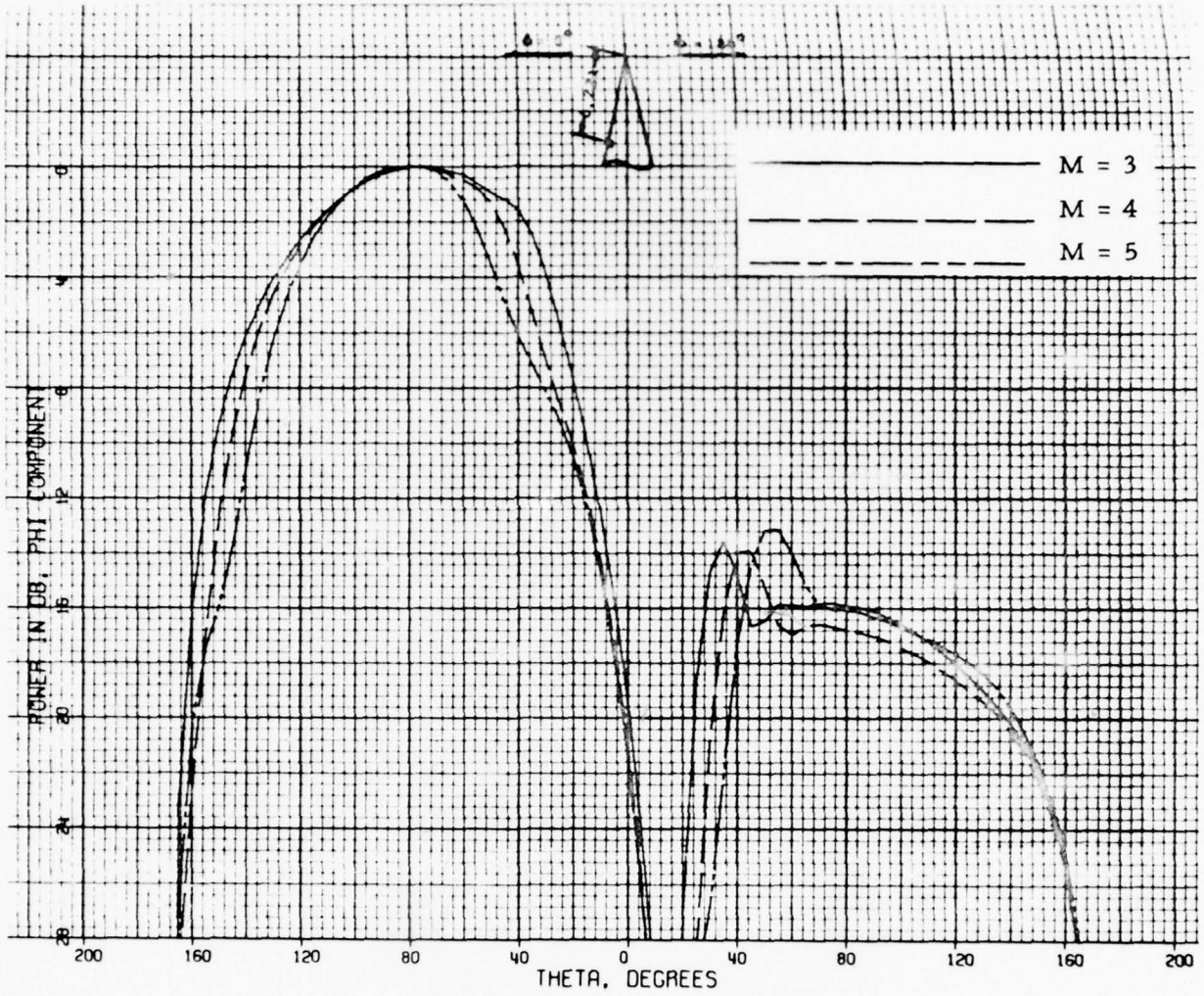

Figure 17. ϕ-Polarized Total Patterns of $\lambda/2$ Radial Slot for $\phi = 0^{o}$, $\phi = 180^{o}$, M = 3, 4 and 5

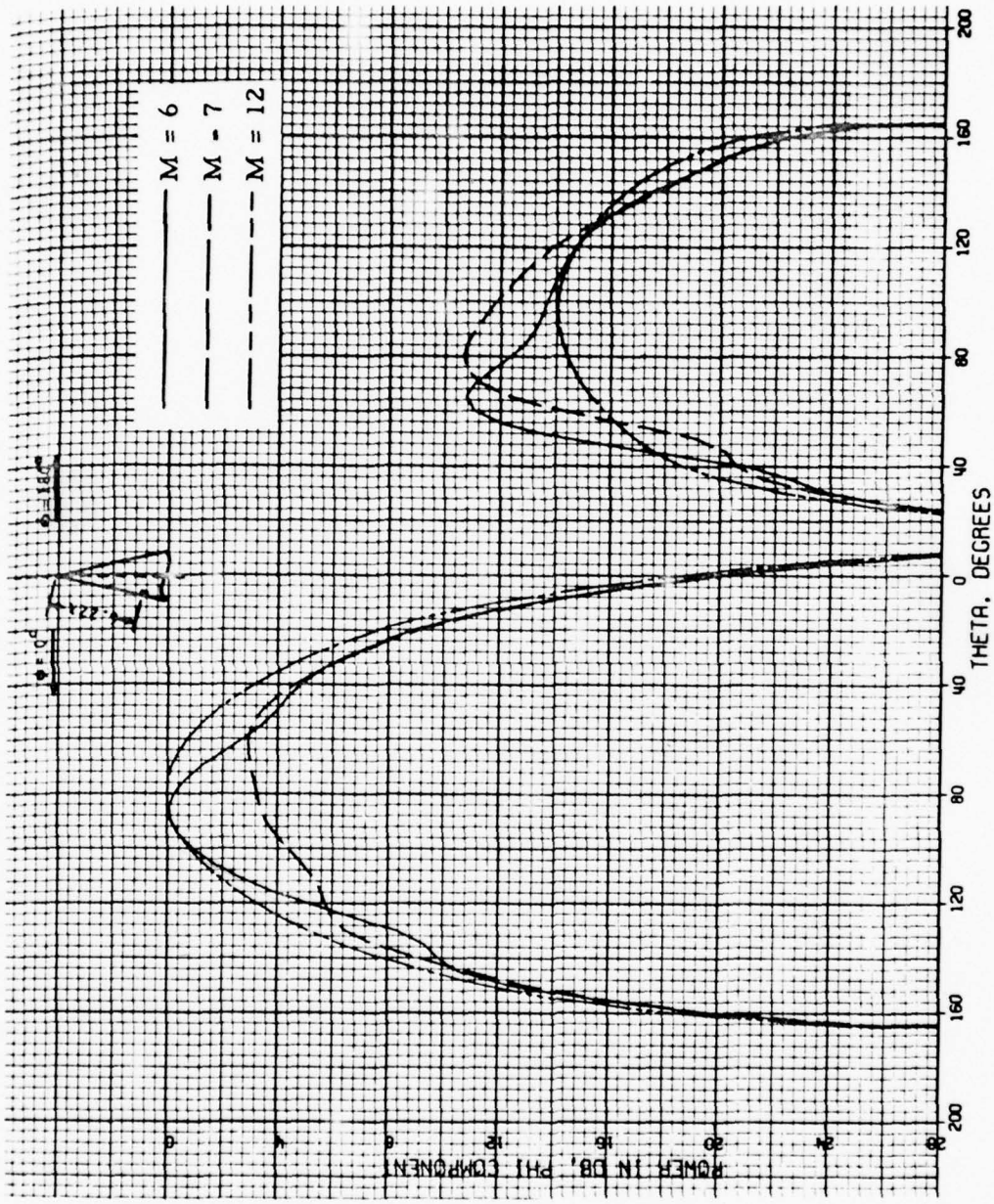

Figure 18. ϕ-Polarized Total Patterns of $\lambda/2$ Radial Slot for $\phi = 0^{o}$, $\phi = 180^{o}$, M = 6, 7, and 12

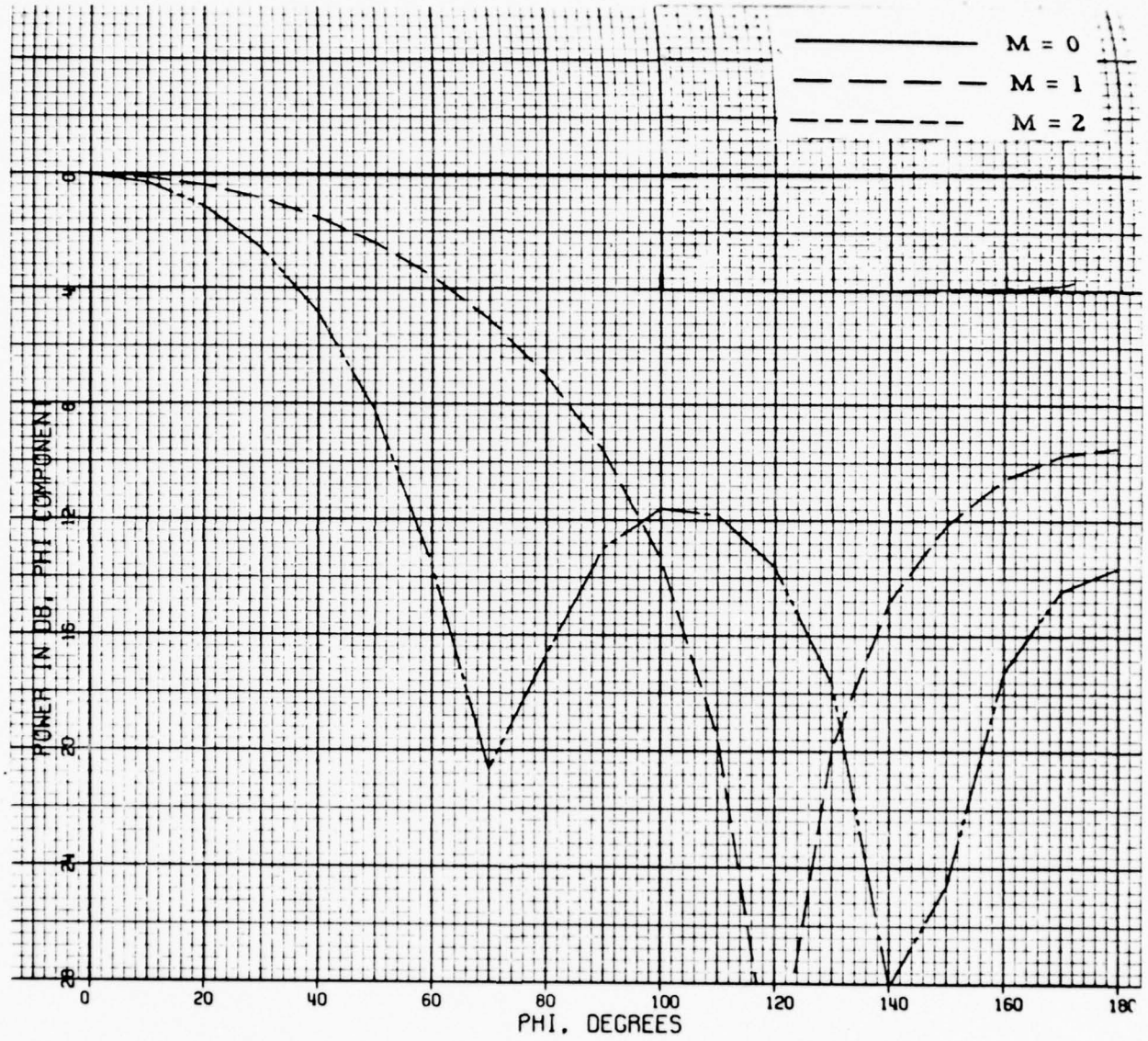

Figure 19. ϕ-Polarized Total Pattern of $\lambda/2$ Radial Slot for $\theta = 80^{\circ}$, M = 0, 1, and 2

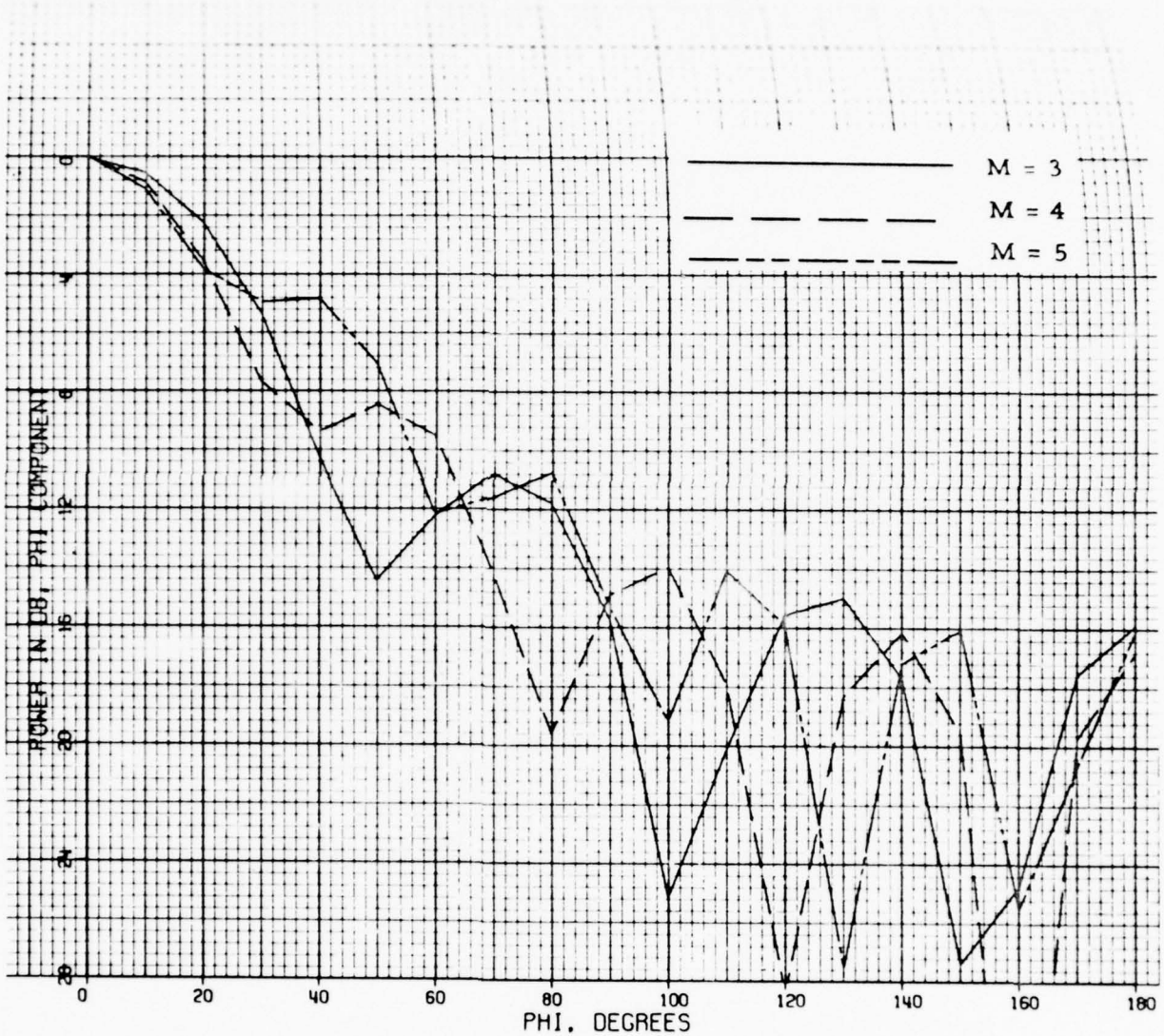

Figure 20. ϕ-Polarized Total Patterns of $\lambda/2$ Radial Slot for $\theta = 80^{\circ}$, M = 3, 4, and 5

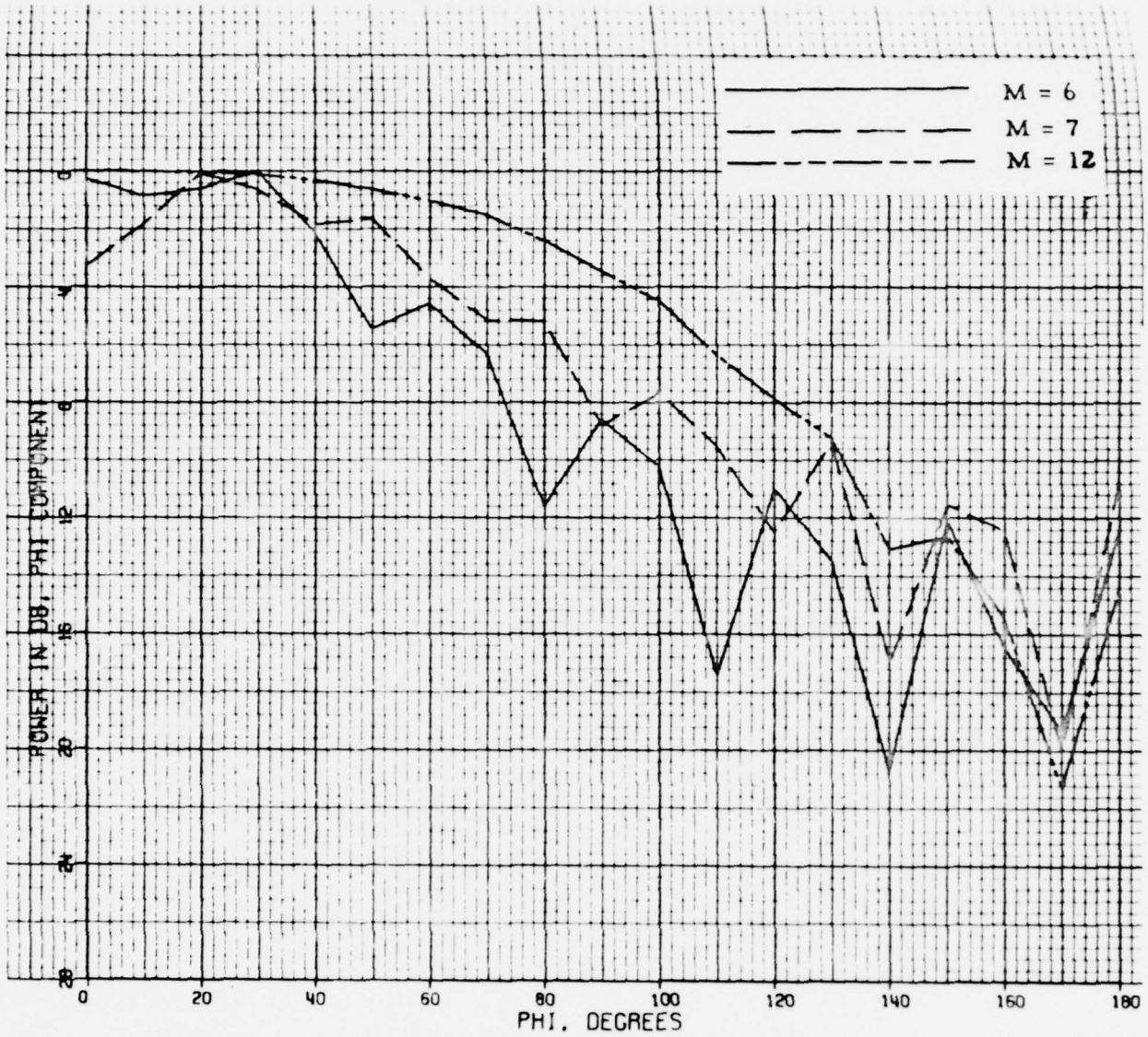

Figure 21. ϕ-Polarized Total Patterns of $\lambda/2$ Radial Slot for $\theta = 80^{\circ}$, M = 6, 7, and 12

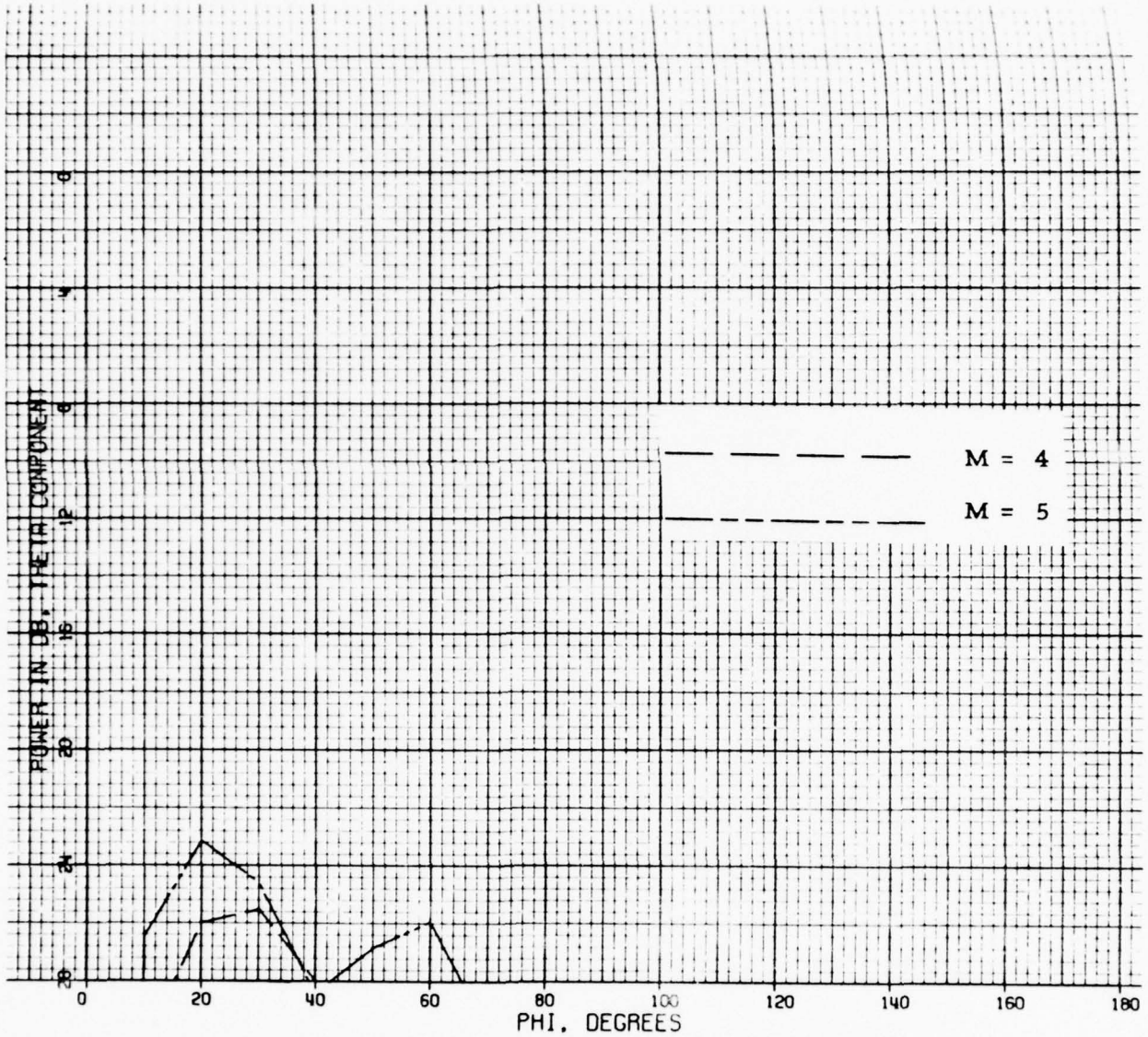

Figure 22. θ-Polarized Total Patterns of λ/2 Radial Slot for θ = 80°, M = 4 and 5

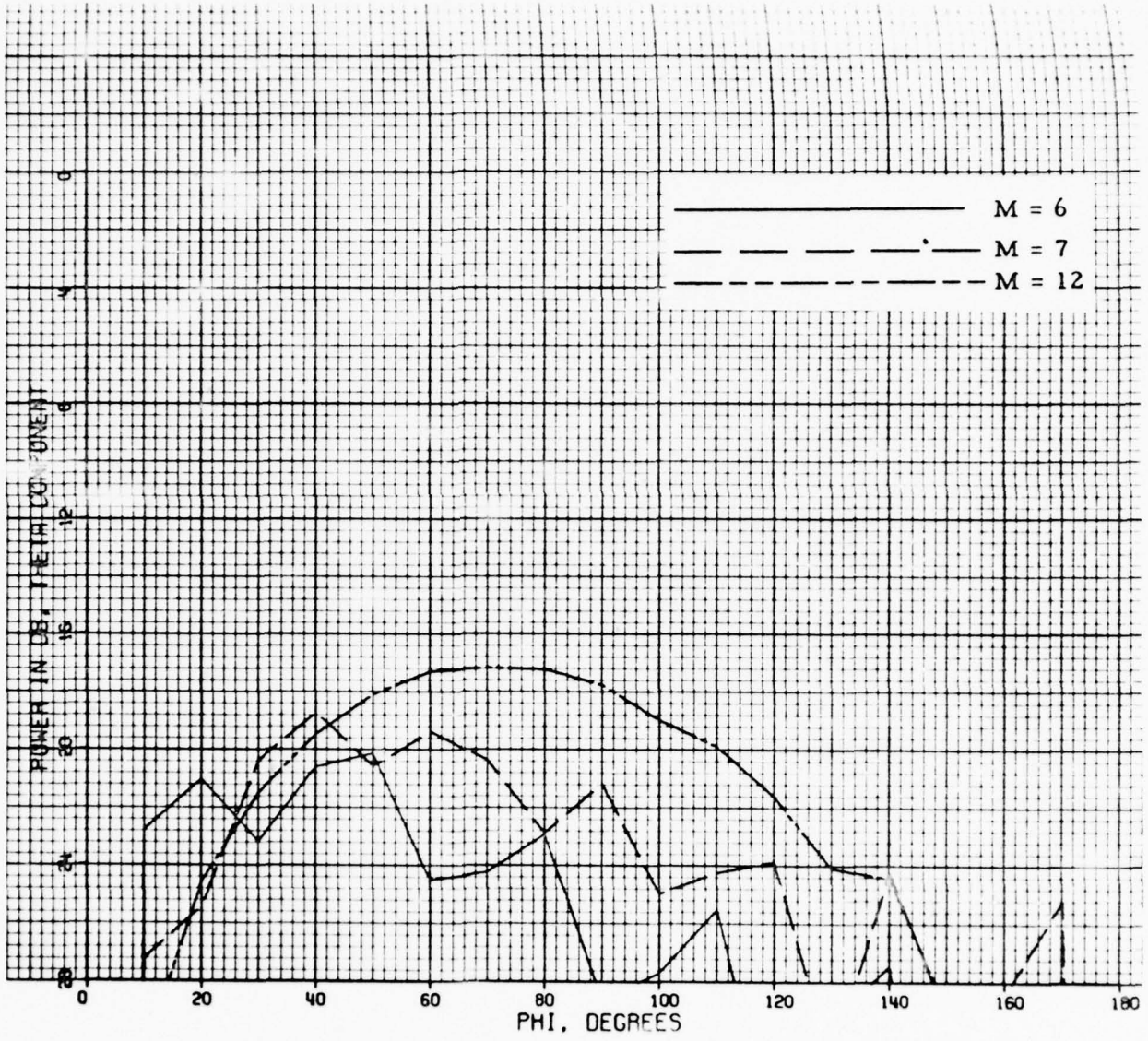

Figure 23. θ-Polarized Total Patterns of λ/2 Radial Slot for $\theta = 80^{\circ}$, M = 6, 7, and 12

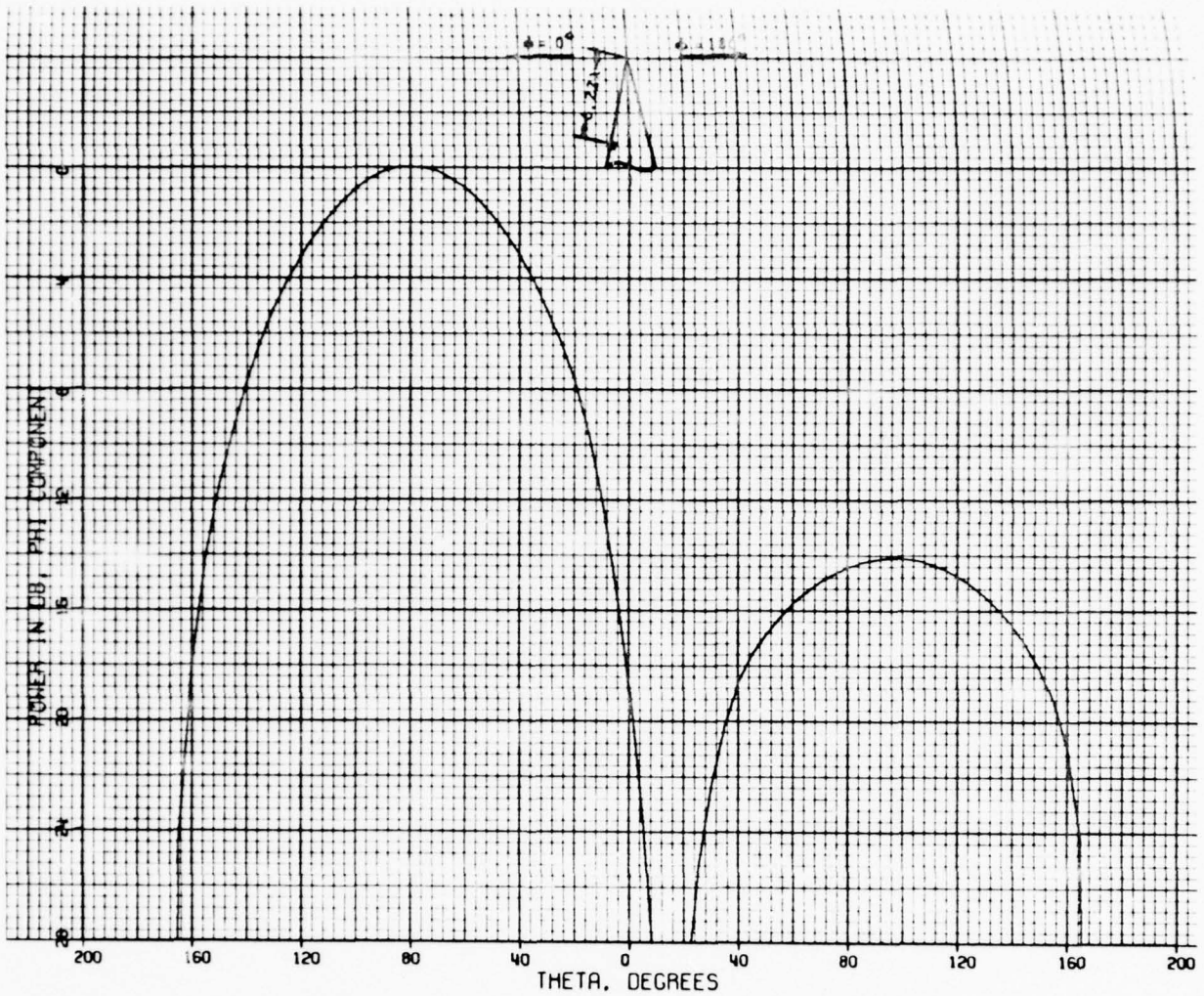

Figure 24. ϕ-Polarized Total Pattern of $\lambda/2$ Radial Slot for $\phi = 0^{o}$, $\phi = 180^{o}$, M = 13

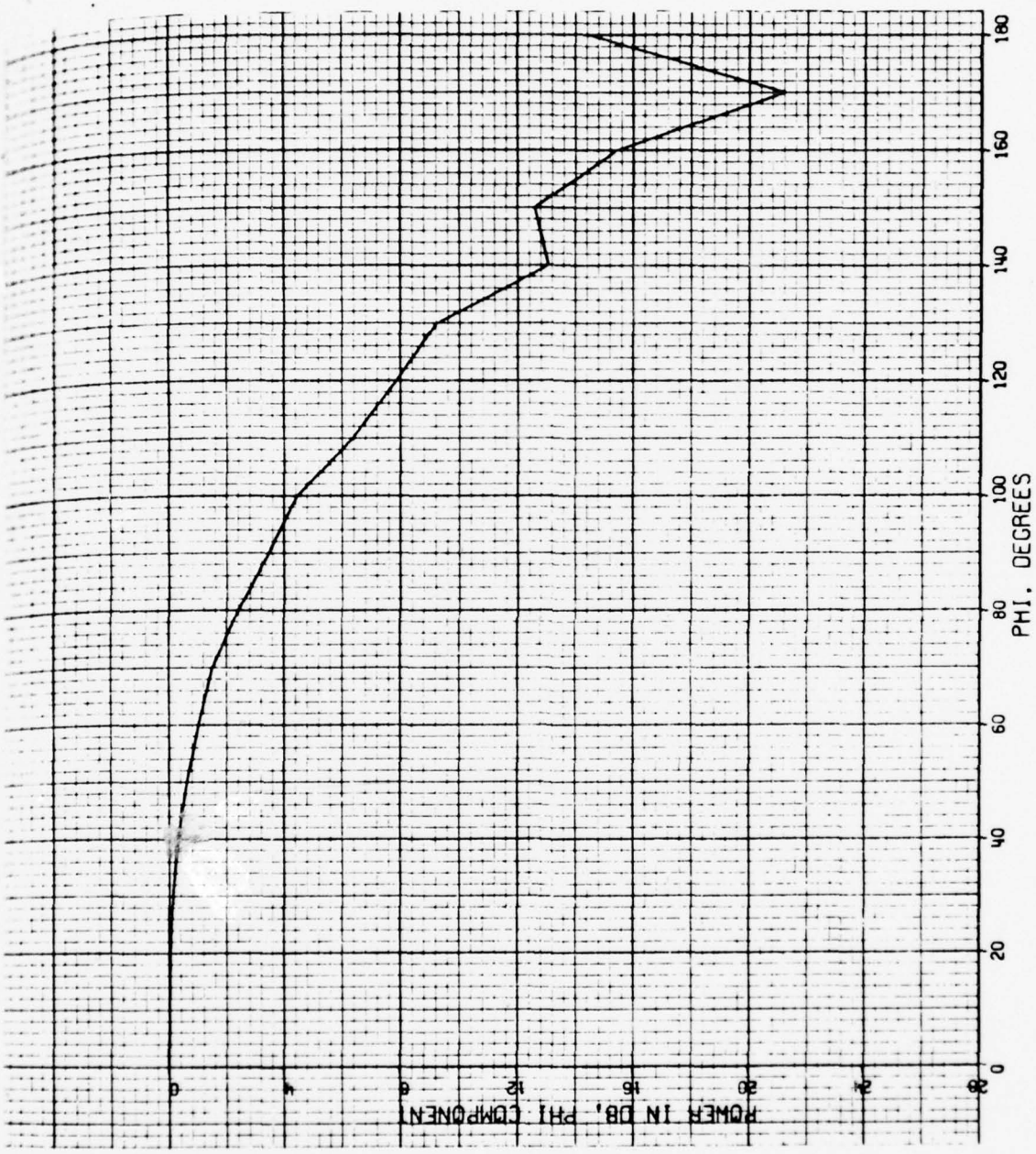

Figure 25. ϕ-Polarized Total Pattern of λ/2 Radial Slot for $\theta = 80^{0}$, M = 13

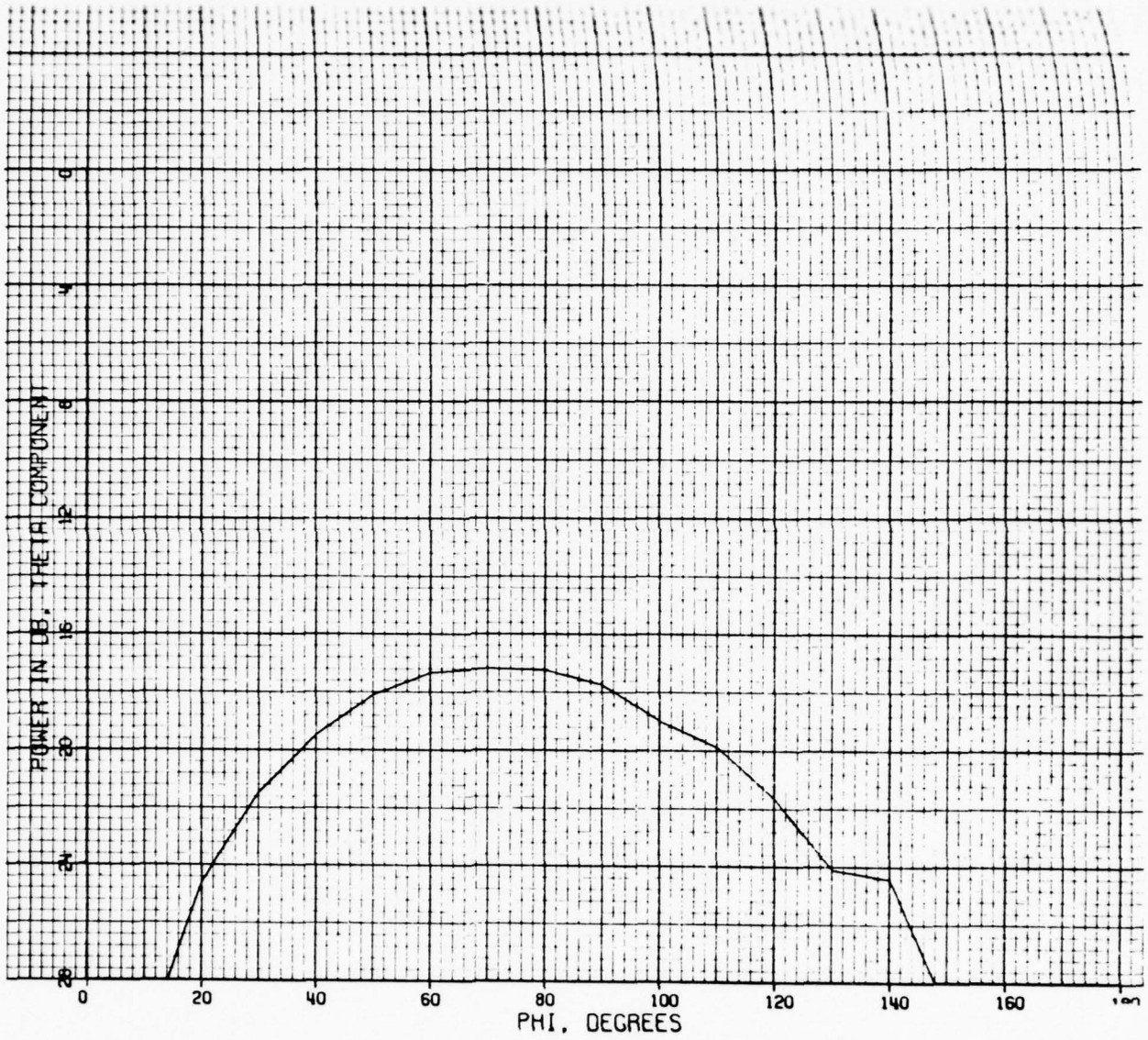

Figure 26. θ-Polarized Total Pattern of λ/2 Radial Slot for $\theta = 80^{o}$, M = 13

Elevation patterns of the same slot located at ka = 30 radians from the tip of the cone were also computed and are shown in Figure 27. As in the circumferential slot for this position, the $\phi = 0^{\circ}$ and the $\phi = 90^{\circ}$ cuts are shown. The maximum of the M = 6 pattern occurs at $\theta = 72^{\circ}$ instead of the expected broadside, $\theta = 80^{\circ}$. This is because of the insufficient number of modes in the truncation of the modal series. All other aspects of the pattern are the same as for the ka = 39 position, indicating that tip diffraction has little effect on the radiation pattern of the radial slot. A greater number of terms must be taken in the modal series, however, as the slot is moved farther away from the tip of the cone. Also, these higher order modes affect mainly the broadside region of the element pattern.

Although we do not have experimental data for the slot described in this section for comparison at this time, the above patterns do look very much like the patterns of a slot on a cylinder tipped 10 degrees from its axis. In further studies of the problem, the above results will be verified experimentally.

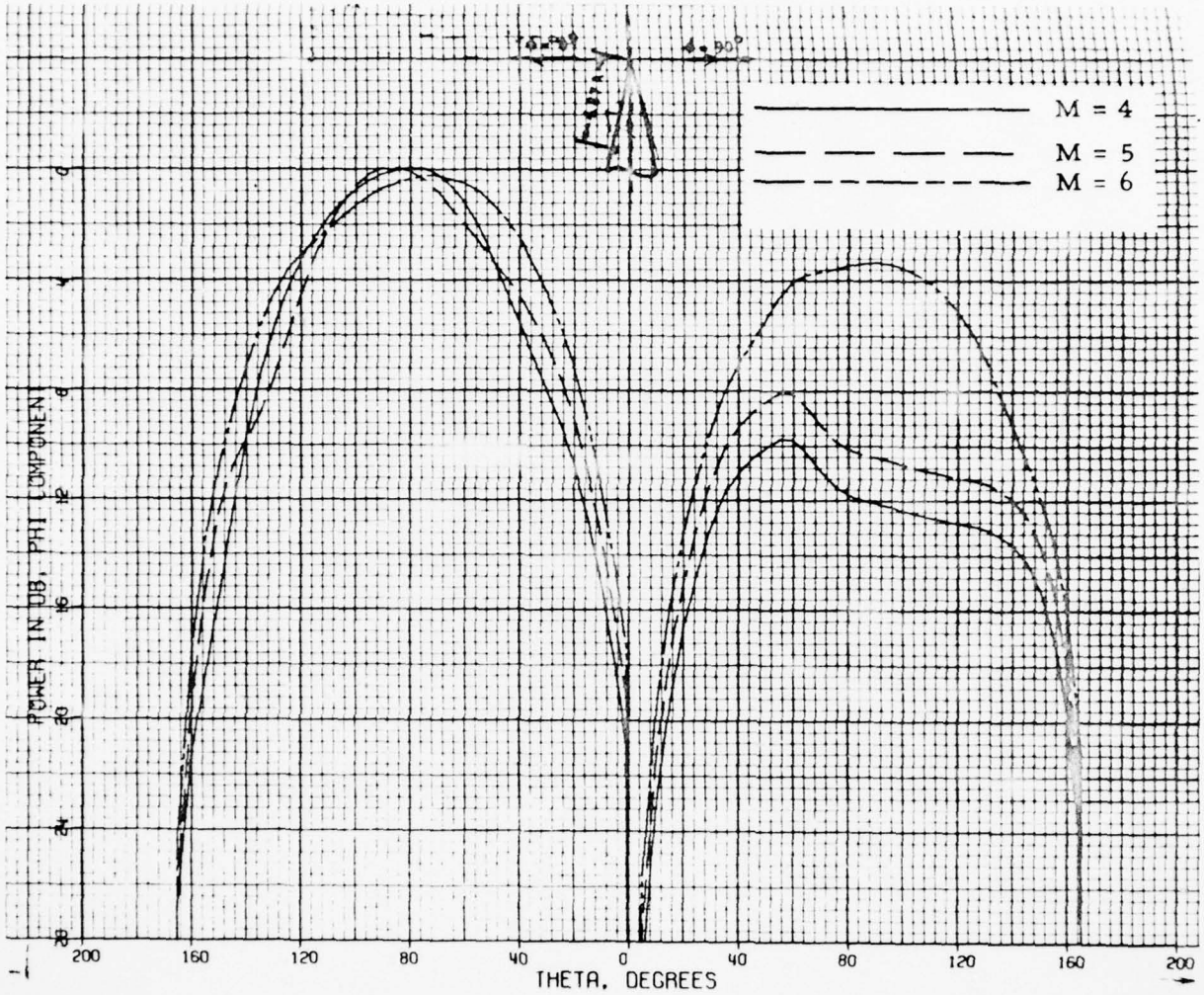

Figure 27. ϕ-Polarized Total Patterns of $\lambda/2$ Radial Slot for $\phi = 0^{o}$, $\phi = 90^{o}$, M = 4, 5, 6, and ka = 30

5.0 RECOMMENDATIONS FOR FURTHER INVESTIGATIONS

The analysis of the computed element patterns from circumferential and radial slots on a sharply tipped cone presented in Section 4 of this report is only a partial one. For more complete understanding of the radiation characteristics of such elements additional investigative work must be performed. Specifically, the developed computer program for the exact element patterns may now be used to compute patterns of slots near the tip of the cone and very far away from the tip. The results can then be analyzed so as to separate the contribution of tip diffraction from the total pattern. Such a procedure not only aids in understanding the radiation characteristics but also will result in more economical pattern calculation as discussed in the next paragraph.

The present analysis has shown that more modes are required in the truncation of the modal series for element locations far away from the tip of the cone. The computation of a higher order mode, however, requires considerable more computer time, for the index of the ν-series in the field expressions is a function of both the order of the mode and the location of the element relative to the tip of the cone. If the contribution of tip diffraction is separated from the total pattern, many repetitive computations would be eliminated and conical array problems will be solved more economically. Such an approach will allow the computation of patterns to verify the equivalence principle pattern synthesis technique.[1]

The computed element patterns of the circumferential slot relatively close to the tip of the cone have shown good agreement with measured patterns. The experimental verification, however, needs to be accomplished for other element positions and orientations. In addition, the present analysis technique could be extended so as to take into consideration mutual coupling effects. The results could then be compared with similar results obtained from the geometrical theory of diffraction.

REFERENCES

1. Kummer, W. H., A. F. Seaton, and A. T. Villeneuve, (1973). "Conformal Antenna Arrays Study," Final Report on Contract N00019-72-C-0212, Report No. 2765, 31/421, Hughes Aircraft Company, January, 1972 to January, 1973.

2. Bargeliotes, P. C., A. F. Seaton, and A. T. Villeneuve (1973), "Dynamic Impedance Matching in Conformal Arrays", Quarterly Report, 1 Jan. to 1 April 1973, Contract N00019-73-C-0127, Hughes Aircraft Company.

3. Pridmore-Brown, D. C., 1972, "Radiation Patterns from Slot-Excited Cones," IEEE Trans. on Antennas and Propagation, Vol. AP-20, No. 6, November, 1972, pp. 815-816.

4. Pridmore-Brown, D. C. and G. Stewart, 1972, "Radiation from Slot Antennas on Cones," IEEE Trans. on Antennas and Propagation Vol. AP-20, No. 1, January, 1972, pp. 30-39.

5. Behnke, M. C., A. T. Villeneuve, and W. H. Kummer, 1972, "Advanced Conformal Array Antenna Techniques," Final Report, February 1971 to January 1972, Contract N00019-71-C-0197, Hughes Aircraft Company.

6. Bailin, L. L. and S. Silver, 1956, "Exterior Electromagnetic Boundary Value Problems for Spheres and Cones," IRE Trans. on Antennas and Propagation, Vol. AP-4, January, 1956, pp. 5-16.

7. Bailin, L. L. and S. Silver, 1957, "Exterior Electromagnetic Boundary Value Problems for Spheres and Cones," IRE Trans. on Antennas and Propagation, Vol. AP-4, January, 1956, pp. 5-16. corrections, IRE Trans, Vol. AP-5, July, 1957, p. 313.

8. Erdélyi, A., et al., Higher Transcendental Functions, Vol. 1, McGraw-Hill Book Company, Inc., New York, 1953, p. 144.

9. Erdélyi, A., et al., Higher Transcendental Functions, Vol. 1, McGraw-Hill Book Company, Inc., New York, 1953, p. 161.

10. Carnahan, B., H. A. Luther and J. O. Wilkes. Applied Numerical Methods, John Wiley and Sons, Inc., New York, 1969, p. 139.

11. Erdélyi, A., et al., Higher Transcendental Functions, Vol. 1, McGraw-Hill Book Company, Inc., N. Y., 1953, p. 147(last Eq.).

12. Erdélyi, A., et al., Higher Transcendental Functions, Vol. 1, McGraw-Hill Book Company, Inc., N. Y., 1953, p. 147, Equation 3.5(5).

13. Abramowitz, M. and I. A. Stegun, Handbook of Mathematical Functions, U.S. Department of Commerce NBS, 1956, p. 480.

14. Jahnke, E., and F. Emde, Tables of Functions, Dover Publications, New York, 1945, p. 128.

15. Watson, G. N., Theory of Bessel Functions, Cambridge University Press, 1952, p. 199.

16. McLachlan, N. W., Bessel Functions for Engineers, Oxford Clarendon Press, 1955, pp. 87-88.

APPENDIX A
COMPUTER PROGRAM FOR CONICAL ARRAY PATTERN ANALYSIS

A FORTRAN IV version of the program used to compute exact element patterns of circumferential and radial slots on a cone is presented at the end of this appendix. Specifically, the program uses the IBM 370 computer system presently available at the Hughes Aircraft Company facilities. The field expressions of Sections 2.2 and 2.3 are the basis for the program. The two different types of slots are considered concurrently when they are located at the same position on the conical surface or individually when located at different positions.

The input data to the program in a specified format specifies the type of slots to be considered, their location on the conical surface, and other parameters necessary for the computation of the field patterns. The program computes both modal and total radiation patterns. The modal patterns provide the necessary information for properly truncating the modal series, while the total pattern information is stored on tape for subsequent use in array analysis. The input parameters required by the READ statement are defined as follows:

THETAO	=	θ_o, supplement of the half-angle of the cone in degrees.
KA	=	position of center of element from the tip in radians.
THETAI	=	initial value of spherical angle θ in degrees.
THETAF	=	final value of spherical angle θ in degrees.

DTH = increment of the spherical angle θ in degrees.

PHI = final value of azimuthal angle ϕ in degrees.

DPHI = increment of the azimuth angle ϕ in degrees. Program always evaluates pattern for $\phi = 0^{o}$.

M = first value of the modal series. Normally M = 0. If M $\neq$ 0, the lower modes are not included in the computations.

MCR = switch specifying the type of slot to be considered. MCR = 1 specifies both circumferential and radial slots individually at same position. MCR = 2 specifies only circumferential slot. MCR = 3 specifies only radial slot.

MVM = upper limit of modal series for circumferential slot.

MVR = upper limit of modal series for radial slot.

Some of the remaining primary parameters of the program are defined as follows:

IT = counter and identifier of different cases considered.

MX = number of terms in the ν - series required for convergence.

PHIN = array of values of the azimuthal angle ϕ.

THETA = the spherical angle θ.

ST = array of values of the spherical angle θ.

NTH = maximum number of θ-values.

NPHI = maximum number of ϕ-values.

LX = total number of points of field evaluation.

LM = DO loop index. LM = 1 outputs patterns of circumferential slot. LM = 2, outputs pattern of radial slot.

Additional relationships between the program variables, printed output and the field component equations are presented for convenience in Table A-1.

In addition to printed output, the program also provides a record of all computed field component values on magnetic tape for further utilization by a separate program. The desired length in inches, the labeling information and the initial and increment values for both axes must be specified in the argument list of the CPLOT3(....) plotting routine. Azimuthal cut plots are obtained only if JS $\neq$ 0 for θ = ST(JS) through θ = ST(JL) degrees in steps of JSTEP. The program terminates with the completion of the computations for the last data card.

TITLE	DENOTES		
	MD = 1 (TM-circ)	MD = 2 (TE-circ)	MD = 3 (Radial)
NU	N^{th} zero of $P^{m}_{\nu\ -1/2}(\cos\theta_o)$	N^{th} zero of $\frac{\partial}{\partial\theta_o} P^{m}_{\nu'-1/2}(\cos\theta_o)$	
DPDNU (RES (J, MD))	$\frac{\partial}{\partial\nu} P^{-m}_{\nu\ -1/2}(\cos\theta_o)$	$\frac{\partial^2}{\partial\nu'\partial\theta_o} P^{-m}_{\nu'-1/2}(\cos\theta_o)$	
COEFFICIENT (BR(J,MD)	$\frac{NU}{NU * NU - .25} * \frac{{}^{j}NU}{DPDNU}$		$NU * \frac{{}^{j}NU}{DPDNU}$
BESSEL FUNCT (BJ (J))	$J_\nu(ka)$	$\frac{\partial}{\partial x}\left[\left(\frac{x}{ka}\right)^{1/2} J_{\nu'}(x)\right]\Big\|_{x=ka}$	$\int_{r_1}^{r_2} \frac{g(r')\ J_{\nu'}(kr')}{r'\sqrt{kr'}}\ dr$
LEGENDRE FUNCT-P	$P^{-m}_{\nu\ -1/2}(\cos\theta)$		
DR-LEGENDRE FUNCT-- PD	$\frac{\partial}{\partial\theta} P^{-m}_{\nu\ -1/2}(\cos\theta)$		
THETA-PARTIAL SUM	$P_{1\theta}$	$P_{2\theta}$	P_θ
PHI-PARTIAL SUM	$P_{1\phi}$	$P_{2\phi}$	P_ϕ
ECT (IT, L) ECF (IT, L) ERT (IT, L) ERF (IT, L)	ECT = E_θ component ECF = E_ϕ component		ERT = E_θ component ERF = E_ϕ component

TABLE A-I

```
      CONICAL ARRAY .
      DIMENSIONING OF THE BJ,RES,AR,BR,NU ARRAYS MUST BE GREATER OR
      EQUAL TO INDEX "MX", THE NUMBER OF ROOTS OF LEGENDRE FUNCTION.
      COMPLEX ECT( 8,665),ECF( 8,665),ERT( 8,665),ERF( 8,665)
      COMPLEX ACT(85),ACF(85),ART(85),ARF(85),AR(120,3),BR(120,3)
      COMPLEX ECTM,ECFM,ERTM,ERFM
      COMPLEX XEN,XNP,PSD,PS,PSDR,PSR,CF1,CF2,ZERO,DJ
      DOUBLE PRECISION BJ,RES,BI,NU(99,2),NU1,NU2,XNU,XNUP1,P,PD,P1,Q
      DOUBLE PRECISION SNT,CST,RAD,DTR,PIO2,TTD,PI
      DIMENSION BJ(99),RES(99,2),PHIN(20),CMP(20),SMP(20),MS(15)
      DIMENSION F(2,15),KAS(15),S(665),SF(665),SMT(20),SMF(20),ST(40)
      DIMENSION ST1(40),ST2(40),ST3(40),ST4(40),SP(40),SFP(40)
      EQUIVALENCE (AR,S),(BR,SF)
      EQUIVALENCE (BJ,SMT), (BJ(21),SMF)
      REAL KA,KAL,KAS
      DATA PI,ZERO,DJ/3.14159265358979,(0.,0.),(0.,1.)/
      DATA JS,JL,JSTEP/17,17,1/
      MCR IS A PARAMETER FOR TYPE OF SLOT.  MCR=1 TREATS CIRCUMF.
      AND RADIAL CASE AT SAME POSITION, KA DISTANCE FROM TIP.
      MCR= 2 TREATS CIRC. ONLY, WHILE MCR=3 TREATS RADIAL ONLY.
C.....DATA JS,JL,JSTEP/.../  SELECTS THE THETA -CUT PLOTS.
  109 FORMAT(1H1,49H THETAO   KA   THETAI THETAF  DTH   PHI   DPHI    DK,
     17X,14HM  MCR MVM MVR)
  110 FORMAT(2X,2F7.3,5F6.2,F8.5,4I4)
  111 FORMAT(3E15.5)
  112 FORMAT(2X,4HMCR=,I2)
  113 FORMAT(2X,11HMCR,LM,KCR=,3I5)
  115 FORMAT(1H1,'CONE ANGLE =',F6.1,' DEGREES, KA =',F8.3,', M =',I2)
  116 FORMAT(1H0,5HMODE I1//3X,1HN,8X,2HNU,19X,11HCOEFFICIENT,20X,
     15HDPDNU,12X,12HBESSEL FUNCT)
  117 FORMAT(1H1, 5HMODE ,I1,5X,4HMCR=,I2)
  118 FORMAT(2X,2(4H NU(,I3,1H,,I2,2H)=,F14.8))
  120 FORMAT(1H0,'THETA =',F6.1,'DEGREES'//3X,1HN,4X,14HDR-LEGEN FUNCT,
     111X,17HTHETA-PARTIAL SUM,10X,1HN,4X,14HLEGENDRE FUNCT,
     111X,17HPHI - PARTIAL SUM)
  121 FORMAT(2(I4,4X,E13.5,5X,1H(,E13.5,3H , ,E13.5,1H)))
  130 FORMAT(I4,F14.8,E20.8,E16.8,2E20.8,F16.8)
  140 FORMAT(1H1,30X,'RADIATION PATTERN,',F4.0,'DEGREE CONE'//
     12X,11HEXCITATION,25HELEM. TYPE(CIRC=1,RAD=2)=,I3,5X,
     118HE-COMP(TH=1,PH=2)=,I3/(3(4X,4HKA =,F7.2,2X,2HM=,I3,2X,
     13HEC=,F7.4)))
  141 FORMAT(1H+,50X,'KA =',F7.2,2X,'M =',I3,2X,'EC =',F7.4/
     1(F24.2,I8,F13.4,F17.2,I8,F13.4))
  143 FORMAT(//1X,10HPHI,THETA=,F5.1,16F7.1/(9X,17F7.1))
  170 FORMAT(F6.1,3X,17F7.1/(9X,17F7.1))
  171 FORMAT(2X,3(1X,3HAR(,I3,1H,,I2,2H)=,2E13.5)/)
  172 FORMAT(2X,3HMD=,I1,2X,E13.5,5X,1H(,E13.5,3H , ,E13.5,1H),
     13X,2E13.5)
```

```
173 FORMAT(2X,4E15.5,4X,2HS(,I3,2H)=,F10.3,2X,2HDB)
180 FORMAT(1HQ,'THETA =',F6.1,'DEGREES'//3X,1H-,4X,14HDR-LEGEN FUNCT,
   111X,17HPHI - PARTIAL SUM,10X,1HN,4X,14HLEGENDRE FUNCT,
   111X,17HTHETA-PARTIAL SUM)
181 FORMAT(4HLLM=,I1,5H MCR=,I1,4H M1=,I2,5H MVM=,I2,5H MVR=,I2,
   14H KA=,F6.2,8H THETAC=,F6.2,6H NPHI=,I3,5H NTH=,I3,4H LX=,I4)
182 FORMAT(4H LM=,I1,5H MCR=,I1,4H M1=,I2,5H MVM=,I2,5H MVR=,I2,
   14H KA=,F6.2,8H THETAC=,F6.2,6H NPHI=,I3,5H NTH=,I3,4H LX=,I4)
184 FORMAT(10F7.2)
185 FORMAT(2E15.7,F9.3,2E15.7,F9.3)
186 FORMAT(//11X,9HECT(IT,L),14X,2HDB,15X,9HECF(IT,L),14X,2HDB)
187 FORMAT(//11X,9HERT(IT,L),14X,2HDB,15X,9HERF(IT,L),14X,2HDB)
188 FORMAT(2X,'***THIS PATTERN CUT IS ZERO AND IS NOT PLOTTED.***')
189 FORMAT(1H1,30X,'RADIATION PATTERN,',F4.0,'DEGREE CONE'//
   12X,11HEXCITATION,25HELEM. TYPE(CIRC=1,RAD=2)=,I3,5X,
   118HE-COMP(TH=1,PH=2)=,I3/(3(4X,4HKA =,F7.2,2X,2HM=,I3)))
191 FORMAT(2X,2F10.3)
192 FORMAT(2X,2I3,5HTEST=,F8.2,3X,5HTESF=,F8.2)
    PIO2 = PI/2.
    STOPI = DSQRT(2./PI)
    HSTOPI = .5*STOPI
    TPI = 2.*PI
    DTR = PI/180.
    IT = 0
    CALL PLOTI
  1 READ(5,110,END=99)THETAO,KA,THETAI,THETAF,DTH,PHI,DPHI,DK,
   1M,MCR,MVM,MVR
    IF(THETAO.EQ.0..AND.KA.EQ.0.) STOP
    IF(THETAO.EQ.0.) THETAO = THETAF
    WRITE(6,109)
    WRITE(6,110)THETAO,KA,THETAI,THETAF,DTH,PHI,DPHI,DK,M,MCR,MVM,MVR
    IF(DPHI.EQ.0.) DPHI=5.
    M1 = M
    IT = IT + 1
    KZR = 0.0
    NPHI=PHI/DPHI + 1.
    KAS(IT) = KA
    STPIKA = SQRT(TPI*KA)
    STPOTP = STPIKA/TPI
    STPOP = STPIKA/PI
    SNTO = DSIN(DTR*THETAO)
    SNTO1 = HSTOPI/SNTO
    SNTO2 = STOPI/SNTO
    AKSO = KA*SNTO
    TAKSO = 2.*AKSO
    PODK = PI/DK
    IM = 0
300 GO TO(310,310,330),MCR
```

```
C     MM IS THE NUMBER OF TERMS CONSIDERED IN THE M-SERIES, AND
C     IS DEFINED BY THE DATA VALUES OF MVM,MVR.
  310 MM = MVM
      GO TO 3
  330 MM = MVR
    3 RM = M
      IM = IM + 1
      MS(IM) = M
      FC = PODK*TAKSO*COS(RM*DK/TAKSO)/((PODK*AKSO)**2 - RM*RM)
      FC1 = FC*STPOTP
      FC2 = FC*STPOP
      F(IT,IM) = FC
    4 MD = 1
      THETA = THETAI
      IA = 1
C     CALCULATE AND STORE COS(MPHI(I)),SIN(MPHI(I))
      DO 2 I = 1,NPHI
      RI = I
      PHIN(I) = (RI - 1.)*DPHI
      RADMPH = RM*DTR*PHIN(I)
      SMP(I) = SIN(RADMPH)
    2 CMP(I) = COS(RADMPH)
C     MX IS NO. OF TERMS IN NU-SERIES REQ. FOR CONVERGENCE.
      MX = KA + 2.*RM + 10.
      WRITE(6,115) THETAO,KA,M
      MP1 = M + 1
      DNU = 180./THETAO
      DO 11 MD = 1,2
      IF(MD.EQ.1.AND.MCR.EQ.3) GO TO 11
    5 XNU = RM + .5 - DNU
      ID = MD - 1
C     CALCULATION OF ZEROES OF LEGENDRE FUNCTIONS,NU,NUPRIME.
      DO 10 J = 1,MX
      NU1 = XNU + DNU - .04
      NU2 = NU1 + .08
      CALL ROOTS(THETAO,NU1,NU2,M,XNU,ID)
C     ID IS PARAMETER FOR MODE.
      CALL RESIDU(THETAO,XNU,M,ID,RES(J,MD))
C     EVALUATE NU-COEF IN NU-SERIES, NOTING THAT RESIDUE FOR
C     RADIAL CASE IS SAME AS FOR MODE 2.
      TTD = XNU/RES(J,MD)
      T = TTD/(XNU**2 - .25)
      TT = TTD
      XNPIM = XNU*PIO2
      XNP = CMPLX(0.,XNPIM)
      XEN = CEXP(XNP)
      BR (J,MD) = T*XEN
      IF(MD.NE.2) GO TO 10
```

```
      BR (J,MD+1) = TT*XEN
   10 NU(J,MD) = XNU
   11 CONTINUE
      WRITE(6,118) ((J,MD,NU(J,MD),MD=1,2),J=1,MX)
      CALCULATION OF BESSEL DEPENDENCE TIMES F(NU)/RESIDUE.
      WRITE(6,112) MCR
      DO 16 MD = 1,3
      IF(MD.LE.2.AND.MCR.EQ.3) GO TO 16
      IF(MD.EQ.3.AND.MCR.EQ.2) GO TO 16
      WRITE(6,116) MD
      K = MD
      IF(MD.EQ.3) K = 2
      EXECUTION OF ST 500 INITIALIZES AR(J,MD) TO PREVENT OVERFLOW.
      IF(MD.EQ.2.AND.M.EQ.0) GO TO 500
      DO 15 J = 1,MX
      XNU = NU(J,K)
      IF(MD.NE.3) GO TO 13
      CALL BESSI(KA,DK,XNU,BJ(J))
      BESSI EVALUATES INTEGRAL FOR RADIAL SLOT CASE
      GO TO 14
   13 CALL BESSEL(KA,XNU,BJ(J))
      IF(MD.EQ.1) GO TO 14
      XNUP1 = XNU + 1.
      CALL BESSEL(KA,XNUP1,B1)
C     FOLLOWING EXPRESSION IS FOR D/DX(X*JNU(X)).
      BJ(J) = (XNU + .5)/KA *BJ(J) - B1
   14 IF(J.LT.6.OR.J.GT.MX-6)
     1WRITE(6,130) J,NU(J,K),BR(J,MD),RES(J,K),BJ(J)
      BJSING = BJ(J)
      AR(J,MD) = BR(J,MD)*BJSING
   15 CONTINUE
      GO TO 16
  500 CONTINUE
      DO 17 J = 1,MX
   17 AR(J,MD) = ZERO
   16 CONTINUE
C     CALCULATION OF LEGENDRE FUNCTIONS AND PARTIAL SUMS.
      IAT = 1.+ (THETAF - THETAI)/DTH
      NAI = THETAI/DTH
      IF(NAI.NE.1) IAT=IAT + 1
      IAM = IAT/2
C     LOOP 18 INITIALIZES THE NU-SERIES TOTAL SUM  FOR EACH NEW M.
      DO 18 I = 1,IAT
      ACT(I) = ZERO
      ACF(I) = ZERO
      ART(I) = ZERO
   18 ARF(I) = ZERO
      CF = RM/SNTO
```

```
      DO 200 MD = 1,2
      IF(MD.EQ.1.AND.MCR.EQ.3) GO TO 200
   19 WRITE(6,117) MD,MCR
      THETA = THETAI
      DO 210 IA = 1,IAT
      GO TO (240,241), MD
  240 IF(IA.EQ.1.OR.IA.EQ.IAM.OR.IA.EQ.IAT) WRITE(6,120) THETA
      GO TO 20
  241 IF(IA.EQ.1.OR.IA.EQ.IAM.OR.IA.EQ.IAT) WRITE(6,180) THETA
   20 RAD = DTR*THETA
      SNT = DSIN(RAD)
      CST = DCOS(RAD)
      ST(IA) = THETA
C.....THE ST1,ST2,ST3,ST4 ARRAYS ARE CREATED FOR PLOTTING ROUTINES.
      ST1(IA) = THETA
      ST2(IA) = THETA
      ST3(IA) = THETA
      ST4(IA) = THETA
      PS = ZERO
      PSD = ZERO
      PSDR = ZERO
      PSR = ZERO
      PSING = 0.
      PDSING = 0.
      P = 0.D0
      P1 = 0.D0
      PD = 0.D0
      DO 30 J = 1,MX
      XNU = NU(J,MD)
      CALL LEGEND(THETA,XNU,MP1,PD,Q,0)
      PDSING = PD
      IF(M)25,25,22
   22 CALL LEGEND(THETA,XNU,M,P1,Q,0)
      PD =RM*CST/SNT*P1 + PD
      PDSING = PD
      CALL LEGEND(THETA,XNU,M,P,Q,0)
      PSING = P
      IF(MCR.EQ.3) GO TO 26
      PS = PS + AR(J,MD)*PSING
   25 PSD = PSD + AR(J,MD) *PDSING
   26 IF(MD.NE.2.OR.MCR.EQ.2) GO TO 27
      PSDR = PSDR + AR(J,MD+1)*PDSING
      PSR = PSR + AR(J,MD+1)*PSING
C     PSDR AND PSR ARE TOTAL SUMS FOR THE RADIAL CASE.
   27 IF(IA.EQ.1.OR.IA.EQ.IAM.OR.IA.EQ.IAT) GO TO 31
      GO TO 30
   31 IF(J.LT.5.OR.J.GT.MX-8) GO TO 32
      GO TO 30
```

```
   32 IF(MCR.EQ.3) GO TO 28
      WRITE(6,121) J,PD,PSD,J,P,PS
   28 IF(MD.NE.2.OR.MCR.EQ.2) GO TO 30
      WRITE(6,121) J,PD,PSDR,J,P,PSR
   30 CONTINUE
      EVALUATION OF FIELD COMPONENTS AT EACH THETA FOR EACH M.
      CF1AR = RM/SNT
      CF1 = CMPLX(0.,CF1AR)
      GO TO(220,230),MD
  220 ACT(IA) = ACT(IA)+ PSD
      ACF(IA) = ACF(IA)- PS*CF1
      GO TO 215
  230 GO TO(235,237,236),MCR
  235 ACT(IA) = ACT(IA) + PS*CF1*CF
      ACF(IA) = ACF(IA) + PSD*CF
  236 ART(IA) = ART(IA) + PSR*CF1
      ARF(IA) = ARF(IA) + PSDR*DJ
      GO TO 215
  237 ACT(IA) = ACT(IA) + PS*CF1*CF
      ACF(IA) = ACF(IA) + PSD*CF
  215 IF(IA.EQ.1) THETA = FLOAT(NAI)*DTH
  210 THETA = THETA + DTH
  200 CONTINUE
C     EVALUATION OF AMPLITUDES AND FINAL FIELD COMPONENTS.
      NTH = IAT
      MT = NTH
      LX = NPHI*NTH
C     KZR IS A COUNTER FOR INITIALIZATION OF THE TOTAL FIELD ARRAYS.
      KZR = KZR + IT
      IF(KZR.GT.IT) GO TO 45
      DO 40 L = 1,LX
      ECT(IT,L) = ZERO
      ECF(IT,L) = ZERO
      ERF(IT,L) = ZERO
   40 ERT(IT,L) = ZERO
   45 CONTINUE
      IF(MCR.EQ.3) GO TO 59
C     THE DO 50 LOOP EVALUATES FIELD COMP. OF CIRCUM. SLOT.
C     ECTM, ECFM ARE THE FIELDS AT A POINT FOR A PARTICULAR  M.
C     ECT, ECF ARE THE TOTAL FIELDS AT A POINT, CIRCUMF. CASE.
      DO 50 I = 1,NPHI
      DO 51 J = 1,NTH
      L = NTH*I - NTH + J
      IF(M.NE.0) GO TO 54
      ECTM = EC1*CMP(I)*ACT(J)
      ECF(IT,L) = (1.E-15,0.)
      SF(L) = -300.
      SFP(J) = SF(L)
```

```
      GO TO 55
   54 ECTM = EC2*CMP(I)*ACT(J)
      ECFM = EC2*SMP(I)*ACF(J)
      IF(CABS(ECFM).LT.1.E-15) ECFM =(1.E-15,0.)
      ECF(IT,L) = ECF(IT,L) + ECFM
      SF(L) = 10.*ALOG10(REAL(ECFM*CONJG(ECFM)))
      SFP(J) = SF(L)
   55 IF(CABS(ECTM).LT.1.E-15) ECTM =(1.E-15,0.)
      ECT(IT,L) = ECT(IT,L) + ECTM
      S(L) = 10.*ALOG10(REAL(ECTM*CONJG(ECTM)))
      SP(J) = S(L)
   51 CONTINUE
      USE "WRITE(6,170) PHIN(I),(SP(J),J=1,NTH) " AND FOR "SFP() HERE.
   50 CONTINUE
      . . . . . .
C     STATEMENTS THROUGH *58* ARE ONLY FOR WRITING OUT MODE PATTERNS.
      WRITE(6,143)(ST(J),J=1,MT)
      DO 56 I = 1,NPHI
      NIN = NTH*(I - 1)
      NIN1 = NIN + 1
      NINMT = NIN + MT
   56 WRITE(6,170) PHIN(I),(S(J),J=NIN1,NINMT)
      IF(M.EQ.0) GO TO 59
      WRITE(6,143)(ST(J),J=1,MT)
      DO 58 I = 1,NPHI
      NIN = NTH*(I - 1)
      NIN1 = NIN + 1
      NINMT = NIN + MT
   58 WRITE(6,170) PHIN(I),(SF(J),J=NIN1,NINMT)
C     . . . . . .
   59 IF(MCR.EQ.2) GO TO 69
C     ERTM, EREM ARE THE FIELDS AT A POINT FOR A PARTICULAR  M.
C     ERT, ERF ARE THE TOTAL FIELDS AT A POINT, RADIAL CASE.
      DO 60 I = 1, NPHI
      DO 61 J = 1,NTH
      L = NTH*I - NTH + J
      IF(M.NE.0) GO TO 64
      EREM = CMP(I)*ARF(J)*SNT01
      ERT(IT,L) = (1.E-15,0.)
      S(L) = -300.
      SP(J) = S(L)
      GO TO 65
   64 EREM = CMP(I)*ARF(J)*SNT02
      ERTM = SMP(I)*ART(J)*SNT02
      IF(CABS(ERTM).LT.1.E-15) ERTM =(1.E-15,0.)
      ERT(IT,L) = ERT(IT,L) + ERTM
      S(L) = 10.*ALOG10(REAL(ERTM*CONJG(ERTM)))
      SP(J) = S(L)
```

```
   65 IF(CABS(EREM).LT.1.E-15) EREM =(1.E-15,0.)
      ERE(IT,L) = ERE(IT,L) + EREM
      SE(L) = 10.*ALOG10(REAL(EREM*CONJG(EREM)))
      SEP(J) = SE(L)
   61 CONTINUE
C     USE "WRITE(6,170) PHIN(I),(SP(J),J=1,NTH) " AND FOR "SEP() HERE.
   60 CONTINUE
C     . . . . . .
C     STATEMENTS THROUGH *68* ARE ONLY FOR WRITING OUT MODE PATTERNS.
      IF(M.EQ.0) GO TO 67
      WRITE(6,143)(ST(J),J=1,MT)
      DO 66 I = 1,NPHI
      NIN = NTH*(I - 1)
      NIN1 = NIN + 1
      NINMT = NIN + MT
   66 WRITE(6,170) PHIN(I),(S(J),J=NIN1,NINMT)
   67 WRITE(6,143) (ST(J),J=1,MT)
      DO 68 I = 1,NPHI
      NIN = NTH*(I - 1)
      NIN1 = NIN + 1
      NINMT = NIN + MT
   68 WRITE(6,170) PHIN(I),(SE(J),J=NIN1,NINMT)
C     . . . . . .
   69 IF(M.GE.MM) GO TO 350
      M = M + 1
      GO TO 3
  350 IF(MCR.NE.1) GO TO 360
      MCR = 3
      ISW = 1
      IF(M.GE.MVR) GO TO 360
      M = M + 1
      GO TO 300
  360 CONTINUE
C     THE "IT" CASE TOTAL PATTERNS ARE COMPUTED  AND PLOTTED BELOW.
      WRITE(6,112) MCR
      THETAC = 180. - THETAO
      IF(ISW.EQ.1) MCR = 1
C.....THE WRITE(10) STATEMENTS WRITE THE COMPUTED DATA ON TAPE.
      WRITE(10) MCR
      DO 400 LM = 1,2
      MZ = MVM - M1 + 1
      IF(LM.EQ.2) MZ = MVR - M1 + 1
      WRITE(6,112) MCR
      IF(MCR.EQ.2.AND.LM.EQ.2) GO TO 400
      IF(MCR.EQ.3.AND.LM.EQ.1) GO TO 400
      KCR = 0
      DO 370 I = 1,NPHI
      TEST = -200.
```

```
      TESF = -200.
      DO 375 J = 1,NTH
      L = NTH*I - NTH + J
      GO TO(371,372),LM
  371 S(L) =10.*ALOG10(REAL(ECT(IT,L)*CONJG(ECT(IT,L))))
      SF(L) =10.*ALOG10(REAL(ECF(IT,L)*CONJG(ECF(IT,L))))
      GO TO 374
  372 S(L) = 10.*ALOG10(REAL(ERT(IT,L)*CONJG(ERT(IT,L))))
      SF(L) = 10.*ALOG10(REAL(ERF(IT,L)*CONJG(ERF(IT,L))))
  374 IF(S(L).GT.TEST) TEST=S(L)
      IF(SF(L).GT.TESF) TESF=SF(L)
  375 CONTINUE
      SMT(I) = TEST
      SMF(I) = TESF
      WRITE(6,192) LM,I,TEST,TESF
  370 CONTINUE
      GO TO (376,377),LM
  376 WRITE(6,181) LM,MCR,M1,MVM,MVR,KA,THETAC,NPHI,NTH,LX
      WRITE(10) LM,MCR,M1,MVM,MVR,KA,THETAC,NPHI,NTH,LX
      WRITE(10) (PHIN(I),I=1,NPHI)
      WRITE(10) (ST(J),J=1,NTH)
      WRITE(6,186)
      WRITE(6,185) (ECT(IT,L),S(L),ECF(IT,L),SF(L),L=1,LX)
      WRITE(10) (ECT(IT,L),S(L),ECF(IT,L),SF(L),L=1,LX)
      GO TO 378
  377 WRITE(6,181) LM,MCR,M1,MVM,MVR,KA,THETAC,NPHI,NTH,LX
      WRITE(10) LM,MCR,M1,MVM,MVR,KA,THETAC,NPHI,NTH,LX
      WRITE(10) (PHIN(I),I=1,NPHI)
      WRITE(10) (ST(J),J=1,NTH)
      WRITE(6,187)
      WRITE(6,185) (ERT(IT,L),S(L),ERF(IT,L),SF(L),L=1,LX)
      WRITE(10) (ERT(IT,L),S(L),ERF(IT,L),SF(L),L=1,LX)
  378 CONTINUE
C     LOOP 410 FINDS LARGEST VALUE IN S(L) AND SF(L) ARRAYS.
      SMTN = -200.
      SMFN = -200.
      DO 410 I = 1,NPHI
      IF(SMT(I).GT.SMTN) SMTN=SMT(I)
  410 IF(SMF(I).GT.SMFN) SMFN=SMF(I)
      SMTT = SMTN
      SMFF = SMFN
      WRITE(6,191) SMTT,SMFF
      SNORM = SMTT
      IF(SMFF.GT.SNORM) SNORM=SMFF
      WRITE(6,191) SMTT,SNORM
  379 KCR = KCR + 1
      WRITE(6,113) MCR,LM,KCR
      GO TO (381,382),LM
```

```
381 WRITE(6,140) THETAC,LM,KCR,(KAS(IT),MS(I),F(IT,I),I=1,MZ)
    GO TO 383
382 WRITE(6,189) THETAC,LM,KCR,(KAS(IT),MS(I),I=1,MZ)
383 WRITE(6,143)(ST(J),J=1,NTH)
    CTF = -70.
    DO 390 I = 1,NPHI
    NIN = NTH*(I - 1)
    NIN1 = NIN + 1
    NINMT = NIN + NTH
    IF(KCR.EQ.2) GO TO 386
    DO 380 J = 1,NTH
    L = NTH*I - NTH + J
    SMT(I),SMF(I) ARE PHI-CUT NORMALIZATIONS.  SMTT,SMFF ARE FOR
C   COMPONENT NORMALZATION.  SNORM=MAX(SMTT,SMFF) OVERALL NORMALIZAT.
    S(L) = S(L) - SNORM
    SF(L) =SF(L) - SNORM
    SP(J) = S(L)
    SFP(J) = SF(L)
380 CONTINUE
385 WRITE(6,170) PHIN(I),(S(J),J=NIN1,NINMT)
C   THE FOLLOWING CARDS CONTROL THE NUMBER OF PLOTS DESIRED.
    IF(I.GT.1) GO TO 390
    IF(SP(2).LT.CTF.AND.SP(3).LT.CTF.AND.SP(6).LT.CTF) GO TO 387
    CALL SYMBOL(1.,7.5,.14,36,0.,-1)
    CALL LEGND1(1.3,7.5,.14,0.,1,'=',1,PHIN(I),0)
    CALL CPLOT3(1,ST,9.,0.,20.,14HTHETA, DEGREES,14,7.,-28.,4.,
   128HPOWER IN DB, THETA COMPONENT,28,NTH,SP)
387 IF(SFP(2).LT.CTF.AND.SFP(3).LT.CTF.AND.SFP(6).LT.CTF) GO TO 390
    CALL SYMBOL(1.,7.5,.14,36,0.,-1)
    CALL LEGND1(1.3,7.5,.14,0.,1,'=',1,PHIN(I),0)
    CALL CPLOT3(1,ST,9.,0.,20.,14HTHETA, DEGREES,14,7.,-28.,4.,
   126HPOWER IN DB, PHI COMPONENT,26,NTH,SFP)
    GO TO 390
386 WRITE(6,170) PHIN(I),(SF(J),J=NIN1,NINMT)
390 CONTINUE
    IF(KCR.EQ.1) GO TO 379
C   THE FOLLOWING CARDS PLOT PATTERNS OF THETA VS. PHI.
C   . . . . . .
    IF(JS.EQ.0) GO TO 400
    IF(JL.GT.NTH) JL=NTH
    DO 590 J = JS,JL,JSTEP
    DO 580 I = 1,NPHI
    L = NTH*I - NTH + J
    SP(I) = S(L)
    SFP(I) = SF(L)
580 CONTINUE
    IF(SP(2).LT.CTF.AND.SP(3).LT.CTF.AND.SP(6).LT.CTF) GO TO 587
    CALL SYMBOL(1.,7.5,.14,37,0.,-1)
```

```
      CALL LEGND1(1.3,7.5,.14,0.,1,'=',1,ST(J),0)
      CALL CPLOT3(1,PHIN,9.,0.,20.,12HPHI, DEGREES,12,7.,-28.,4.,
     128HPOWER IN DB, THETA COMPONENT,28,NPHI,SP)
  587 IF(SFP(2).LT.CTF.AND.SFP(3).LT.CTF.AND.SFP(6).LT.CTF) GO TO 590
      CALL SYMBOL(1.,7.5,.14,37,0.,-1)
      CALL LEGND1(1.3,7.5,.14,0.,1,'=',1,ST(J),0)
      CALL CPLOT3(1,PHIN,9.,0.,20.,12HPHI, DEGREES,12,7.,-28.,4.,
     126HPOWER IN DB, PHI COMPONENT,26,NPHI,SFP)
  590 CONTINUE
C     . . . . . .
  400 CONTINUE
      GO TO 1
   99 CONTINUE
      ENDFILE 10
      CALL PLOT(0.,0.,999)
      STOP
      END
```

```
      SUBROUTINE BESSEL(X,NU,JNUX)
      DOUBLE PRECISION NU,JNUX,XX
      REAL*8 DBSJ1
      XX = X
      IF(X.GT.100..OR.NU.GT.100.) GO TO 100
      JNUX = DBSJ1(XX,NU)
      RETURN
  100 CALL BESEXT(XX,NU,JNUX)
      RETURN
      END


      SUBROUTINE BESEXT(XX,NU,JNUXL)
      COMMON/BESWRK/L1,L2,A(700)
      REAL*8 XX,NU,JNUXL,A
C     THE BESEXT SUBROUTINE RETURNS THE VALUE OF THE BESSEL
C     FUNCTION OF ORDER P.LT.400 AND ARGUMENT X.LT.400. LARGER ORDERS
C     AND ARGUMENTS ARE CONSIDERED BY EXTENDING THE DIMENSION OF A,L1.
      L1 = 700
      K = NU
      CALL DBSJ2(XX,NU,A)
      JNUXL = A(K+1)
      RETURN
      END


      SUBROUTINE BESSI(KA,DK,NU,RINT)
C     THIS IS AN INTEGRATION PROGRAM USING SIMPSON'S 3/8 RULE.
C     NR IS THE NUMBER OF INCREMENTS ON RK AXIS, MULTIPLE OF 3.
      DIMENSION F(4)
      DOUBLE PRECISION NU,RINT,BJ
      REAL KA
      DATA NR/15/
      R1K = KA - DK/2.
      R2K = KA + DK/2.
      RN = NR
      HR = (R2K - R1K)/RN
      A = 0.0
      RK = R1K
      DO 30 I = 1,NR,3
      DO 20 J = 1,4,1
      RKP = RK**(-1.5)
      CALL BESSEL(RK,NU,BJ)
      GOR = COS(RK - KA)
      F(J) = RKP*BJ*GOR
      IF(J.EQ.4) GO TO 30
   20 RK = RK + HR
   30 A = A + (3./8.)*HR*(F(1) + 3.*F(2) + 3.*F(3) + F(4))
      RINT = A
      RETURN
      END
```

```
      SUBROUTINE LEGEND(THETA,NU,M,PNU,P1,IR)
      DOUBLE PRECISION P1,P2,CF,DA,A,PNU,RMGM
      DOUBLE PRECISION PI,CSDA,SNDA,CSA,SNA,T,X,F,RAD,B,C,TX,Y,NU
      DATA PI/3.14159265358979/
      RAD = THETA*PI/180.
      Y = 2.*DSIN(RAD)
      DA = RAD + .5*PI
      RM = M
      N = (70.+RM+RM) -NU
      IF(NU.GT.(69.+RM+RM)) N = -1
      SNDA = DSIN(DA)
      CSDA = DCOS(DA)
      RN = N
      NU = NU + (RN+2.)
      J = 0
      EM2 = RM*RM
      IF(NU*RAD.LT.9.) GO TO 50
   10 NU = NU - 1.
      A = NU*RAD + (.25+.5*RM)*PI
      SNA = DSIN(A)
      CSA = DCOS(A)
      C = 1.
      P2 = P1
      T = 1.
      P1 = SNA
   20 T = -T*((C-.5)**2 - EM2)/(C*Y*(NU+C))
      SNA = SNA*CSDA + CSA*SNDA
      CSA = (CSA - SNA*SNDA)/CSDA
      P1 = P1 + T*SNA
      C = C + 1.
      IF(DABS(T).GT.1.D-9.AND.C.LT.35.) GO TO 20
      B = .25 - EM2
      IF(N.EQ.(-1)) GO TO 40
      J = J + 1
      IF(J.EQ.1) GO TO 10
      C = NU + 2.
      TX = 2.*DCOS(RAD)
      NT = (N+1)/2
      DO 30 J = 1,NT
      C = C - 2.
      P2 = TX*P1 - (1.+B/(C*(C+1.)))*P2
   30 P1 = TX*P2 - (1.+B/(C*(C-1.)))*P1
      J = 2 - MOD(N+1,2)
      NU = NU - RN
      IF(J.EQ.2) P1=P2
      IF(IR.EQ.1) RETURN TO SUBROOTS FOR COMPLETION OF ROOTS.
   40 IF(IR.EQ.1) RETURN
      X = NU +RM - .5
```

```
      T = NU +RM - .5
      IF(M.EQ.0) X=1.
      IF(M.LT.2) GO TO 45
      DO 44 I = 2,M
      T = T-1.
   44 X = X*T
   45 IF(NU.GT.110.) GO TO 46
      CALL GAMRAT(NU,M,GR,1)
      CF = 2./DSQRT(PI*Y)*X*GR
      PNU = CF*P1
      RETURN
   46 T = 1./(16.*NU)
      CF = 2./DSQRT(PI*Y*NU)*X*(1.-2.*T*(1.-T))
      PNU = CF*P1
      RETURN
   50 NU = NU -RN - 2.
      (NU*RAD.LE.9) NOW EXECUTING.
      F = NU*NU - .25
      X = DCOS(RAD)
      Y = (1. - X)/2.
      P1 = 1.
      T = 1.
      C = 0.
   60 C = C + 1.
      T = -T*(F - C*(C-1.))/(RM+C)*Y/C
      P1 = P1 + T
      IF(DABS(T).GT.1.D-9.AND.C.LT.25.) GO TO 60
      CALL GAMRAT(NU,M,GR,2)
      RMGM = RM + 1.
      GM1 = GAMMAR(RMGM)
      IF(NU.LT.100.) CF = GR/GM1
      IF(NU.GE.100.) CF = NU**(M+M)/GM1
      PNU = CF*(((1.-X)/(1.+X))**(.5*RM))*((-1.)**M)*P1
      RETURN
      END
```

```
      SUBROUTINE RESIDU(THETA,NU,M,ID,DPDNU)
      SUB-RESIDUE RETURNS DPDNU,THETAD. WHEN ID=0 AND ITS
      THETA DERIVATIVE WHEN ID=1.
      DOUBLE PRECISION PI,F,RAD,CST,SNT,DPDNU,DPNU2D,NU,P2,PNU2
      DIMENSION F(4)
      DATA PI,H/3.14159265358979,.0001/
      NU = NU - 2.*H
      I = 1
   10 CALL LEGEND(THETA,NU,M,F(I),P2,0)
      IF(ID.EQ.0) GO TO 15
      MP1 = M+1
      CALL LEGEND(THETA,NU,MP1,PNU2,P2,0)
      RAD = THETA*PI/180.
      CST = DCOS(RAD)
      SNT = DSIN(RAD)
      RM = M
      F(I) =RM* CST/SNT*F(I) + PNU2
   15 I = I + 1
      NU = NU + H
      IF(I.EQ.3) NU = NU + H
      IF(I.LT.5) GO TO 10
      DPDNU = (F(1)-8.*F(2)+8.*F(3)-F(4))/(12.*H)
      NU = NU - 3.*H
      RETURN
      END


      FUNCTION GAMMAR(X)
      DOUBLE PRECISION X
      IF(X.GT.1.) GO TO 2
      Z = X
    1 IF(Z.GT.0.) GO TO 3
      Z = Z + 1.
      GO TO 1
    2 Z = X - 1.
    3 T1 = Z + .5
      TZG = T1 + 5.
      T1 = TZG**T1
      T1 = EXP(-TZG)*T1*2.50662827465
      GAMZ = T1*(1.+76.18009173/(Z+1.) -86.50532033/(Z+2.)
     1+24.01409822/(Z+3.) -1.231739516/(Z+4.) +.120858003E-2/
     1(Z+5.) -.536382E-5/(Z+6.))
      IF(X.GT.1.)GO TO 5
    4 GAMZ = GAMZ/Z
      IF(Z.EQ.X) GO TO 5
      Z = Z - 1.
      GO TO 4
    5 GAMMAR = GAMZ
      RETURN
      END
```

```
      SUBROUTINE ROOTS(THETA,NU1,NU2,M,NU,ID)
C     ROOTS OF PNU ARE OBTAINED WHEN ID=0, OF DPDTHETA WHEN ID=1.
      DOUBLE PRECISION PI,EPS
      DOUBLE PRECISION NU,NU1,NU2,NUL,P2,Q,PNU,RAD,FP,FPS,FPL,SCT,SNT
      DATA PI,EPS/3.1415926535 8979,1.D-7/
   26 FORMAT(14H ITN,NU,FP,FPS,I5,3E15.8)
      NU = NU1
      ITN = 0
   10 CALL LEGEND(THETA,NU,M,PNU,FP,1)
      IF(ID.EQ.0) GO TO 15
      MP1 = M + 1
      CALL LEGEND(THETA,NU,MP1,PNU,P2,1)
      RAD = THETA*PI/180.
      CST = DCOS(RAD)
      SNT = DSIN(RAD)
      RM = M
      FP = RM*CST*FP + (NU+RM+.5)*SNT*P2
   15 Q = NU2
      ITN = ITN +1
      IF(ITN.EQ.1) GO TO 20
      FPS = FP - FPL
      IF(DABS(FPS).LT.EPS) FPS = DSIGN(EPS,FPS)
      Q = NUL - (NU - NUL)/FPS*FPL
   20 NUL = NU
      FPL = FP
      NU = Q
      IF(DABS(NU-NUL).LT.EPS) RETURN
      IF(ITN.GT.20) GO TO 30
      GO TO 10
   30 WRITE(6,26) ITN,NU,FP,FPS
      RETURN
      END
```

```
      SUBROUTINE GAMRAT(NU,M,GR,IG)
C     SUB-GAMRAT CALCULATES AND RETURNS THE RATIO OF TWO GAMMA
C     FUNCTIONS.. G(NU+.5)/G(NU+1.) AND G(NU+RM+.5)/G(NU-RM+.5).
      DOUBLE PRECISION NU,X,D1
   10 FORMAT(3E20.10)
      RM = M
      IF(IG.EQ.2) GO TO 30
      KNU = NU
      D = NU - FLOAT(KNU)
      D1 = D + 1.
      X = D + .5
      RAT1 = X/D1
      Y = GAMMAR(X)/GAMMAR(D1)
      IF(KNU.EQ.0) RAT1 = 1.
      Y = Y*RAT1
      IF(KNU.LT.2) GO TO 25
      DO 20 I = 2,KNU
      D1 = D1 + 1.
      X = X + 1.
      RAT = X/D1
   20 Y = Y*RAT
   25 GR = Y
      RETURN
   30 IF(M.EQ.0) GO TO 50
      S = NU + RM - .5
      T = S
      MT = 2*M - 1
      DO 40 I = 1,MT
      T = T - 1.
   40 S = S*T
      GO TO 60
   50 S = 1.
   60 GR = S
      RETURN
      END
```

APPENDIX B

COMPUTER PROGRAM FOR MODAL OR TOTAL FIELD PATTERNS

This program is also written for the IBM 370 system and provides complete field patterns and plots selective cuts of modal or sum patterns. The field component data is provided by one to three magnetic tapes generated by the general program of Appendix A. This auxiliary program allows for detailed study of the modal series without costly recomputations of the general program.

Most of the program parameters have the same meaning as in the program of Appendix A. Other parameter definitions are as follows:

NTAPE = number of data tapes to be read.
If NTAPE = 1 only tape identified by NC will be read.

NC = Tape unit number.

IT = Counter for the total number of complete files read from all the tapes. Must be ≤ to first subscript of the E-arrays.

Scaling and labeling information must be provided in the arguments of the plot subroutines. Multiple graphs will be drawn with the present listing in all plots. The complete listing of the program is included in the following pages.

```
C       POWER PATTERNS AND PLOTS OF CONICAL ARRAY PROBLEM.
C       INPUT TO THIS PROGRAM IS TAKEN FROM TAPE .
        COMPLEX ECT(11,665),ECF(11,665),ERT(11,665),ERF(11,665)
        COMPLEX ECTT,ECFF,ERTT,ERFF
        REAL KA,KAA
        COMMON /CFLD/ECTT(665),ECFF(665)/RFLD/ERTT(665),ERFF(665)
        COMMON /PVS/  PHIN(20),ST(40),S(665),SF(665)
        COMMON/KAMA/KAA(15),M1A(15),MVMA(15),MVRA(15)
        DATA NTAPE/2/
        DATA NTAPE/1/
  181 FORMAT(4H1LM=,I1,5H MCR=,I1,4H M1=,I2,5H MVM=,I2,5H MVR=,I2,
       14H KA=,F6.2,8H THETAC=,F6.2,6H NPHI=,I3,5H NTH=,I3,4H LX=,I4)
  182 FORMAT(4H LM=,I1,5H MCR=,I1,4H M1=,I2,5H MVM=,I2,5H MVR=,I2,
       14H KA=,F6.2,8H THETAC=,F6.2,6H NPHI=,I3,5H NTH=,I3,4H LX=,I4)
  185 FORMAT(2E15.7,F9.3,2E15.7,F9.3)
  186 FORMAT(//11X,9HECT(IT,L),14X,2HDB,15X,9HECF(IT,L),14X,2HDB)
  187 FORMAT(//11X,9HERT(IT,L),14X,2HDB,15X,9HERF(IT,L),14X,2HDB)
  188 FORMAT(4E15.7)
        CALL PLOTI
        NC = 10
        IT = 0.
    1   IT = IT + 1
        IF(IT.EQ.10.AND.NC.EQ.11) GO TO 310
        READ(NC,END=310) MCR
        GO TO (301,301,302),MCR
C       IT CAN REPRESENT A MODE OR A DIFFERENT ELEMENT POSITION.
  301   READ(NC) LM,MCR,M1,MVM,MVR,KA,THETAC,NPHI,NTH,LX
        READ(NC) (PHIN(I),I=1,NPHI)
        READ(NC) (ST(J),J=1,NTH)
        READ(NC) (ECT(IT,L),S(L),ECF(IT,L),SF(L),L=1,LX)
        KAA(IT) = KA
        M1A(IT) = M1
        MVMA(IT) = MVM
        MVRA(IT) = MVR
C       USE "WRITE(6,185) (ECT(IT,L),S(L),ECF(IT,L),SF(L),L=1,LX)" HERE.
        IF(MCR.EQ.1) GO TO 302
        GO TO 300
  302   READ(NC) LM,MCR,M1,MVM,MVR,KA,THETAC,NPHI,NTH,LX
        READ(NC) (PHIN(I),I=1,NPHI)
        READ(NC) (ST(J),J=1,NTH)
        READ(NC) (ERT(IT,L),S(L),ERF(IT,L),SF(L),L=1,LX)
        KAA(IT) = KA
        M1A(IT) = M1
        MVMA(IT) = MVM
        MVRA(IT) = MVR
C       USE "WRITE(6,185) (ERT(IT,L),S(L),ERF(IT,L),SF(L),L=1,LX)" HERE.
  300   GO TO 1
  310   IT = IT - 1
```

```
      IF(NTAPE.EQ.1) GO TO 312
      IF(NC.EQ.12) GO TO 312
      IF(NC.EQ.11) GO TO 311
      NC = 11
      GO TO 1
  311 NC = 12
      GO TO 1
  312 CONTINUE
      DO 340 II = 1,IT
      IF(MCR.EQ.3) GO TO 317
      DO 316 I = II,II
      DO 315 L = 1,LX
      ECTT(L) = ECTT(L) + ECT(I,L)
  315 ECFF(L) = ECFF(L) + ECF(I,L)
  316 CONTINUE
  317 IF(MCR.EQ.2) GO TO 330
      DO 321 I = II,II
      DO 320 L = 1,LX
      ERTT(L) = ERTT(L) + ERT(I,L)
  320 ERFF(L) = ERFF(L) + ERF(I,L)
  321 CONTINUE
  330 CONTINUE
C     THE FOLLOWING "IF" STATEMENT IS TO BE USED ONLY WHEN
C     HIGHER ORDER MODE  PATTERNS IN SUCCESSION ARE REQUIRED.
      CALL PHICUT(II,MCR,M1,MVM,MVR,KA,THETAC,NPHI,NTH,LX)
      IF(II.EQ.3.OR.II.EQ.6.OR.II.EQ.9) GO TO 340
      CALL PLOT(-37.,0.,-3)
  340 CONTINUE
      CALL PLOT(0.,0.,999)
  999 CONTINUE
      STOP
      END
```

```
      SUBROUTINE PHICUT(IT,MCR,M1,MVM,MVR,KA,THETAC,NPHI,NTH,LX)
      DIMENSION SMT(20),SMF(20),SP(40),SFP(40)
      COMPLEX ECTT,ECFF,ERTT,ERFF
      REAL KA,KAA
      COMMON /CFLD/ECTT(665),ECFF(665)/RFLD/ERTT(665),ERFF(665)
      COMMON /PVS/  PHIN(20),ST(40),S(665),SF(665)
      COMMON/KAMA/KAA(15),M1A(15),MVMA(15),MVRA(15)
.....EXECUTE 'DATA JS,LL,JSTEP/0,0,1/' LAST IF THETA-CUTS NOT DESIRED.
      DATA JS,JL,JSTEP/ 0, 0,1/
      DATA JS,JL,JSTEP/17,17,1/
  113 FORMAT(2X,12HMCR,LMP,KCR=,3I5)
  140 FORMAT(1H1,30X,'RADIATION PATTERN,',F4.0,'DEGREE CONE'//
     12X,11HEXCITATION,25HELEM. TYPE(CIRC=1,RAD=2)=,I3,5X,
     118HE-COMP(TH=1,PH=2)=,I3/(3(4X,4HKA =,F7.2,2X,3HM1=,I3,2X,
     14HMVM=,I3,2X,4HMVR=,I3)))
  143 FORMAT(//1X,10HPHI,THETA=,F5.1,16F7.1/(9X,17F7.1))
  170 FORMAT(F6.1,3X,17F7.1/(9X,17F7.1))
  181 FORMAT(4H1LM=,I1,5H MCR=,I1,4H M1=,I2,5H MVM=,I2,5H MVR=,I2,
     14H KA=,F6.2,8H THETAC=,F6.2,6H NPHI=,I3,5H NTH=,I3,4H LX=,I3)
  185 FORMAT(2E15.7,F9.3,2E15.7,F9.3)
  191 FORMAT(2X,2F10.3)
  192 FORMAT(2X,2I3,5HTEST=,F8.2,3X,5HTESF=,F8.2)
.....THE FOLLOWING TWO STATEMENTS DETERMINE CURVE IDENTIFIER
.....FOR THE 'CSEG' PLOTTING ROUTINE.....
      IT1 = IT - 1
      KL = MOD(IT1,3)
      DO 400 LMP = 1,2
      IF(MCR.EQ.2.AND.LMP.EQ.2) GO TO 400
      IF(MCR.EQ.3.AND.LMP.EQ.1) GO TO 400
      KCR = 0
      DO 370 I = 1,NPHI
      TEST = -200.
      TESF = -200.
      DO 375 J = 1,NTH
      L = NTH*I - NTH + J
      GO TO(371,372),LMP
  371 S(L) = 10.*ALOG10(REAL(ECTT(L)*CONJG(ECTT(L))))
      SF(L) = 10.*ALOG10(REAL(ECFF(L)*CONJG(ECFF(L))))
      GO TO 374
  372 S(L) = 10.*ALOG10(REAL(ERTT(L)*CONJG(ERTT(L))))
      SF(L) = 10.*ALOG10(REAL(ERFF(L)*CONJG(ERFF(L))))
  374 IF(S(L).GT.TEST) TEST=S(L)
      IF(SF(L).GT.TESF) TESF=SF(L)
  375 CONTINUE
      SMT(I) = TEST
      SMF(I) = TESF
      WRITE(6,192) LMP,I,TEST,TESF
  370 CONTINUE
```

```
      WRITE(6,191) (SMT(I),SMF(I),I=1,NPHI)
      GO TO (376,377),LMP
  376 WRITE(6,181) LMP,MCR,M1A(IT),MVMA(IT),MVRA(IT),KAA(IT),
     1THETAC,NPHI,NTH,LX
C     USE "WRITE(6,185) (ECTT(L),S(L),ECFF(L),SF(L),L=1,LX)" HERE.
      GO TO 378
  377 WRITE(6,181) LMP,MCR,M1A(IT),MVMA(IT),MVRA(IT),KAA(IT),
     1THETAC,NPHI,NTH,LX
C     USE "WRITE(6,185) (ERTT(L),S(L),ERFF(L),SF(L),L=1,LX)" HERE.
  378 CONTINUE
C     LOOP 410 FINDS LARGEST VALUE IN S(L) AND SF(L) ARRAYS.
      SMTN = -200.
      SMFN = -200.
      DO 410 I = 1,NPHI
      IF(SMT(I).GT.SMTN) SMTN=SMT(I)
  410 IF(SMF(I).GT.SMFN) SMFN=SMF(I)
      SMTT = SMTN
      SMFF = SMFN
      WRITE(6,191) SMTT,SMFF
      SNORM = SMTT
      IF(SMFF.GT.SNORM) SNORM=SMFF
      WRITE(6,191) SMTT,SNORM
  379 KCR = KCR + 1
      WRITE(6,113) MCR,LMP,KCR
      WRITE(6,140) THETAC,LMP,KCR,(KAA(I),M1A(I),MVMA(I),MVRA(I),I=1,IT)
      WRITE(6,143)(ST(J),J=1,NTH)
      CTF = -70.
      DO 390 I = 1,NPHI
      NIN = NTH*(I - 1)
      NIN1 = NIN + 1
      NINMT = NIN + NTH
      IF(KCR.EQ.2) GO TO 386
C     "SNORM" NORMALIZES PATTERNS WITH RESPECT TO LARGEST VALUE
C     OF BOTH FIELD COMPONENTS.   "SMTT" AND "SMFF" ARE FOR
C     INDIVIDUAL COMPONENT NORMALIZATION.
      DO 380 J = 1,NTH
      L = NTH*I - NTH + J
      S(L) = S(L) - SNORM
      SF(L) =SF(L) - SNORM
      SP(J) = S(L)
      SFP(J) = SF(L)
  380 CONTINUE
  385 WRITE(6,170) PHIN(I),(S(J),J=NIN1,NINMT)
      IF(I.GT.1.AND.I.LT.NPHI) GO TO 390
      IF(SP(2).LT.CTF.AND.SP(3).LT.CTF.AND.SP(6).LT.CTF) GO TO 387
  387 IF(SFP(2).LT.CTF.AND.SFP(3).LT.CTF.AND.SFP(6).LT.CTF) GO TO 390
      GO TO 390
  386 WRITE(6,170) PHIN(I),(SF(J),J=NIN1,NINMT)
```

```
390 CONTINUE
    IF(KCR.EQ.1) GO TO 379
    CALL SUB-FBCUT(KL,.....) FOR CONTINUOUS PLOT OF PHI=0 AND PHI=180.
    CALL FBCUT(KL,NTH,NPHI,LX,LMP)
    THE FOLLOWING CARDS PLOT PATTERNS OF THETA VS. PHI.
    . . . . . .
    IF(JS.EQ.0) GO TO 591
    IF(JL.GT.NTH) JL=NTH
    DO 590 J = JS,JL,JSTEP
    DO 580 I = 1,NPHI
    L = NTH*I - NTH + J
    SP(I) = S(L)
    SFP(I) = SF(L)
580 CONTINUE
    CALL PBPLOT(KL,PHIN,9.,0.,20.,12HPHI, DEGREES,12,
   1SP,7.,28.,-4.,28HPOWER IN DB, THETA COMPONENT,28,NPHI,1)
    CALL PBPLOT(KL,PHIN,9.,0.,20.,12HPHI, DEGREES,12,
  1SFP,7.,28.,-4.,26HPOWER IN DB, PHI COMPONENT,26,NPHI,1)
    IF(IT.EQ.3.OR.IT.EQ.6.OR.IT.EQ.9) GO TO 590
    IF(LMP.EQ.2) CALL PLOT(-24.,0.,-3)
590 CONTINUE
591 CONTINUE
    . . . . . .
    IF(IT.EQ.3.OR.IT.EQ.6.OR.IT.EQ.9) GO TO 400
    IF(LMP.EQ.2) CALL PLOT(-13.,0.,-3)
    . . . . . .
400 CONTINUE
900 RETURN
    END
```

```
      SUBROUTINE PBPLOT(K,X,XN,XS,DX,XLAB,NLX,Y,YN,YS,DY,YLAB,NLY,NP,ID)
      DIMENSION X(80),Y(80),XLAB(10),YLAB(10)
.....ID=1 GIVES SINGLE INCREMENT SCALE. ........
.....ID = 2 GIVES TWO-INCREMENT SCALE........
      NX = XN
      NY = YN
      XI = XS
      YI = YS
      NX1 = NX + 1
      NY1 = NY + 1
      IF(K.NE.0) GO TO 30
      DRAW AND LABEL THE X-AXIS.
      CALL PLOT(0.,0.,-3)
      DO 10 I = 1,NX1
      CALL PLOT(0.,-.07,2)
      CALL NUMBER(-.07,-.21,.10,XI,0.,-1)
      'IF STATEMENT' CHANGES INCREMENT FOR ALL POSITIVE SCALE.
      GO TO (11,9), ID
    9 IF(I-5) 11,11,12
   11 XI = XI + DX
      GO TO 13
   12 XI = XI - DX
   13 CALL PLOT(0.,0.,3)
      IF(I.EQ.NX1) GO TO 10
      CALL PLOT(1.,0.,-2)
   10 CONTINUE
      CALL PLOT(-XN,0.,-3)
      AX = XN/2. -.14*(6./7.)*NLX/2.
      CALL SYMBOL(AX,-.42,.14,XLAB,0.,NLX)
      DRAW AND LABEL THE Y-AXIS.
      CALL PLOT(0.,0.,-3)
      DO 20 I = 1,NY1
      CALL PLOT(-.07,0.,2)
      CALL NUMBER(-.14,-.07,.10,YI,90.,-1)
      YI = YI + DY
      CALL PLOT(0.,0.,3)
      IF(I.EQ.NY1) GO TO 20
      CALL PLOT(0.,1.,-2)
   20 CONTINUE
      CALL PLOT(0.,-YN,-3)
      AY = YN/2. -.14*(6./7.)*NLY/2.
      CALL SYMBOL(-.35,AY,.14,YLAB,90.,NLY)
C     THE CURVE MAY BE DRAWN BY 'CALL LINE' IN THE X-Y ARRAYS ARE FIRST
C     FIRST CONVERTED INTO INCHES.  'CALL CSCEG' CONVERTS AUTOMATICALLY.
C.....'ST-30' SELECTS THE TWO-INCREMENT OR THE ONE-INCREMENT AXIS.
   30 GO TO(31,32), ID
   31 CALL CSEG(0,K,NP,X,XN,XS,DX,Y,YN,-YS,-DY)
      GO TO 33
```

```
   32 CALL CSEG(0,K,NP,X,XN,-XS,-DX,Y,YN,-YS,-DY)
C     SET NEW ORIGIN 3 INCHES BEYOND PRESENT PLOT.
   33 CALL PLOT(XN+3.,0.,-3)
      RETURN
      END


      SUBROUTINE FBCUT(IT,NTH,NPHI,LX,LMP)
C     'SUB-FBCUT' PLOTS THE PHI=0 AND PHI=180 CUTS ON SAME PLOT.
      DIMENSION STT(80),SPP(80),SFPP(80)
      COMMON /PVS/PHIN(20),ST(40),S(665),SF(665)
  143 FORMAT(//1X,10HPHI,THETA=,F5.1,16F7.1/(9X,17F7.1))
  144 FORMAT(2X, 5I5)
  170 FORMAT(F6.1,3X,17F7.1/(9X,17F7.1))
      DO 600 J = 1,NTH
      JU = NTH + J
      LN = NTH + 1 - J
      LL = LX - NTH + J
      STT(J) = -ST(LN)
      STT(JU) = ST(J)
      SPP(J) = S(LN)
      SPP(JU) = S(LL)
      SFPP(J) = SF(LN)
      SFPP(JU) = SF(LL)
  600 CONTINUE
C     THE ARRAYS ARE READY FOR USE BY PBPLOT ROUTINES FOR PLOTTING.
      NT2 = 2*NTH
      NT1 = NTH + 1
      WRITE(6,144) LX,NTH,NPHI,NT2,NT1
      GO TO (610,611), LMP
  610 CALL PBPLOT(IT,STT,10.,200.,-40.,14HTHETA, DEGREES,14,
     1SPP,7.,28.,-4.,28HPOWER IN DB, THETA COMPONENT,28,NT2,2)
      WRITE(6,143) (STT(J),J=1,NTH)
      WRITE(6,170) PHIN(1),(SPP(J),J=1,NTH)
      WRITE(6,143) (STT(J),J=NT1,NT2)
      WRITE(6,170) PHIN(NPHI),(SPP(J),J=NT1,NT2)
      GO TO 612
  611 CALL PBPLOT(IT,STT,10.,200.,-40.,14HTHETA, DEGREES,14,
     1SFPP,7.,28.,-4.,26HPOWER IN DB, PHI COMPONENT,26,NT2,2)
      WRITE(6,143) (STT(J),J=1,NTH)
      WRITE(6,170) PHIN(1),(SFPP(J),J=1,NTH)
      WRITE(6,143) (STT(J),J=NT1,NT2)
      WRITE(6,170) PHIN(NPHI),(SFPP(J),J=NT1,NT2)
  612 CONTINUE
      RETURN
      END


      BLOCK DATA
      COMPLEX ECTT,ECFF,ERTT,ERFF
      COMMON /CFLD/ECTT(665),ECFF(665)/RFLD/ERTT(665),ERFF(665)
      COMPLEX ECTT/665*(1.E-15,0.)/,ECFF/665*(1.E-15,0.)/
      COMPLEX ERTT/665*(1.E-15,0.)/,ERFF/665*(1.E-15,0.)/
      END
```

APPENDIX C

EXPANSIONS FOR THE COMPUTATION OF THE BESSEL FUNCTION $J_\nu(x)$

In the event that library routines are not available three different expansions may be used for the Bessel functions $J_\nu(x)$ for different ranges of x and ν.

For $x \lesssim 35$ and $\nu \geq x$, the power series expansion[14]

$$J_\nu(x) = \frac{\left(\frac{x}{2}\right)^\nu}{\nu!} \sum_{k=o}^{\infty} \frac{1}{k!} \frac{\nu!}{(\nu+k)!} \left(\frac{jx}{2}\right)^{2k} \qquad \text{(C-1)}$$

is used. A more convenient form of (C-I) suitable for computation is given by

$$J_\nu(x) = \frac{\left(\frac{x}{2}\right)^\nu}{\Gamma(\nu+1)} \left[1 - S_1 + S_1 S_2 - S_1 S_2 S_3 + \ldots\ldots\right] \qquad \text{(C-2)}$$

where $S_i = \dfrac{\left(\frac{x}{2}\right)^2}{(\nu+i)\, i}$

The asymptotic expansion [15] is used to represent the Bessel function for $35 < x \leq 130$ and $\nu \leq 3\sqrt{x}$.

$$J_\nu(x) = \left(\frac{2}{\pi x}\right)^{1/2} \left[\cos\left(x - \frac{\pi}{2}(\nu+\tfrac{1}{2})\right) \sum_{m=o}^{\infty} (-1)^m \frac{(\nu, 2m)}{(2x)^{2m}}\right. \qquad \text{(C-3)}$$

$$\left. - \sin\left(x - \frac{\pi}{2}(\nu+\tfrac{1}{2})\right) \sum_{m=o}^{\infty} (-1)^m \frac{(\nu, 2m+1)}{(2x)^{2m+1}}\right]$$

where (ν, m) is Hankel's symbol defined by

$$(\nu, m) = \frac{2^{-2m}}{m!} \left\{(4\nu^2 - 1)(4\nu^2 - 3^2) \ldots [4\nu^2 - (2m-1)^2]\right\} \qquad \text{(C-4)}$$

$$= \Gamma\left(\tfrac{1}{2} + \nu + m\right) \Big/ \left[m!\ \Gamma\left(\tfrac{1}{2} + \nu - m\right)\right]$$

The Meissel expansion [16] valid for ν real, large and positive is used to represent the Bessel function for $x > 130$ and $\nu > 3\sqrt{x}$. This expansion is included here for convenient reference.

$$J_\nu(\nu+\epsilon) = \frac{T}{48^{1/6}} + \left(\frac{3}{4}\right)^{1/6} U \qquad \text{(C-5)}$$

where

$$T = \frac{\Gamma\left(\frac{1}{3}\right)}{\pi(\nu+\epsilon)^{1/3}} \sum_{r=0}^{\infty} T_r(\epsilon)\left[\frac{6}{\nu+\epsilon}\right]^r$$

$$U = \frac{\Gamma\left(\frac{2}{3}\right)}{\pi(\nu+\epsilon)^{2/3}} \sum_{r=0}^{\infty} U_r(\epsilon)\left[\frac{6}{\nu+\epsilon}\right]^r$$

and $T_0(\epsilon) = 1$ $\qquad T_1(\epsilon) = \frac{\epsilon}{45} - \frac{\epsilon^3}{18}$

$U_0(\epsilon) = \epsilon$ $\qquad U_1(\epsilon) = -\frac{1}{420} + \frac{\epsilon^2}{36} - \frac{\epsilon^4}{36}$

$$T_2(\epsilon) = -\frac{1}{8100} + \frac{\epsilon^2}{648} - \frac{7\epsilon^4}{3240} + \frac{\epsilon^6}{1620}$$

$$U_2(\epsilon) = -\frac{13}{283500} + \frac{19\epsilon^3}{11340} - \frac{\epsilon^5}{810} + \frac{\epsilon^7}{4536}$$

Taking $x = \nu + \epsilon$ and $\epsilon = x - \nu$, the above expansion of the first three terms becomes:

$$J_\nu(x) = C_1 x^{-1/3}\left[450 + \frac{\epsilon}{x}(60 - 150\epsilon^2) + \frac{1}{x^2}[-2 + 25\epsilon^2 - 35\epsilon^4 + 10\epsilon^5]\right]$$
$$-C_2 x^{-5/3}\left[450 - 31500 x \epsilon - 5250\epsilon^2[1 - \epsilon^2]\right. \qquad \text{(C-6)}$$
$$\left. + \frac{\epsilon}{x}[52 - 1900\epsilon^2 + 1400\epsilon^4 - 2500\epsilon^6]\right]$$

where $C_1 = \frac{\Gamma(1/3)}{450\,\pi\,(48)^{1/6}}$

$$C_2 + \frac{(3/4)^{1/6}\,\Gamma(2/3)}{31500\,\pi}$$

DISTRIBUTION

Commander
Naval Air Systems Command
Department of the Navy
Washington, D. C. 20360
Attn: AIR-53321A
AIR-360
AIR-50174 (4)
AIR-310B (5)

Commander
Naval Ordnance Systems Command
Department of the Navy
Washington, D. C. 20360
Attn: ORD-034

Director
Office of Naval Research
800 North Quincy Street
Arlington, Virginia 22217
Attn: ONR-427

Raytheon Company
Missile Systems Division
Hartlwell Road
Bedford, Massachusetts 01730
Attn: Mr. Walter Jeros,
MS S2-32

Commander
Department of the Air Force
Air Force Avionics Laboratory
Electronic Warfare Division
Wright-Patterson Air Force Base
Ohio 45433
Attn: Mr. Harold Weber

Commanding Officer
Naval Air Development Center
Warminster, Pennsylvania 18974
Attn: Mr. Jerry Guarini, AER-2

Director Naval Research Laboratory
Washington, D. C. 20390
Attn: Code 5360
Code 5350
Code 5256

Commanding Officer
Naval Avionics Facility
Indianapolis, Indiana 46218
Attn: Mr. Paul Brink

Commander
Naval Electronics Laboratory Center
San Diego, California 92152
Attn: Code 2330

General Dynamics
Electronics Division
P. O. Box 81127
San Diego, California 92138
Attn: Dr. G. Tricoles

Director
Electro-Sciences Laboratory
Ohio State University
1320 Kinnear Road
Columbus, Ohio 43212
Attn: Mr. Robert Fouty

Sperry-Rand Corporation
Sperry Gyroscope Division
Microwave Engineering Department
Great Neck, New York 11020
Attn: Dr. Robert J. Tims

Commander
Air Force Cambridge Research Lab.
Laurence G. Hanscom Field
Bedford, Massachusetts 01730
Attn: Mr. Philip Blacksmith

McDonnell Douglas Astronautics Co.
5301 Bolsa Avenue
Huntington Beach, California 92647
Attn: Mr. John Wright/Mail Stop 9
Department A3-830/BB10

Teledyne Ryan Company
5650 Kearny Mesa Road
San Diego, California 92119
Attn: Mr. H. Penner

DISTRIBUTION - Continued

Advanced Sensor Laboratory
U.S. Army Missile Command
Redstone Arsenal
Huntsville, Alabama 35809
Attn: Mr. W. Lindberg

Harry Diamond Laboratories
Microwave Research and
Development Branch
Connecticut Avenue and Van Ness Street, N. W.
Washington, D. C. 20438
Attn: Mr. Howard S. Jones, Jr.

Dr. Norbert N. Bojarski
16 Circle Drive
Moorestown, New Jersey 08057

REPORT DOCUMENTATION PAGE		READ INSTRUCTIONS BEFORE COMPLETING FORM
1. REPORT NUMBER	2. GOVT ACCESSION NO.	3. RECIPIENT'S CATALOG NUMBER
4. TITLE (and Subtitle) Dynamic Impedance Matching in Conformal Arrays		5. TYPE OF REPORT & PERIOD COVERED Final Report January 1973 to January 1974
		6. PERFORMING ORG. REPORT NUMBER 2265.307184, HAC Ref. No. C-7488
7. AUTHOR(s) Peter C. Bargeliotes Wolfgang H. Kummer Alfred T. Villeneuve		8. CONTRACT OR GRANT NUMBER(s) N00019-73-C-0127
9. PERFORMING ORGANIZATION NAME AND ADDRESS Hughes Aircraft Company Culver City, California 90230		10. PROGRAM ELEMENT, PROJECT, TASK AREA & WORK UNIT NUMBERS
11. CONTROLLING OFFICE NAME AND ADDRESS Air Systems Command Department of the Navy Washington, D. C.		12. REPORT DATE January 1974 13. NUMBER OF PAGES 91
14. MONITORING AGENCY NAME & ADDRESS(if different from Controlling Office)		15. SECURITY CLASS. (of this report) Unclassified 15a. DECLASSIFICATION DOWNGRADING SCHEDULE

16. DISTRIBUTION STATEMENT (of this Report)
Distribution limited to U.S. Agencies only; (Test and Evaluation)(January 1974). Other requests for this document must be referred to Commander, Naval Air Systems Command, AIR-310B, Washington, D. C. 20360

APPROVED FOR PUBLIC RELEASE:
DISTRIBUTION UNLIMITED

17. DISTRIBUTION STATEMENT (of the abstract entered in Block 20, if different from Report)

18. SUPPLEMENTARY NOTES

19. KEY WORDS (Continue on reverse side if necessary and identify by block number)
Antenna, conformal, conical, array, element, pattern, slot, modal series, Computer Programs

20. ABSTRACT (Continue on reverse side if necessary and identify by block number)
An exact element pattern from slots on a conducting cone with a full cone angle of 20 degrees was investigated during this period. The exact element pattern was computed from expressions of two potential functions representing the modal fields of arbitrary apertures on the conducting cone. Special subroutines were written for the accurate computation of the special functions of the modal series. The various expressions used in the computer program for these functions and the complete program itself are included in the report.
Continued

20. ABSTRACT - Continued

A comprehensive analysis of the modal series patterns is presented in graphical form for circumferential and radial slots at 39 radians from the cone tip. In the case of the circumferentially oriented slot, the computed patterns agree very well with available measured patterns. Recommendations for further investigative work on the topic of conformal arrays are also included. Computer programs using FORTRAN IV, IBM 370/158 are included.